Entrainment in forced Winfree systems

Zhang, Yongjiao

DOI:
10.33612/diss.143454306

Entrainment in Forced Winfree Systems

Yongjiao Zhang

rijksuniversiteit
groningen

The research for this doctoral dissertation has been carried out at the Faculty of Science and Engineering, University of Groningen, The Netherlands, within the Bernoulli Institute for Mathematics, Computer Science and Artificial Intelligence. This work was financially supported by the China Scholarship Council.

Entrainment in Forced Winfree Systems

PhD Thesis Rijksuniversiteit Groningen

university of groningen

Entrainment in Forced Winfree Systems

PhD thesis

to obtain the degree of PhD at the
University of Groningen
on the authority of the
Rector Magnificus Prof. C. Wijmenga
and in accordance with
the decision by the College of Deans

This thesis will be defended in public on

Monday 9 November 2020 at 11.00 hours

by

Yongjiao Zhang

born on 20 November 1988
in Liaoning, China

Supervisor
Prof. H. W. Broer

Co-supervisor
Dr. K. Efstathiou

Assessment Committee

Prof. A. Jorba
Prof. G. Vegter
Prof. L. Wang

Dedicated to my beloved family
献给我亲爱的家人
♡

Contents

Chapter 1

Introduction

We present a brief history of the concept of synchronization and an overview of its applications focusing on the synchronization in circadian rhythms. Then we discuss the main research questions and ideas of the project, and we give an outline of this thesis.

1.1 A Brief History of Synchronization

The story of synchronization begins in 1665 with Christiaan Huygens [87], the famous Dutch mathematician, astronomer and physicist. By observing his inventor pendulum clocks while he was lying in bed because of a minor illness, he noticed that two pendulums were swinging in perfect synchrony through a beam shown in Fig. 1.1. The pendulums would adjust their motions to form the same rhythms of oscillation, even after the rhythm was disturbed by a perturbation.

Huygens [88] gave a description and explanation of synchronization. The synchronized pendulum was caused by the imperceptible motion of the beam. In modern terminology, we call this phenomenon mutual synchronization. The weak interaction between the pendulums is called coupling.

In 1727, synchronization in a large population was firstly reported by a Dutchman Engelbert Kaempfer [139]. His observation of synchronization in a swarm of insects was the start of description of synchronization in a large group.

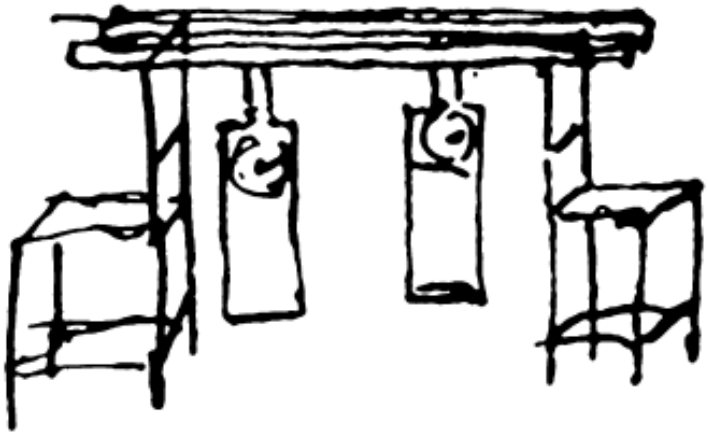

Figure 1.1: Original drawing from Christiaan Huygens explaining the synchronzation of two hanging pendulum clocks

In 1896, John William Strutt and Baron Rayleigh in their book "The theory of sound" [172] observed that two coupled organ pipes speak in absolute unison. This observation started the study of mutual synchronization in acoustical systems.

Synchronization was further developed by William Henry Eccles and J.H Vincent [53] theoretically and experimentally in 1920. They invented a triode generator by taking advantage of the synchronization of two generators which had two different frequencies at the beginning but they shared a common frequency in the end. A few years later, Edward Appleton and Balthasar van der Pol [11] showed that the frequency of a triode generator was entrained to an external signal, even though the signal connected the generator weakly with a slightly different frequency.

In 1935, the American biologist Hugh M. Smith [167] reported that in Thailand thousands of fireflies could flash on and off in synchrony. His finding also contributed to the synchronization in collective behaviour. Something similar was mentioned in Harvery's book [77] that male fireflies of some species gather on trees and start to blink at individual frequencies in order to search for females. Soon they all flash on and off in perfect synchrony. This phenomenon was observed

by tourists and studied by other scholars. In the 1940s, Buck [36, 37] did a series of experiments on the synchronous fireflies. However, how they reached such perfect unison in the whole tree for all fireflies was unknown.

At that time, it was not clear how the rhythmic behaviors were formed or how single cells joined the periodic behavior. What sorts of interactions between cells could result in such a mutual synchronization? Or what led the neurons or the insects firing or flashing simultaneously in a group? Is this governed by a leader or caused by the environment? Inspired by these questions, mathematicians tried to study them in different ways.

In 1958, Norbert Wiener [192] studied the spectrum of human brain waves and firstly hypothesized that there was a population of oscillators in the brain that interact with each other by pulling on each other's frequencies. This phenomenon is called collective synchronization [191]. He also attempted to account for the alpha rhythms with Fourier integrals [192]. Due to the complex neuron network in the brain, this method did not work.

Motivated by Wiener's work, in 1967, Arthur Winfree [194] was the first to successfully use a mathematical model to describe collective synchronization of biological oscillators. He formulated a set of governing equations based on the assumption that biological oscillators could be considered as self-sustained nearly identical oscillators. Without thinking about the oscillator's amplitude, he simplified the nonlinear dynamics of large populations. Before Winfree, Brian Goodwin [66] already considered biological oscillators as physical oscillators. But unlike Goodwin's 3-variable model about intra action among the cells, Winfree considered general interactions among biological oscillators in the whole population. Moreover, he assumed these oscillators were weakly coupled. This assumption meant that each oscillator had a stable limit cycle and they would never move far from their limit cycles.

Winfree explored what types of oscillatory processes and interactions could result in the mutual synchronization, and what peculiarities might be noted in the resultant pattern of temporal organization. In Winfree model, the dynamics of N coupled oscillators is given by

the first-order differential equations

$$\dot{\theta}_i = \omega_i + R(\theta_i)\frac{K}{N}\sum_{j=1}^{N} P(\theta_j), \tag{1.1}$$

for $i = 1, 2, ..., N$, where the parameter K determines the strength of the coupling between oscillators, the state of the i-th oscillator is described by a phase $\theta_i \in \mathbb{S}^1 = \mathbb{R}/2\pi\mathbb{Z}$ and its natural frequency $\omega_i \in \mathbb{R}$.

The response (or, sensitivity) function $R(\theta)$ and the forcing (or, influence) function $P(\theta)$ describe the interaction between oscillators. $R(\theta)$ is also called the phase-response curve or the phase-resetting curve, which determines how the phase changes under perturbations. In circadian rhythms, the phase-response curve will vary with the season, sleep disorders and external interferences. $P(\theta)$ represents how each oscillator influences the others.

The natural frequencies were randomly chosen from a probability distribution. With numerical simulations and analytical approximations, Winfree found that the oscillators would keep their natural frequencies if the width of the distribution of natural frequencies is large. It meant the oscillators were running incoherently. Winfree also showed that the system could reach a synchronized state if the coupling strength is large enough or if the width of the distribution of natural frequencies is small enough. The breakthrough of Winfree's research was that the system could impulsively freeze into either synchrony or death by reaching a critical threshold of system parameters.

Only a few years after Winfree's pioneering work, Kuramoto proposed a simpler model which is more mathematically tractable. The Kuramoto model has numerous variations and has been widely applied in different problems [5]. It has received increasing attention and motivated a great deal of study on synchronization.

1.2 Applications of Synchronization

The study of synchronization and collective behavior has drawn great attention. The understanding of the common properties of network

synchronization and its underlying mechanisms can be applied in various disciplines including physics, chemistry, engineering and economy. We will primarily focus on its applications in biology and neuroscience.

Biological synchronization and rhythmic phenomena at cellular level can be exemplified by pacemaker cells in the heart [136,175]. Experiments on animals [91, 116] supported the notion that pacemakers in the heart can be regarded as a population of coupled oscillators and synchronization occured by self-organizing. Sherman et al. [162–164] studied the synchronization on pancreatic beta-cells mathematically. A.K Ghosh [65] reported synchronization in metabolic yeast cells.

Biological synchronization at a population level has been extensively studied as well. Besides the common examples of flashing fireflies [34,35,54] and crickets that chirp in unison [183], other examples, periodical cicada and Japanese tree frog could synchronize in calling behavior was mentioned in some studies [6–8, 85]. Myxobacteria were modeled for synchronization in pattern formation and traveling waves [89]. In recent years, much interest has been invested in studying the synchronization and swarming behaviors involving mobile agents [28, 59, 62, 130, 131, 179]. Synchronization often happens in animal groups, such as flocking birds [72] and schooling fish [131]. Synchronized behaviors in social groupings is not only for animals, but also for humans. The synchronization of women's menstrual cycles among friends or roommates was investigated in some studies [67, 114, 121]. Some other researchers have noticed the rhythmic clapping from audiences in concert halls [124–126] and coordinated moves among a group of dancers [170].

Synchronization plays a pivotal role in neural activities. On the one side, neural oscillations and synchronization have been linked to many intellectual functions. In recent years, some research has explored the connection between synchronized neurons in a network and its functional properties. Juergen Fell and Nikolai Axmacher [56] demonstrated that synchronization plays a vital role in human memory processes. Neuronal synchronization in the cerebral cortex have been found to be essential for computation [61] and cognitive functions [185], control of movements [111], decision making [195], attention [60,165] and respiratory rhythms [39]. On the other side, synchronization dysfunction may lead to abnormal function in our bodies and

impair our health. The loss of synchrony in the heart could result in cardiac arrhythmias [3,47]. There is also work implying that synchronization is associated to epilepsy [157, 177], Parkinson's disease [76], schizophrenia [176, 177], and autism spectrum disorder [176]. How precisely the exact proper functions are affected by certain synchrony patterns or synchronization mechanism is still not fully understood. But further research of the synchronization mechanism could help to reduce the risk of death and improve life quality [19, 32, 122].

Of course the applications of synchronization is far more than in biology and neuroscience, it is broadly used in other aspects as well.

The most celebrated applications in physics and chemistry are laser arrays [92] and Josephson junctions arrays [188, 193]. Other applications include the analysis of chemical oscillations [102, 201], charge-density wave transport [169], neutrino oscillations [51], triode generators [139], and spin glass [166]. In engineering, synchronization is applied to power grids [57], microwave oscillations [200], beam steering [41,80] and antenna technology [115]. In economy, synchronization is used for analysis of goods markets [90] and the global economic activity [71], measuring market movements [58], and stock arrangement [110].

1.3 Circadian Rhythms and Entrainment

The first observation for synchronization in circadian rhythms was in 1729. The French astronomer and mathematician, Jean-Jacques Dortous de Mairan [155] had observed an interesting phenomenon in his experiments on a haricot bean. He noticed that with the alternation of day and night, the leaves of a haricot bean underwent a corresponding periodic cycle of moving up and down. This variation of behavior did not continue when the plant was put in the darkness. Mairan showed that the period of daily rhythms of the plants was synchronized to the period of the alternation of light. This phenomenon is called entrainment. The external stimulus or environmental factor, such as the change of light and darkness, which entrains or synchronizes an

organism's biological rhythms is called Zeitgeber. Entrainment is one of the cornerstones of circadian systems.

Rhythmic behavior is widely present in the physiological processes of living organisms, from plants to simple animals and humans. The circadian rhythm is a roughly 24 hour sleep and wakefulness cycle, seeing the sunlight, sleeping at night. The entire body is synchronized to and driven by the light-dark cycle. Observations on synchronization in circadian rhythms have also been made in organs, tissues, cells and intra-cellular elements [24, 78, 144]. In mammalian brains, there is a circadian clock consisting of thousands of neurons residing in the suprachiasmatic nucleus (SCN) in the hypothalamus governing their daily rhythmic behaviors [25, 79, 141, 180, 182]. Research on studying circadian rhythms and some experiments on rodents suggested that the circadian pacemaker controls this daily activity-inactivity cycle by keeping trace of dawn and dusk [141]. It is known that a single clock cell exhibits a robust circadian rhythm in its firing rate, and thus each cell is regarded as a self-sustained oscillator. External signals, such as the seasonal change, rotation of the earth, illuminance, temperature, pressure and other environmental variation could also influence the rhythmic behaviors, and entrain the dynamics of living organisms to a 24 h day [84, 99, 117, 189]. The behavior and entrainment properties of a single neuron's response to Zeitgeber is well established [18,26,55].

However, in the SCN, neurons mutually synchronize even without any environmental assistance. Research has shown that with the absence of any environmental input, the internal period of biological clocks differs from 24h, it is longer than that for humans [16, 29, 70, 149, 199], and shorter than that for animals [83] and plants [75]. Therefore, the exact 24-h light-dark living cycle results from the environmental entrainment and must be externally imposed. Complex interactions between the neurons and environment work together in the suprachiasmatic nucleus where the synchronization and entrainment happens. Biological clocks are innate, but the circadian rhythms are very adaptable: they are synchronized, influenced or driven by the environment.

Entrainment is essential for the proper functioning of biological clock. Living behaviors are not functional alone, they are also influenced by the environment. Thus, there are many situations where we

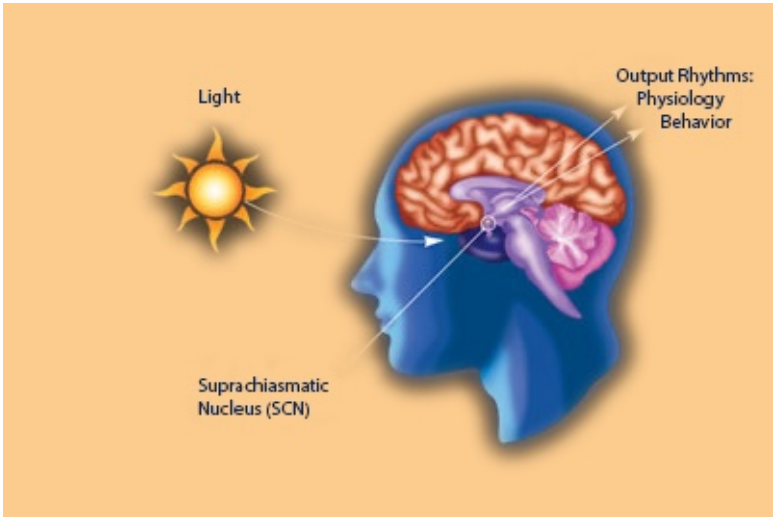

Figure 1.2: Rhythmic behaviors are governed by the circadian cells in the suprachiasmatic nucleus, and it is influenced by Zeitgeber such as light.

not only think of the system itself, but also we need to consider the system with a periodic forcing. Some examples are the contraction of a heart assisted by the cardiac pacemaker [139], or the treatment with hormonal pills for women's menstrual cycle [173]. Periodic stimulation of a system could give rise to various patterns, depending on the strength of the stimulation and its frequency. But sometimes synchronization disorders might bring some trouble to us, such as fuzzy-headedness and errors in judgment caused by jet lag. With respect to the impact of synchronization on human life, we would like to know how the circadian pacemaker affects our everyday lives. The significance and motivation of knowing more about circadian rhythms is that we can keep a synchronized life to the daily dark-light cycle, which also means a healthy life. In addition, by understanding how our body adapts to the dark-light daily cycle, we will be able to understand sleep better, which is a main component of healthy ageing.

How synchronization and entrainment mechanisms work within the SCN neurons is little known and remains one of the main open problems in the field of circadian rhythms. However, mathematical

modeling of circadian systems can provide some understanding of the mechanisms responsible for the circadian oscillation or the possible explanation of the circadian behavior. Some of these models are oscillator models [98, 142, 181, 190] and some are data driven models [33]. Asgari-Targhi and Klerman [17] classify the circadian modeling at organism level [46,98,142,194], biochemical and molecular level [66] and multicellular level [49]. At molecular level, the mathematical model emphasizes the feedback loop in the circadian clock. But at organism level, it focuses more on the interaction between pacers. Entrainment of circadian systems has been studied on both levels [23, 132, 153]. A lot of work has been done on entrainment of circadian rhythms, such as the amplitude of circadian entrainment [31, 104, 107], the stability of circadian entrainment [27, 132], the entrainment range of circadian clocks [1,15], entrainment properties [14,152,174], required light intensity for entrainment of human circadian rhythms [196] and timescale of entrainment [68]. The key point of the entrainment problem so far is how Zeitgeber properties determine entrainment and how the entrainment of these rhythms is affected by the free-running period.

1.4 Winfree Model and Kuramoto Model

Theoretical investigations of collective synchronization include Winfree's pioneering model [194] and Kuramoto's significant extension work [101] on studying the collective behavior of oscillator populations. Other models such as Kuramoto-Sakaguchi [159], forced Kuramoto model [40, 128], second order Kuramoto model [57] and some variations of Kuramoto models are also widely studied. Some research about synchronization focuses on the connectivity and strength of interactions between oscillators [21, 82, 135], and synchronization patterns [13, 161]. Many analytical methods have been developed, such as the self-consistent method [103], stability analysis in the continuum limit [171], and Watanabe-Strogatz method [187, 188]. Moreover, Edward Ott and Thomas M. Antonsen developed a method to lower the dimension of the systems [128]. Other explorations of synchronization

in large population system include [13, 40, 129].

Based on some facts from physics and biology, many scholars have studied large systems of coupled oscillators subjected to a periodic external drive. The problem of exogenous entrainment of an endogenously oscillating synchronized population of oscillators described by the Kuramoto model has been considered. Sakaguchi [158, 160] firstly studied the periodically forced Kuramoto model with self-consistent method, and found oscillators could be synchronized with the external forcing and sometimes the system was self-synchronized at a different frequency from that of the forcing. Since then, more complicated questions, such as the connecting ways between oscillators, asymmetric coupling, on forced Kuramoto model have been studied. Radicchi et al. [147] studied Kuramoto oscillators, driven by one pacemaker, but the oscillators are only coupled with their nearest neighbors. Kori et al. [95, 96] introduced a forced system with an asymmetric coupling strength matrix and proved that entrainment is influenced by the network depth, average distance from the pacemaker to the network, with hierarchical organization. Childs et al. [40] studied the bifurcation diagram of Kuramoto oscillators forced by a pacemaker. Lu et at. [109] considered a sinusoidally forced Kuramoto model and applied it to study how human circadian rhythms are affected by jet-lag and how to reach the reentrainment. Antonsen et al. [10] focused on the stationary states and their stability under a periodic external drive of large systems of coupled oscillators, and provided a method to reduce the dimensionality of the system [128]. Oleksandr et al. [143] discovered that the population field potential is entrained to the pacemaker while individual oscillators are phase desynchronized in the forced Kuramoto model. The exponential synchronization rate of Kuramoto oscillators is analyzed in the presence of a pacemaker [186]. Tarun et al. [156] studied the entrainment of the synchronized solutions under a periodic external driving, including that of stability of the entrained solutions. Recently, research indicates that the topology of the network and the set of forced nodes influences global synchronization of forced Kuramoto oscillators [120]. In the Kuramoto-Sakaguchi model, Baibolatov et al. proved that the external forcing entrains the mean-field [20]. Yuan et al. [202] studied the dynamics of a generalized Kuramoto model with an external pinning force.

Some of this research on large population problems are based on the Winfree model or focus on the Kuramoto model. The major difference between the Winfree and Kuramoto phase oscillator models is that the former has interactions described by a phase product structure and the latter a phase-difference structure. However, there is a much close relationship between them. Choosing the response function $R(\theta) = \sigma - \sin(\theta + \beta)$ and the forcing function $P(\theta) = a_n(1 + \cos(\theta))^n$ in Eq.(1.1), there is a reduction from Winfree model to Kuramoto-Sakaguchi model, Eq.(1.2) with the assumption of weak coupling and nearly identical oscillators by averaging approximation method. This gives the following dynamics:

$$\dot{\theta}_i = \omega_i + \frac{K}{N} \sum_{j=1}^{N} \sin(\theta_j - \theta_i - \beta). \tag{1.2}$$

Setting the phase delay $\beta = 0$, we obtain the Kuramoto model, Eq.(1.3).

$$\dot{\theta}_i = \omega_i + \frac{K}{N} \sum_{j=1}^{N} \sin(\theta_j - \theta_i). \tag{1.3}$$

Compared to Kuramoto model, the analysis of the Winfree model remains a challenging problem and the progress is scarce. Different forms of phase response curves have been chosen in Winfree model [13, 63, 145]. A recent research [94] has been done on the Winfree model with additive white noise which generate noise-induced oscillations and make the equilibria unstable. Diego [134] has considered the chimera states in the Winfree system that consist of two coupled subpopulations.

The Winfree model does not conserve the total phase as the Kuramoto model does. For this reason the Winfree model has richer dynamical features compared to reduced phase models. In this paper, we focus on the synchronization of Winfree model with a periodic forcing, and only all-to-all network is considered.

1.5 Main Questions of the Thesis

Entrainment is a fundamental property of circadian behaviors. In order to understand it better, it is of interest to study the interaction of coupled oscillators [106]. The external periodic driving may come from the 24-hour light-dark cycle, which entrains the oscillatory neurons in the circadian clock and leads to entrained behaviors [189]. The rhythmic external input can also be the process of information streams in the visual cortex [178]. Even it can be the electrode implantation in the deep brain stimulation for curing Parkinson's disease [22]. Studying the effect on entrainment of periodically external force on oscillators is not only of theoretical interest [140,148], but also of practical importance [95, 139, 143]. As we have introduced, Winfree considered the model at the level of intercellular interactions with simplifications. He also demonstrated that the limit cycle oscillators captured amplitude and phase dynamics in circadian rhythms.

In this thesis, we computationally study a basic setup in circadian rhythms described by Winfree system under periodic forcing which means a population of interacting neurons receiving an external periodic input. The first question is whether the oscillators in a forced Winfree system become entrained to the driving frequency and produce regular rhythms. Particularly, what is the driving force's impact? How the external force influences the synchronization and drives the oscillators to be synchronized in the network and how easily a group of oscillators can be entrained by the external periodic force?

The second question we study is the mechanism of the entrainment. How do the parameters (the strength of the external forcing, the average oscillator frequency, the drive frequency, and the coupling strength between oscillators) influence the synchronization? What dynamics does this system have and how the parameters influence the dynamics?

It will be also interesting to know what is the situation for the oscillators coming from two different populations.

1.6 Outline of the Thesis

In Chapter 2, we consider a network of coupled Winfree oscillators under the influence of an external periodic forcing. Our focus is on entrainment, the synchronization of individual oscillators to the forcing. This is quantitatively described through the entrainment degree, that is, the percentage of entrained oscillators. Through a series of numerical experiments we study the entrainment degree for different coupling strengths, forcing strengths, and distributions of natural frequencies of the Winfree oscillators. We consider three types of distributions, delta distribution (identical oscillators), uniform distribution, and Lorentz distribution, and we compare the results. In all cases the mean natural frequency equals the frequency of the external forcing. Moreover, for the Lorentz distribution we use the Ott-Antonsen approximation to obtain a low-dimensional description of the dynamics and we use this to compute the entrainment degree and obtain a better understanding of entrainment.

In Chapter 3, we focus on the frequency detuning in the Winfree system with periodic forcing. The detuning here refers to the difference between the mean natural frequency and that of the external force. In this case, the entrainment properties of the system and the differences with the non-detuned system in Chapter 2 are addressed.

In Chapter 4, we investigate two populations with different mean frequency interacting with each other in the periodic forced Winfree system as an extension of the thesis and point out some future research directions.

In the last chapter, the conclusions of this thesis are presented, as well as some limitations.

Chapter 2

Entrainment of Winfree System under External Forcing

2.1 Introduction

The Winfree model was introduced in [194] to describe the *synchronization* of biological oscillators. It is the first paradigmatic model proposed to study synchronization in large populations and it exhibits very rich dynamics. The dynamics of N coupled oscillators is given by the first-order differential equations

$$\dot{\theta}_i = \omega_i + R(\theta_i)\frac{K}{N}\sum_{j=1}^{N} P(\theta_j), \tag{2.1}$$

for $i = 1, 2, ..., N$, where the parameter K determines the strength of the coupling between oscillators, the state of the i-th oscillator is described by a phase $\theta_i \in \mathbb{S}^1 = \mathbb{R}/2\pi\mathbb{Z}$, and its natural frequency is $\omega_i \in \mathbb{R}$.

The functions $R(\theta)$ and $P(\theta)$ are associated to the interaction between oscillators. The *response* (or, sensitivity) function $R(\theta)$ signifies how an oscillator responds to the effect of other oscillators or its environment. The *forcing* (or, influence) function $P(\theta)$ represents how each oscillator influences the others. Through this simple interaction

model, very rich dynamics of the system can appear even for benign choices of the functions $R(\theta)$ and $P(\theta)$. Winfree showed that the system can reach a synchronized state if the coupling strength is large enough or if the width of the distribution of natural frequencies is small enough. Other types of dynamics are also possible. For example, for

$$R(\theta) = -\sin\theta, \qquad P(\theta) = 1 + \cos\theta, \tag{2.2}$$

a choice of response and forcing functions that will be the basis also for this work, other observed states include *death*, *partial locking*, and *partial death*; see [13] and Sec. 2.4.2.

The Kuramoto model [100], introduced a few years later after the Winfree model, is analytically more tractable and for symmetric and unimodal natural frequency distributions of the oscillators it exhibits simpler dynamics—either locking or incoherence. The great explanatory power and the simplicity of the Kuramoto model were two of the main reasons that motivated its subsequent study, and the explosion of theoretical and numerical work focusing on understanding its properties. We indicatively mention here Kuramoto's own self-consistent analysis [100]; Crawford's work on the stability of the incoherent state [43–45]; the Watanabe-Strogatz theory [187]; and the low-dimensional Ott-Antonsen ansatz [128]. We refer to [12, 150, 168] for thorough reviews of the Kuramoto model, the role it has played on the question of synchronization, and its many generalizations leading to rich dynamics beyond locking and incoherence.

Despite the fact that the Kuramoto model has been the focus of most research activity, there has been recently also significant work aiming to understand the more complicated behavior of the Winfree model. Ariaratnam and Strogatz [13] considered a Winfree model with interaction functions as in Eq. (2.2) and a uniform distribution of natural frequencies in an interval $[1-\gamma, 1+\gamma]$. For this system, different types of dynamics are described in [13], and the regions in parameter space (K, γ) corresponding to each type are identified using a combination of numerical computations and theoretical analysis. In particular, all of the bifurcation curves, except the one corresponding to transition from *locking* to *partial locking*, were analytically determined in [13]. We review the types of dynamics in Sec. 2.4.2. Quinn *et*

al. [145,146] continued this work and used the Poincaré-Lindstedt perturbation method to understand the transition from locking to partial locking. They have shown that the corresponding bifurcation curve becomes singular as N goes to ∞, while it remains well-behaved for finite N, establishing that the transition to the continuum limit can be quite subtle. In [129], Oukil *et al.* give criteria for synchronization in a network of Winfree oscillators. Ha *et al.* in [74] consider the strong coupling regime of Winfree oscillators and prove convergence to an equilibrium solution—*oscillator death* in the terminology of [13]. In [73] the emergence of different types of dynamics is studied for Winfree oscillators on locally connected networks.

The Ott-Antonsen ansatz has also been used for the study of dynamics of Winfree oscillators. We refer to work by Pazánd Montbrió [134] and Gallego *et al.* [64] who have considered the Ott-Antonsen ansatz for a variety of pulse types and sinusoidal response functions in Winfree oscillators. In particular, in [64] two different synchronization scenarios are identified and distinguished via the mutation of a Bogdanov-Takens point. A generalization of the Winfree model has been studied by Laing [106] using again the Ott-Antonsen ansatz in the same spirit as in [134].

Our work is motivated by problems related to circadian rhythms and, in particular, the entrainment of organisms to the daily dark-light cycle. Describing the pacer cells in the suprachiasmatic nucleus as Winfree oscillators [194], we are interested in the effect of a periodic external forcing to their dynamics. Thus, we consider the forced Winfree system

$$\dot{\theta}_i = \omega_i + \frac{K}{N}\sum_{j=1}^{N} R(\theta_i)P(\theta_j) + \varepsilon R_Z(\theta_i)P_Z(t), \tag{2.3}$$

for $i = 1, 2, \ldots, N$. The additional term, $\varepsilon R_Z(\theta_i)P_Z(t)$, where "$Z$" stands for "Zeitgeber", represents the interaction of the i-th oscillator with its environment. The parameter ε represents the strength of this interaction. The *external forcing* function $P_Z(t)$ represents the influence of the environment, while the *external response* function $R_Z(\theta)$ represents how each oscillator responds to the external influence.

This is a very general model and to proceed we will make several assumptions. First, we will consider the interaction functions $R(\theta)$ and $P(\theta)$ given in Eq. (2.2). Then, we will assume that $P_Z(t)$ is a 2π-periodic function of time t so that it models the periodic effect of the dark-light cycle. Finally, we make the assumption that the response function to the external forcing and to other oscillators is the same, that is, $R_Z(\theta) = R(\theta)$, and that the external forcing function P_Z has the same form as the influence function P. Summarizing, we consider the following model describing a system of forced Winfree oscillators:

$$\dot{\theta}_i = \omega_i - \frac{K}{N}\sum_{j=1}^{N} \sin\theta_i(1+\cos\theta_j) - \varepsilon \sin\theta_i(1+\cos t), \tag{2.4}$$

for $i = 1, 2, ..., N$.

We will consider three types of unimodal natural frequency distributions. In all cases the mean value Ω of the natural frequencies is chosen to be $\Omega = 1$, that is, equal to the frequency of the external forcing. The more general problems of unimodal distributions with mean value $\Omega \neq 1$ and bimodal distributions will be considered in a forthcoming paper.

The first, and simplest, case is that of identical oscillators, that is, $\omega_i = \Omega = 1$ for $i = 1, \ldots, N$. Results for this case will serve as a baseline with which to compare the results that we obtain for the other two natural frequency distributions. The second case is the uniform natural frequency distribution with support in $[\Omega - \delta, \Omega + \delta]$. The third natural frequency distribution that we consider in this paper is the Lorentz distribution

$$g(\omega) = \frac{\gamma}{\pi((\omega - \Omega)^2 + \gamma^2)}, \tag{2.5}$$

which has non-compact support and will allow to use the Ott-Antonsen ansatz for the study of the system.

The main aim of our paper is to describe the collective dynamics of forced Winfree oscillators and to understand the entrainment of oscillators to the external forcing. One important question here is how to characterize the collective dynamics and quantify entrainment. The latter is done through the *entrainment degree* which is defined as the

ratio of oscillators that are entrained (synchronized to the external forcing). The *order parameter*,

$$z = re^{\mathrm{i}\psi} = \frac{1}{N}\sum_{j=1}^{N} e^{\mathrm{i}\theta_j},$$

has been extensively used in the literature to describe the collective dynamics. However, as we later show, there is only a weak relation between the dynamical behavior of the order parameter in our system and the corresponding entrainment degree. In particular, there are a few cases where one can deduce whether the system has a very high or very low entrainment degree from specific types of dynamical behavior of the order parameter. Nevertheless, there are also many intermediate cases where a direct connection is not possible. Our approach for connecting these two quantities is to consider the order parameter predicted by the Ott-Antonsen ansatz and using the resulting low-dimensional dynamics to compute a corresponding entrainment degree. The question on whether one can define an appropriate collective variable, similar to the order parameter, from which one can directly read off the entrainment degree remains open.

We now give a brief outline of the paper. In Sec. 2.2 we study in detail the dynamics of a single oscillator under the influence of the external forcing. That is, we consider the case $K = 0$ where each oscillator decouples from the rest but is still forced by the Zeitgeber. Moreover, we define the *entrainment degree*, that is, the ratio of oscillators that synchronize to the Zeitgeber and give an analytic expression for the degree in the case $K = 0$. In Sec. 2.3 we consider the case of identical oscillators, we numerically compute the entrainment degree that depends on parameters (ε, K), and we give a theoretical explanation of the numerical results. In Sec. 2.4 we describe the collective dynamics of the system in the case of non-identical oscillators whose natural frequencies follow a uniform or Lorentz distribution. After discussing numerical results on the entrainment degree, we extend the classification scheme of dynamical types in [13] to the new types of dynamics that appear with the introduction of the external forcing. Moreover, we consider the evolution of the order parameter and how it reflects the different types of dynamics. In Sec. 2.5 we re-

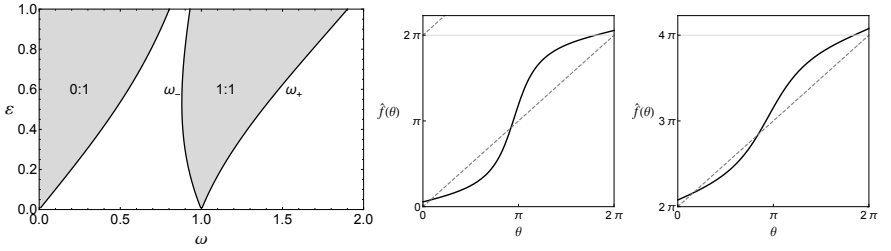

(a) Resonance tongues (b) Poincaré map $\omega = 0.05$, $\varepsilon = 0.2$ (c) Poincaré map $\omega = 1.05$, $\varepsilon = 0.2$

Figure 2.1: (a) The two main resonance tongues, 0:1 and 1:1, for the single oscillator dynamics, Eq. (2.6). (b,c) Graphs of the Poincaré map lift $\hat{f}_{\omega,\varepsilon}$ for different values of the parameters. Intersections with the dashed lines $\theta + 2k\pi$, $k \in \mathbb{Z}$, correspond to fixed points θ_p of the Poincaré map $f_{\omega,\varepsilon}$.

port on the low-dimensional dynamics of the system by applying the Ott-Antonsen ansatz. We study the bifurcations of the obtained dynamics and we use these dynamics to establish a connection between the order parameter (mean-field) and the entrainment degree. We conclude the paper in Sec. 2.6.

2.2 Single Oscillator Dynamics and Entrainment Degree

We first consider the dynamics of a single Winfree oscillator interacting only with the environment and not with other oscillators in the ensemble. The techniques we use to study this simple case (e.g., Poincaré maps, circle maps, resonance tongues, entrainment degree) will carry over to the study of the general system in subsequent sections. The dynamics in this case is given by the non-autonomous first-order differential equation

$$\dot{\theta} = \omega - \varepsilon \sin\theta\,(1 + \cos t), \tag{2.6}$$

that is, Eq. (2.4) with $K = 0$, where we have dropped the index i.

To study the dynamics of Eq. (2.6) we introduce the Poincaré map $f_{\omega,\varepsilon}(\theta)$ which for an initial condition $\theta \in \mathbb{S}^1$ at $t = 0$ gives the phase at time $t = 2\pi$, that is, after one period of the forcing. This defines the Poincaré map as a function $f_{\omega,\varepsilon} : \mathbb{S}^1 \to \mathbb{S}^1$. However, it is also convenient to work with a *lift* of the Poincaré map $\hat{f}_{\omega,\varepsilon} : \mathbb{R} \to \mathbb{R}$ defined by solving Eq. (2.6) with $\theta \in \mathbb{R}$.

The map $f_{\omega,\varepsilon}(\theta)$ is a circle map and thus the corresponding theory applies here, see [48]. In particular, we expect to find resonance tongues in the (ω, ε) parameter plane. When the natural frequency ω is inside the k:1 resonance tongue for a given value of ε, the Poincaré map $f_{\omega,\varepsilon}(\theta)$ has two fixed points, one stable and one unstable. These correspond to points θ_p where $\hat{f}_{\omega,\varepsilon}(\theta_p) = \theta_p + 2k\pi$ for some $k \in \mathbb{Z}$. Stability corresponds to $|\hat{f}'_{\omega,\varepsilon}(\theta_p)| < 1$ and instability to $|\hat{f}'_{\omega,\varepsilon}(\theta_p)| > 1$. The boundaries of the resonance tongues are determined by a saddle-node bifurcation where the stable and unstable fixed points collide and disappear, i.e., by $\hat{f}_{\omega,\varepsilon}(\theta_p) = \theta_p + 2k\pi$ and the additional condition $\hat{f}'_{\omega,\varepsilon}(\theta_p) = 1$. The main resonance tongues 0:1 and 1:1, the boundaries of which have been computed through numerical continuation of the corresponding saddle-node bifurcations, are shown in Fig. 2.1a.

The graph of the lift $\hat{f}_{\omega,\varepsilon}$ for two values of ω with $\varepsilon = 0.2$ is depicted in Fig. 2.1b and 2.1c. In Fig. 2.1b, corresponding to parameters in the 0:1 resonance zone, we have that $\hat{f}_{\omega,\varepsilon}(\theta_p) = \theta_p$, implying that the phase θ becomes constant after sufficiently large time. In contrast, in Fig. 2.1c, corresponding to parameters in the 1:1 resonance zone, we have that $\hat{f}_{\omega,\varepsilon}(\theta_p) = \theta_p + 2\pi$. This implies that the phase θ increases by 2π when time t increases by 2π, for t sufficiently large. Even though in both cases we have a fixed point of the Poincaré map, only in the latter case, corresponding to parameters in the 1:1 resonance zone, we can say that the oscillator *entrains* to the forcing, in the sense that the oscillator makes exactly one full cycle for each cycle of the forcing.

To characterize entrainment in an ensemble of oscillators, we define the *entrainment degree* d_e as a measure of the effect of the external forcing. Specifically, we define

$$d_e = \frac{N_e}{N}, \tag{2.7}$$

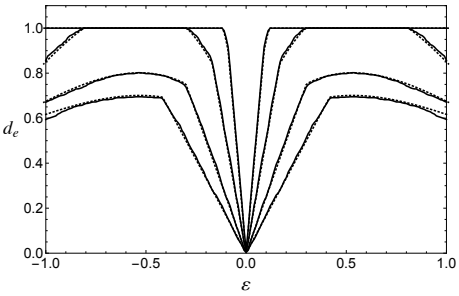

(a) Uniform distribution, $K = 0$. From top to bottom: $\delta = 0.05$, 0.1, 0.2, 0.3.

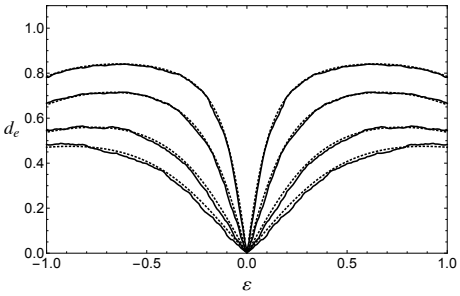

(b) Lorentz distribution, $K = 0$. From top to bottom: $\gamma = 0.05$, 0.1, 0.2, 0.3.

Figure 2.2: Entrainment degrees for different distributions and values of their scale parameter for $K = 0$. The numerically computed entrainment degrees (solid curves) are compared with the theoretically computed ones (dotted curves). In both figures, $N = 1000$ oscillators have been integrated for time $T = 2000$ with time-step $\mathrm{d}t = 0.1$. An oscillator is considered to be entrained if its rotation number ρ satisfies $|\rho - 1| < 0.01$.

where N_e is the number of oscillators having rotation number $\rho = 1$, that is, equal to the frequency of the external forcing. Recall that for an oscillator with initial phase $\theta_i(0)$, the *rotation number* is defined by

$$\rho_i = \lim_{t\to\infty} \frac{\theta_i(t) - \theta_i(0)}{t},$$

provided that the limit exists, see [48]. Oscillators with the same rotation number attain the same average frequency (and thus an asymptotically constant phase difference) after large enough time. Since Eq. (2.7) involves the rotation numbers of the oscillators it is meaningful in the limit $t \to \infty$ and when each oscillator has a well-defined rotation number.

The entrainment degree for $K = 0$ can be theoretically determined by considering for a given distribution and given value of ε how many oscillators fall within the 1:1 resonance zone. More specifically, let $\omega_-(\varepsilon) < \omega_+(\varepsilon)$ be the two boundary curves of the 1:1 resonance zone,

see Fig. 2.1a, and let $g(\omega)$ be the natural frequency distribution of the oscillators. Then for $K = 0$ we have

$$d_e(\varepsilon) = \int_{\omega_-(\varepsilon)}^{\omega_+(\varepsilon)} g(\omega)\,\mathrm{d}\omega. \tag{2.8}$$

The theoretically predicted values of $d_e(\varepsilon)$ are compared to numerical computations in Fig. 2.2 for uniform and Lorentz distributions.

We observe that for $K = 0$ the entrainment degree is an even function of ε. This is a direct consequence of the fact that Eq. (2.6) is invariant under the map $(\varepsilon, \theta) \mapsto (-\varepsilon, \theta + \pi)$.

Moreover, as the scale parameter of the distribution increases the entrainment degree is decreased. The reason is that increasing the scale parameter implies that a larger proportion of oscillators falls outside the resonance tongue. This is also the reason that the degree entrainment for the Lorentz distribution is, in general, smaller than that for the uniform distribution and, in particular, for the non-compactly supported Lorentz distribution we never have $d_e = 1$.

2.3 Identical Oscillators

We now turn our attention to the general case of coupled oscillators, i.e., $K \neq 0$. As a baseline, we first consider here the case of identical oscillators where $\omega_i = 1$ for all oscillators. The numerically computed entrainment degree as a function of the parameters (ε, K) is shown for this case in Fig. 2.3b. There are only two regions. Either all oscillators are entrained to the forcing (red), or no oscillators are entrained (dark blue). This is a result of the (numerically verified) fact that for all values of ε and K all oscillators attain exactly the same rotation number. However the precise details are not the same for all (ε, K) values.

The key to understanding the dynamics of this case is the synchronized dynamics, taking place on the *synchronized manifold*,

$$\Sigma = \{\theta \in (\mathbb{S}^1)^n : \theta_1 = \cdots = \theta_N =: \theta_s\}.$$

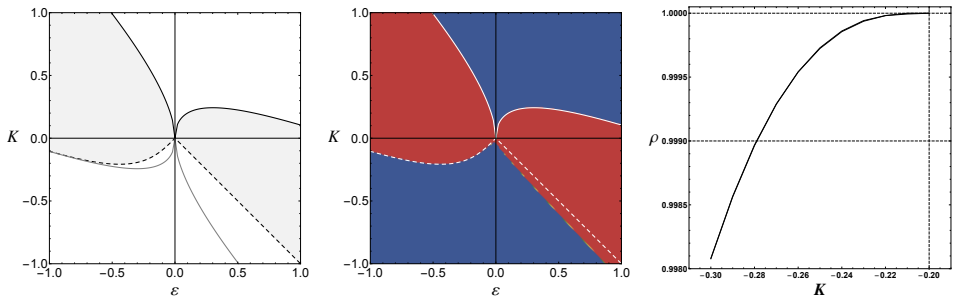

(a) (b) (c)

Figure 2.3: (a) Boundaries of the 1:1 resonance tongue on the (ε, K)-plane for the synchronized dynamics and the curve $K_n(\varepsilon)$ corresponding to loss of normal stability. The upper boundary of the tongue is represented by the thick black curve and the lower boundary by the light gray curve. The curve $K_n(\varepsilon)$ is represented by the dashed curve. The gray area is the theoretically predicted area of entrainment for identical oscillators with $\omega_i = 1$. (b) Numerically computed entrainment degree for $N = 1000$ identical oscillators with $\omega_i = 1$, $i = 1, \ldots, N$, and random initial phases $\theta_i(0)$ chosen uniformly in $[0, 2\pi)$. An oscillator is considered to be entrained if its rotation number ρ_i satisfies $|\rho_i - 1| < 10^{-3}$. The red color represents complete entrainment, $d_e = 1$, and the dark blue color represents no entrainment, $d_e = 0$. The solid and dashed curves are as in (a) and represent the boundaries of the theoretically predicted entrainment region. (c) Rotation number for $\varepsilon = 0.2$ and K close to $K_n(\varepsilon) = -\varepsilon$ computed for time $T = 10^6$. The numerical curve shown here can be approximated by $\rho = 1 - b(\varepsilon)|K + \varepsilon|^{a(\varepsilon)}$ with $K \leq -\varepsilon$.

The manifold $\Sigma \simeq \mathbb{S}^1$ is invariant under the dynamics induced by Eq. (2.4). In particular, the dynamics on Σ is given by

$$\dot{\theta}_s = \omega - \sin\theta_s \left[K(1+\cos\theta_s) + \varepsilon(1+\cos t)\right]. \tag{2.9}$$

Therefore, the dynamics on $\Sigma \simeq \mathbb{S}^1$ is that of an externally forced flow on $\mathbb{S}^1$. The corresponding Poincaré map is the circle map $F_s : \Sigma \to \Sigma$ obtained by following the flow of the synchronized dynamics for time 2π. Similarly to the discussion in Sec. 2.2 we can also talk here about the lift of F_s and resonance tongues. We are again interested in the 1:1 resonance tongue, corresponding to entrainment to the external forcing. The tongue will be here a subset of the three-space (ω, ε, K). However, we are here interested only in the case $\omega = 1$ so we can consider only the intersection of the tongue with the (ε, K)-plane. The numerically computed resonance tongue boundaries are shown in Fig. 2.3a by a black solid curve for $K \geq 0$ and a gray solid curve for $K \leq 0$. The tongue is invariant under the mapping $(\varepsilon, K) \mapsto (-\varepsilon, -K)$.

Let $\theta_s(t)$ be the periodic orbit of period $T = 2\pi$ of the synchronized dynamics, corresponding to the stable fixed point of the Poincaré map F_s in the 1:1 resonance tongue. The linear stability of $\theta_s(t)$ with respect to deviations in the direction of Σ (i.e., deviations that correspond to synchronized states) is determined through the variational equation

$$(\delta\theta_s)^{\cdot} = (S(t) + K\sin^2\theta_s(t))(\delta\theta_s),$$

where

$$S(t) = -\cos\theta_s(t)\left[K(1+\cos\theta_s(t)) + \varepsilon(1+\cos t)\right],$$

and stability implies that

$$\lambda_s = \int_0^{2\pi} \left(S(t) + K\sin^2\theta_s(t)\right)\, dt < 0.$$

To determine the normal stability of the periodic orbit $\theta_s(t)$ let

$$u_i = \theta_i - \theta_{i+1}, \text{ for } i = 1, \ldots, N-1 \text{ and } u_N = \theta_N.$$

On Σ we have $u_i = 0$, $i = 1, \ldots, N-1$, and $u_N = \theta_s$. The variational equations for the u_i, $i = 1, \ldots, N-1$, representing deviations from the synchronized manifold are given by

$$(\delta u_i)^{\cdot} = S(t)(\delta u_i), \quad i = 1, \ldots, N-1,$$

and therefore the *normal stability* of the periodic orbit $\theta_s(t)$ is determined by the sign of

$$\lambda_\perp = \int_0^{2\pi} S(t)\, dt = \lambda_s - K \int_0^T \sin^2 \theta_s(t)\, dt.$$

The last relation implies that the stable periodic orbit of the synchronized dynamics ($\lambda_s < 0$) is also normally stable for $K > 0$. However, for $K < 0$, the last term in the previous equation can become large enough to make $\lambda_\perp > 0$, that is, to make the periodic orbit $\theta_s(t)$ normally unstable. We have numerically computed for each value of ε the value $K_n(\varepsilon)$ of K where the stable periodic orbit loses $\theta_s(t)$ normal stability. The resulting curve $K_n(\varepsilon)$ is shown by the black dashed curve in Fig. 2.3a.

Determining the local stability of $\theta_s(t)$ that we have been discussing is not sufficient to reach global conclusions. In particular, it leaves open the possibility that the periodic orbit $\theta_s(t)$ is linearly stable but not globally attracting. We have numerically checked that this does not occur: when the system is in the 1:1 resonance tongue of F_s and $K > K_n(\varepsilon)$, that is, when $\theta_s(t)$ is linearly stable, randomly chosen initial phases converge to $\theta_s(t)$ and thus all oscillators entrain, see Fig. 2.3b. This explains why the upper boundary of the entrainment region is given by the upper boundary of the 1:1 resonance tongue of the synchronized dynamics while the lower boundary is given by the curve $K = K_n(\varepsilon)$.

Remark 2.3.1. The obtained straight line $K_n(\varepsilon) = -\varepsilon$ for $\varepsilon > 0$ can be easily explained. For $K = -\varepsilon$ the equation for synchronized manifold θ_l becomes

$$\dot{\theta}_l = 1 - \varepsilon \sin \theta_l (\cos t - \cos \theta_l),$$

with the obvious (periodic) solution $\theta_l(t) = t$ which can be shown to be stable for $\varepsilon > 0$ and for which a straightforward computation gives $S(t) = 0$ and thus $\lambda_\perp = 0$.

Remark 2.3.2. The match between the numerics and the curve $K_n(\varepsilon)$ seems to not be perfect for $\varepsilon > 0$, as shown in Fig. 2.3b. This turns out to be a numerical artifact. The computation of the entrainment degree in Fig. 2.3b is done by integrating the dynamics for time $T = 2 \cdot 10^4$ which leads to an estimation error for the rotation number of the order of 10^{-4}. For this reason we have set the threshold to identify entrained oscillators to 10^{-3}, that is, an oscillator is marked as entrained if $|\rho_i - 1| < 10^{-3}$, and with this threshold we see the small mismatch in Fig. 2.3b. A longer integration, which allows for a more accurate estimate of the rotation number, indicates that there is no mismatch. In particular, computing the rotation number by integrating the dynamics for time $T = 10^6$ (and corresponding estimation error of the order of 10^{-6}) for fixed $\varepsilon = 0.2$ and K near $K_n(\varepsilon) = -0.2$ we obtain the picture in Fig. 2.3c. The longer integration indicates that the rotation number equals 1 for $K \geq -0.2$ and it falls slowly for $K < -0.2$; in particular, it becomes 0.999 at $K \approxeq -0.28$. Therefore, with threshold 10^{-3} all states with K between $K \approxeq -0.28$ and $K = -0.2$ are erroneously considered as entrained thus leading to the observed mismatch. Setting the threshold to 10^{-4} would improve the result but only slightly: states with K between $K \approxeq -0.23$ and $K = -0.2$ would still be erroneously considered as entrained.

2.4 Non-Identical Oscillators

Moving beyond the case of identical oscillators we now turn our attention to oscillators whose natural frequencies follow either a uniform or a Lorentz distribution with different values of scale parameters. We first present the numerically computed entrainment degree for these distributions. Then we consider, *state diagrams* showing for each oscillator in an ensemble the relation between its natural frequency and the corresponding, numerically computed, rotation number. Different types of dynamics are characterized in terms of such diagrams. Finally, we consider the time evolution of the *order parameter*

$$z = re^{\mathrm{i}\phi} = x + \mathrm{i}y := \frac{1}{N}\sum_{j=1}^{N} e^{\mathrm{i}\theta_j}. \tag{2.10}$$

Since the external forcing is 2π-periodic we will plot both the continuous evolution $z(t)$, $t \in \mathbb{R}$, of the order parameter as a planar curve, but also the discrete values $z(t_k)$, $t_k = 2k\pi$ with $k \in \mathbb{Z}_{\geq 0}$. In Sec. 2.5 we will compare the evolution of the order parameter in the case of a Lorentz distribution of natural frequencies to the corresponding evolution obtained through the Ott-Antonsen ansatz.

2.4.1 Entrainment degree

We have made a series of numerical simulations to compute the entrainment degree d_e for different parameter values of the system. In the simulations we have used $N = 1000$ oscillators with initial phases uniformly distributed in the interval $[0, 2\pi]$, that is, starting close to the incoherent state. We have let the system evolve for time $T = 2 \cdot 10^4$, using a fourth-order Runge-Kutta method with fixed time step $\mathrm{d}t = 0.1$, and then we have computed a finite-time approximation of the rotation number for the i-th oscillator by

$$\rho_i(T) = \frac{1}{T}(\theta_i(T) - \theta_i(0)).$$

An oscillator has been marked as entrained, and thus contributed to the number of entrained oscillators, N_e, when $|\rho_i(T) - 1| < 10^{-3}$. The results of these computations are shown in Fig. 2.4 and Fig. 2.5, for the uniform and the Lorentz distribution respectively, on the (ε, K) parameter plane and for different fixed values of their respective scale parameters.

The first observation, mirroring the situation for $K = 0$ (see Sec. 2.2), is that d_e decreases as the scale parameter increases, that is, as the distribution becomes wider. Moreover, while d_e attains the values 1 (complete entrainment) and 0 (no entrainment) for certain parameter values with the uniform distribution, this is not the case for the Lorentz distribution. Both of these observations should be expected, since oscillators are more easily entrained when their natural frequency is close to the forcing frequency. Moreover, the fact that the Lorentz distribution has non-compact support implies that there are always going to be some oscillators that can be entrained through the collective dynamics and, correspondingly, some for which this does

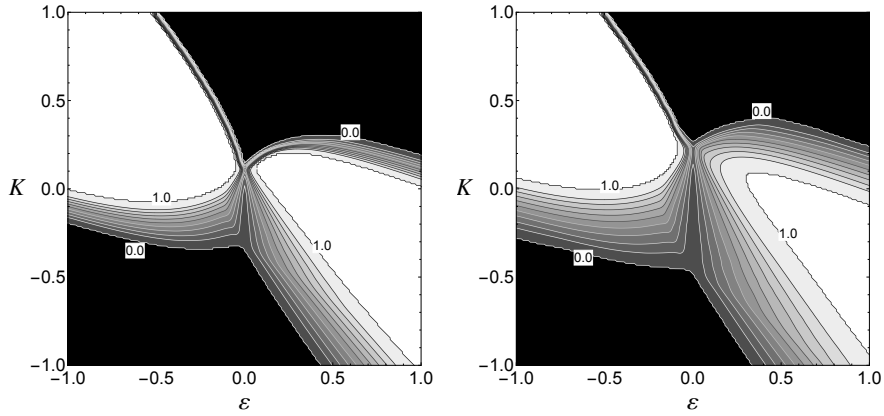

(a) Uniform, $\delta = 0.05$

(b) Uniform, $\delta = 0.1$

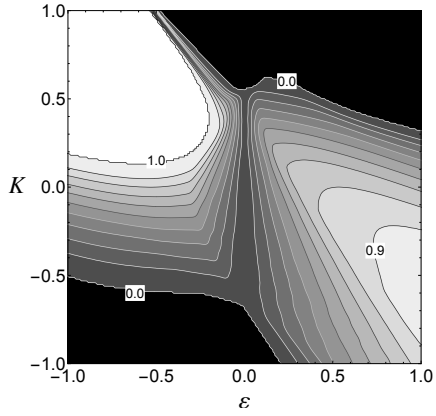

(c) Uniform, $\delta = 0.2$

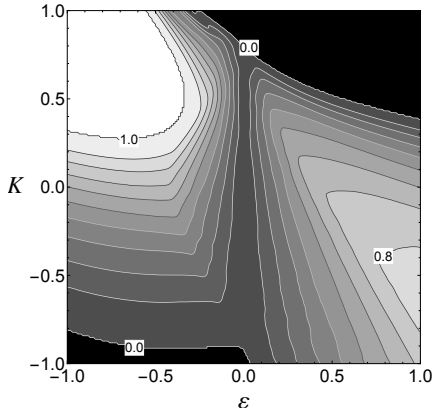

(d) Uniform, $\delta = 0.3$

Figure 2.4: Entrainment degree for uniform distribution (a-d) in the parameter space (ε, K) for fixed values of the scale parameters. Lighter gray levels represent larger entrainment degrees. Contours are equally spaced with step $\Delta d_e = 0.1$. In the computations $N = 1000$ oscillators were used; see the text for more details.

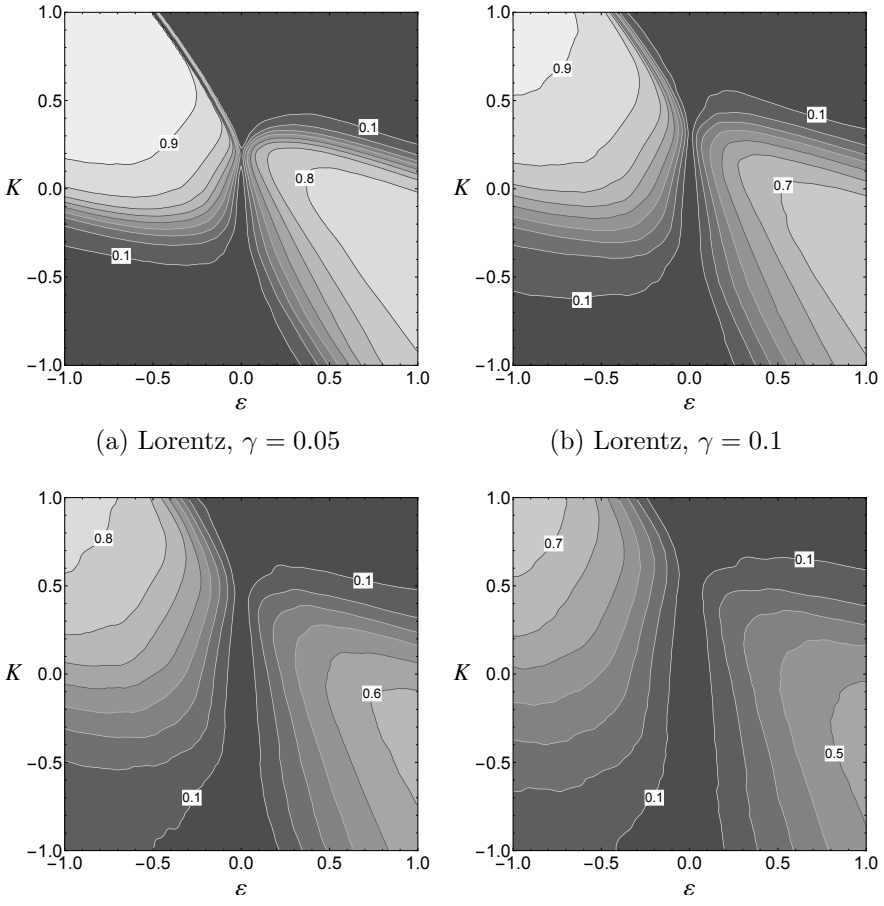

(a) Lorentz, $\gamma = 0.05$

(b) Lorentz, $\gamma = 0.1$

(c) Lorentz, $\gamma = 0.2$

(d) Lorentz, $\gamma = 0.3$

Figure 2.5: Entrainment degree for Lorentz distribution (a-d) in the parameter space (ε, K) for fixed values of the scale parameters. Lighter gray levels represent larger entrainment degrees. Contours are equally spaced with step $\Delta d_e = 0.1$. In the computations $N = 1000$ oscillators were used; see the text for more details.

not happen. Therefore, for the Lorentz distribution we can never have the two extremes: complete entrainment or no entrainment. For the most narrow distributions (uniform with $\delta = 0.05$ and Lorentz with $\gamma = 0.05$) we observe similarities with the entrainment degree that we numerically computed for the case of identical oscillators, see Fig. 2.3b.

2.4.2 Dynamical states

Ariaratnam and Strogatz [13] have considered the Winfree system, Eq. (2.4), with a uniform distribution of natural frequencies in the interval $[1-\delta, 1+\delta]$ and no forcing, i.e., $\varepsilon = 0$. They have identified 5 main different types of dynamics which they call incoherence, locking, death, partial locking, and partial death. The classification of the dynamics is done in terms of *state diagrams* depicting the functional dependence of the rotation numbers ρ_i on the natural frequency ω_i. In particular, incoherence corresponds to the rotation number being a strictly increasing function of the natural frequency, Fig. 2.6a; locking, to all oscillators having the same rotation number $\rho_i = \rho \neq 0$, Fig. 2.6b; death, to all oscillators having rotation number $\rho_i = 0$, Fig. 2.6c; partial locking, to a mixed locking / incoherence state, Fig. 2.6d; and partial death, to a mixed death / incoherence state, Fig. 2.6e.

Note that this sharp classification of different states can be done for distributions with compact support, such as the uniform distribution, but does not work equally well for distributions with non-compact support, such as the Lorentz distribution. In particular, distributions with compact support allow for the existence of *pure states* where all oscillators have the same rotation number. In the classification scheme above, locking and death are pure states, while partial death and partial locking will be called *mixed states*.

The introduction of the forcing enriches the dynamics, resulting in several new types. The main change introduced by the external forcing is the possibility of entrainment of the oscillators to the forcing and also the possibility of states that mix entrainment with locking, death, or incoherence. Note that, even though entrained oscillators have the same rotation number $\rho_i = 1$, we distinguish here entrainment from locking: an oscillator is entrained if $\rho_i = 1$ and it is locked if it

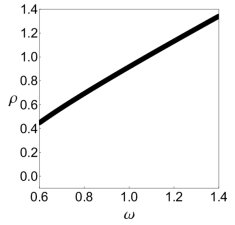

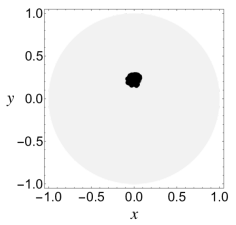

(a) Incoherence: $K = 0.4$, $\varepsilon = 0$, $\delta = 0.4$

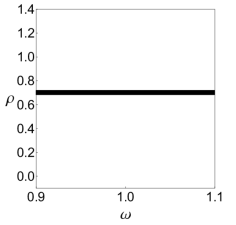

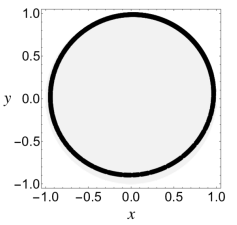

(b) Locking: $K = 0.6$, $\varepsilon = 0$, $\delta = 0.1$

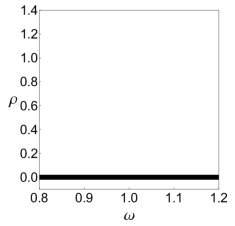

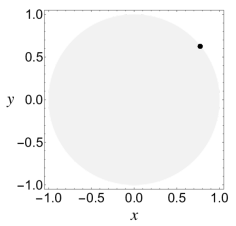

(c) Death: $K = 0.9$, $\varepsilon = 0$, $\delta = 0.2$

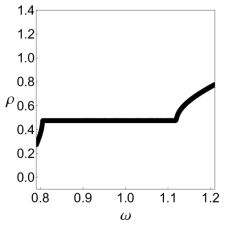

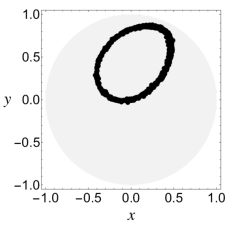

(d) Partial locking: $K = 0.75$, $\varepsilon = 0$, $\delta = 0.21$

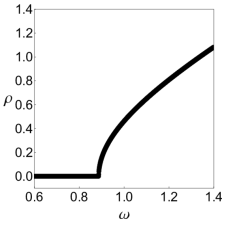

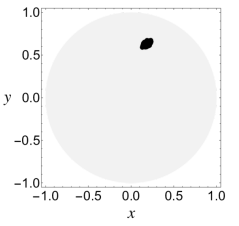

(e) Partial death: $K = 0.75$, $\varepsilon = 0$, $\delta = 0.4$

Figure 2.6: Each panel shows a state diagram for Winfree oscillators with uniform natural frequency distribution (left) and the corresponding evolution of the order parameter (right). States without external forcing ($\varepsilon = 0$), as defined in [13], and corresponding evolutions are shown in panels.

belongs in a group of oscillators that share a common rotation number, $\rho_i = \rho_{\text{group}} \neq 1$.

A few of the new dynamics states that appear for $\varepsilon \neq 0$ are shown in Fig. 2.7. In these examples we have integrated the system with $N = 1000$ oscillators for time $T = 2000$ with initial phases $\theta_i(0)$

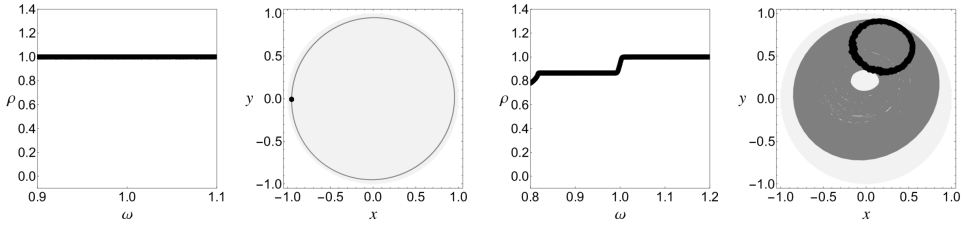

(a) Entrainment: $K = 0.2$, $\varepsilon = -0.2$, $\delta = 0.1$

(b) Mixed entrainment / locking: $K = 0.6$, $\varepsilon = -0.18$, $\delta = 0.2$

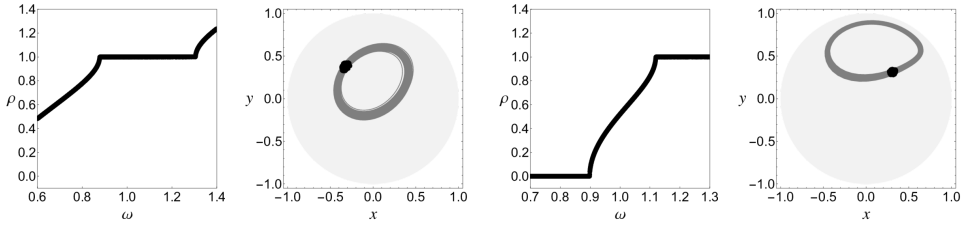

(c) Partial entrainment: $K = 0.6$, $\varepsilon = -0.2$, $\delta = 0.4$

(d) Mixed entrainment / death: $K = 0.4$, $\varepsilon = 0.5$, $\delta = 0.3$

Figure 2.7: Each panel shows a state diagram for Winfree oscillators with uniform natural frequency distribution (left) and the corresponding evolution of the order parameter (right). Panels (a-d) show states in the case of external forcing ($\varepsilon \neq 0$). In the evolution pictures dark gray curves represent the continuous time evolution $(x(t), y(t))$ of the order parameter while black points represent the stroboscopic image $(x(2k\pi), y(2k\pi))$, $k \in \mathbb{Z}$. The order parameter is constrained in the unit disk, represented here by light gray..

chosen uniformly in $[0, 2\pi]$ and natural frequencies ω_i chosen uniformly (equally spaced) in the interval $[1-\delta, 1+\delta]$. In the entrainment state in Fig. 2.7a all oscillators have been synchronized to the external forcing, that is, they all have $\rho_i = 1$. In our terminology, entrainment is also a pure state. Fig. 2.7b shows a mixed entrainment / locking state, while Fig. 2.7c shows partial entrainment—here entrainment coexists with incoherence. Finally, Fig. 2.7d depicts a mixed entrainment / death state. Note that the mixed entrainment / locking and entrainment / death states also contain intervals of incoherence. Because of the proliferation of new types of dynamics, and the fact that sometimes

the boundaries between them are not well-defined, we will refrain from giving a more formal definition of these new states.

In the case of a Lorentz distribution it is more difficult to provide a meaningful distinction between states since there are no pure states. The reason for the latter is that the distribution has a non-compact support and therefore oscillators at the "tails" of the distribution can have very different dynamical behavior to oscillators in the "bulk". We present examples of different states for a Lorentz distribution in Fig. 2.8 and in Fig. 2.9. In these examples we have integrated again the system with $N = 1000$ oscillators for time $T = 2000$ with initial phases $\theta_i(0)$ chosen uniformly in $[0, 2\pi]$. The natural frequencies ω_i are chosen from a Lorentz distribution $g(\omega)$ with mean 1 and scale parameter γ. Even in cases such as shown in Fig. 2.8a and 2.8b where most oscillators have been entrained or died there are still smaller populations outside the bulk that exhibit different behavior.

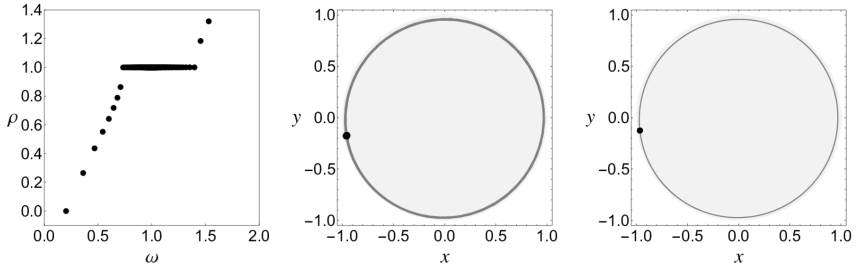

(a) Entrainment: $K = 0.2$, $\varepsilon = -0.5$, $\gamma = 0.01$; $d_e = 0.985$

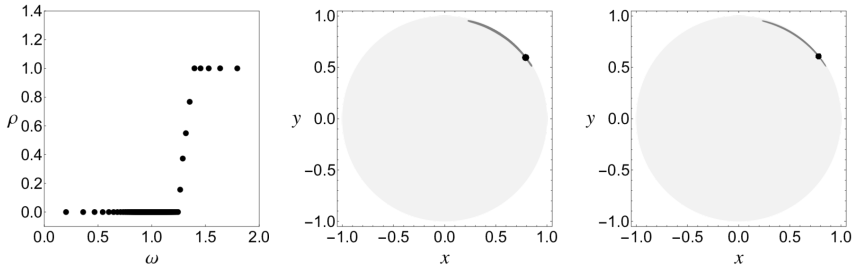

(b) Death: $K = 0.5$, $\varepsilon = 0.6$, $\gamma = 0.01$; $d_e = 0.006$

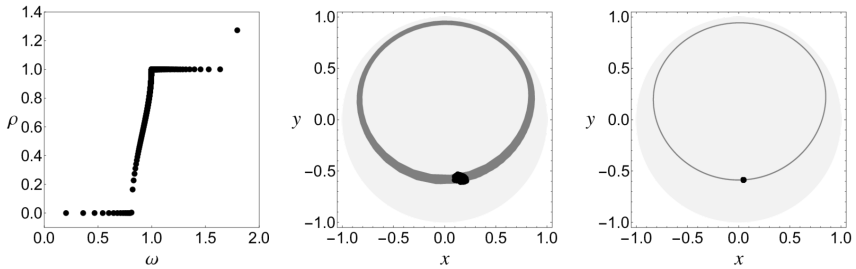

(c) Mixed entrainment / death: $K = 0.18$, $\varepsilon = 0.74$, $\gamma = 0.01$; $d_e = 0.558$

Figure 2.8: Dynamics for Winfree oscillators whose natural frequencies follow a Lorentz distribution with scale γ. Each panel depicts the dynamic state diagram (ρ_i vs ω_i), the corresponding evolution of the order parameter, and the evolution of the order parameter as obtained through the Ott-Antonsen ansatz, see Eq. (2.22). For each panel we also give the value of the corresponding entrainment degree d_e. In the order parameter plots dark gray curves represent the continuous time evolution $(x(t), y(t))$, while discrete points represent the stroboscopic image $(x(2k\pi), y(2k\pi))$. The order parameter is constrained in the unit disk, represented here by light gray.

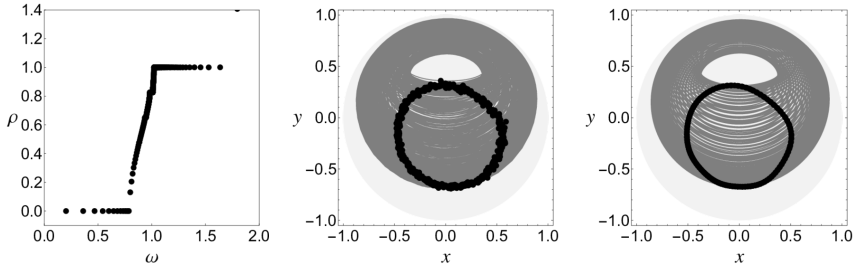

(a) Mixed entrainment / death: $K = 0.23$, $\varepsilon = 0.64$, $\gamma = 0.01$; $d_e = 0.129$

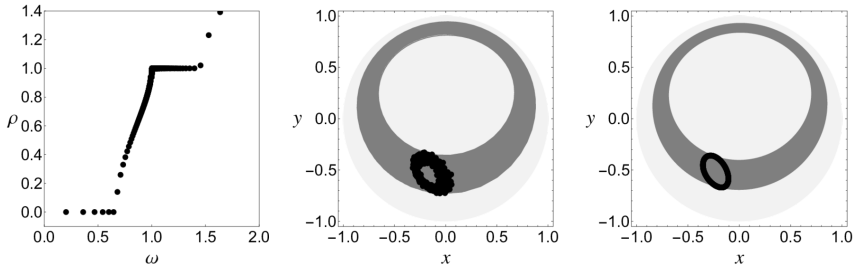

(b) Mixed entrainment / death: $K = 0.24$, $\varepsilon = 0.46$, $\gamma = 0.01$; $d_e = 0.398$

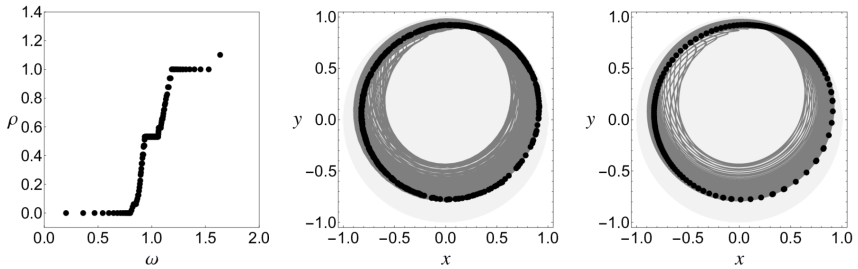

(c) Mixed entrainment / locking / death: $K = 0.39$, $\varepsilon = 0.51$, $\gamma = 0.01$; $d_e = 0.017$

Figure 2.9: Dynamics for Winfree oscillators whose natural frequencies follow a Lorentz distribution with scale γ. Each panel depicts the dynamic state diagram (ρ_i vs ω_i), the corresponding evolution of the order parameter, and the evolution of the order parameter as obtained through the Ott-Antonsen ansatz, see Eq. (2.22). For each panel we also give the value of the corresponding entrainment degree d_e. In the order parameter plots dark gray curves represent the continuous time evolution $(x(t), y(t))$, while discrete points represent the stroboscopic image $(x(2k\pi), y(2k\pi))$. The order parameter is constrained in the unit disk, represented here by light gray.

2.4.3 Order parameter evolution

The order parameter, Eq. (2.10), is often used to characterize the degree of synchronization in a network of coupled oscillators [100]. Even though there is no direct correspondence between the evolution of the order parameter and the entrainment degree we briefly discuss the situation in specific examples.

We first consider the case of a uniform distribution for which we have discussed different types of state diagrams in Sec. 2.4.2. For the state diagrams presented in Fig. 2.6 we consider the corresponding time evolution of the order parameter. We integrate the dynamics of the system starting with the same initial conditions as those used to produce the corresponding state diagrams in the previous section. The time evolution of the order parameter $z = x + \mathrm{i}y$ is shown in Fig. 2.7 for time from $T = 1000$ to $T = 2000$ as a continuous gray curve. Moreover, we present in the same picture the corresponding stroboscopic image of the evolution of the order parameter, where the value of the order parameter is only shown at times $2k\pi$, $k \in \mathbb{Z}$, resembling a Poincaré map.

The comparison of the state diagrams and the evolution of the order parameter in Fig. 2.6 reveals some interesting patterns. In the case of incoherence, Fig. 2.6a, the ensemble of motions with different rotation numbers destructively interfere to produce an almost constant order parameter. In the case of locking at a common rotation number ρ, Fig. 2.6b, the modulus of the order parameter is close to 1 and its phase rotates with angular velocity ρ. In the stroboscopic image we observe quasi-periodic motion depending on the (ir-)rationality of ρ. In the case of death, Fig. 2.6c, the modulus of the order parameter is again close to 1 but its phase is almost constant. In the case of partial locking, Fig. 2.6d, the order parameter almost fills out a disk which is a result of the combination of destructive interference of the incoherent part and the rotation induced by the locked part. Partial death, Fig. 2.6e, strongly resembles incoherence but the modulus of the order parameter is closer to 1. There does not seem to be a sharp criterion in terms of the evolution of the order parameter that would allow us to distinguish between the two cases. In entrainment, Fig. 2.7c, the order parameter evolves in a very similar way to locking

but there is only one point in the stroboscopic image, as a result of the fact that $\rho = 1$ for all oscillators. In the last three panels, Fig. 2.7(b-d) we observe that the order parameter fills out an annulus. We note that in the first two of the three panels the annulus has winding number 1 while in the last one it has winding number 0.

In the case of the Lorentz distribution the corresponding evolution of the order parameter is shown in Fig. 2.8 and in Fig. 2.9 (middle picture in each of the panels). In panel Fig. 2.8a the evolution for a state where almost all oscillators are entrained ($d_e = 0.985$) is shown. We observe that the stroboscopic image of the orbit consists of a single point while the continuous-time orbit (dark gray curve) winds around the origin and it lies very close to the unit circle. In panel Fig. 2.8b the evolution for a state where almost all oscillators are dead ($d_e = 0.006$) is shown. The stroboscopic image consists again of a single point, however, we observe that the continuous-time orbit makes very small oscillations along an arc close to the unit circle and it does not wind around the origin.

In panels Fig. 2.8(a) and Fig. 2.9(a-c) we depict four evolutions of the order parameter that all correspond to mixed entrainment / death or mixed entrainment / locking /death states but have different entrainment degrees ranging from very small ($d_e = 0.017$) to significant ($d_e = 0.558$). The evolution depicted in Fig. 2.8c is similar to the one in the case of entrainment in Fig. 2.8a; the difference is that the continuous-time orbit is not very close to the unit circle.

From the discussion for the evolution of the order parameter for uniform and for Lorentz distribution of natural frequencies we conclude that there are some evolutions that can be easily recognized as (almost complete) entrainment or (almost complete) death. These correspond to Fig. 2.7a and Fig. 2.6c for the uniform distribution, and Fig. 2.8a and Fig. 2.8b for the Lorentz distribution. However, there are many other intermediate cases where it is not straightforward to read the entrainment degree from the evolution of the order parameter—we will return to this issue in Sec. 2.5.3.

2.5 Low-dimensional Dynamics

In this part, we analyze the system with a Lorentz distribution of natural frequencies using the Ott-Antonsen method [128]. After deriving the Ott-Antonsen equations for the system, we compare the results of the Poincaré map with the numerical results for the full system, observing striking similarities. Moreover, we perform a bifurcation analysis of the limit cycles and fixed points of the Poincaré map on the (ε, K) space for different values of the scale parameter γ.

2.5.1 Derivation of the Ott-Antonsen equations

We consider the continuum limit where the ensemble of discrete oscillators is replaced by a continuous distribution $\rho(\theta, t, \omega)$ expressing the probability density that an oscillator of natural frequency ω has phase θ at time t. The density ρ satisfies the normalization condition

$$\int_0^{2\pi} \rho(\theta, t, \omega)\, d\theta = 1,$$

and the continuity equation

$$\frac{\partial \rho}{\partial t} + \frac{\partial}{\partial \theta}(\rho v) = 0, \tag{2.11}$$

representing the conservation of the number of oscillators. In the continuity equation, v is the velocity of each oscillator, and it is given by

$$v = \dot{\theta} = \omega - K \sin\theta \langle 1 + \cos\theta \rangle - \varepsilon \sin\theta (1 + \cos t), \tag{2.12}$$

where we denote by

$$\langle f(\theta) \rangle = \int_0^{2\pi} \int_{-\infty}^{\infty} f(\theta) \rho(\theta, t, \omega) g(\omega)\, \mathrm{d}\theta\, \mathrm{d}\omega, \tag{2.13}$$

the average value of $f(\theta)$. The order parameter, defined in the discrete case by Eq. (2.10), is given in the continuum limit by

$$z(t) = \langle e^{\mathrm{i}\theta} \rangle = \int_0^{2\pi} \int_{-\infty}^{\infty} e^{\mathrm{i}\theta} \rho(\theta, t, \omega) g(\omega)\, \mathrm{d}\theta\, \mathrm{d}\omega, \tag{2.14}$$

thus

$$\langle 1 + \cos\theta \rangle = 1 + \mathrm{Re}(z(t)). \tag{2.15}$$

The distribution $\rho(\theta, t, \omega)$ is 2π-periodic in θ. We assume that ρ has a Fourier series expansion, given by

$$\rho(\theta, t, \omega) = \frac{1}{2\pi} \sum_{n=-\infty}^{\infty} c_n(t, \omega) e^{\mathrm{i}n\theta}, \tag{2.16}$$

where $c_{-n} = \overline{c_n}$ and $c_0 = 1$. Substituting Eq. (2.12) and Eq. (2.16) into the continuity equation, Eq. (2.11), and using Eq. (2.15), we obtain the evolution equation for the Fourier coefficients

$$\frac{\partial c_n}{\partial t} + \mathrm{i}n\omega c_n + \frac{n}{2}\big(K(1 + \mathrm{Re}(z(t))) + \varepsilon(1 + \cos t)\big)(c_{n+1} - c_{n-1}) = 0. \tag{2.17}$$

Following the Ott-Antonsen ansatz, we consider distributions with $c_n(t, \omega) = \alpha(t, \omega)^n$, for $n \geq 1$. Consequently, $c_n = \overline{c}_{|n|} = \overline{\alpha}^{|n|}$ for $n \leq -1$. Substituting the expression for c_n into Eq. (2.17) we find

$$\frac{\mathrm{d}\alpha}{\mathrm{d}t} + \mathrm{i}\,\omega\alpha + \frac{1}{2}\big(K(1 + \mathrm{Re}(z(t))) + \varepsilon(1 + \cos t)\big)(\alpha^2 - 1) = 0. \tag{2.18}$$

Using the Fourier series representation of ρ and the Ott-Antonsen ansatz we find that

$$z(t) = \int_{-\infty}^{\infty} c_{-1}(t, \omega) g(\omega)\, \mathrm{d}\omega = \int_{-\infty}^{\infty} \overline{\alpha(t, \omega)} g(\omega)\, \mathrm{d}\omega. \tag{2.19}$$

Considering the case where $g(\omega)$ is the Lorentz distribution, Eq. (2.5), we obtain by calculating the residue at the pole $\Omega - \mathrm{i}\gamma$ of $g(\omega)$ at the lower complex half-plane that

$$z(t) = \overline{\alpha(t, \Omega - \mathrm{i}\gamma)}. \tag{2.20}$$

Finally, considering the complex conjugate of Eq. (2.18) for $\omega = \Omega - \mathrm{i}\gamma$ we find that the evolution of the order parameter is given by

$$\frac{\mathrm{d}z}{\mathrm{d}t} + (\gamma - \mathrm{i}\,\Omega)z + \frac{1}{2}\big(K(1 + \mathrm{Re}(z)) + \varepsilon(1 + \cos t)\big)(z^2 - 1) = 0. \tag{2.21}$$

Writing $z = x + \mathrm{i}y$ and separating the real and imaginary parts of Eq. (2.21), we obtain the equations

$$\frac{\mathrm{d}x}{\mathrm{d}t} = -\gamma x - \Omega y + \frac{1}{2}(1 - x^2 + y^2)\big[K(1+x) + \varepsilon(1+\cos t)\big], \quad (2.22a)$$

$$\frac{\mathrm{d}y}{\mathrm{d}t} = \Omega x - \gamma y - xy\,\big[K(1+x) + \varepsilon(1+\cos t)\big]. \quad (2.22b)$$

Remark 2.5.1. The Lorentz distribution is an example for which we can explicitly compute the integral in Eq. (2.19). This computation is not always feasible for other distributions and, in particular, it is not feasible for the uniform distribution. For this reason we restrict the discussion in this section to the Lorentz distribution.

Remark 2.5.2. The relative simplicity of the equation for z depends on the simplicity of the response and influence functions, R and P respectively, in Eq. (2.3). In the case where the influence function P is a trigonometric polynomial in θ of the form $P(\theta) = Q(\cos\theta, \sin\theta)$, the Ott-Antonsen ansatz gives equations similar to Eq. (2.22) with the term $(1+x)$ replaced by $Q(x, y)$. However, when R contains harmonics of degree $n \geq 2$ the Ott-Antonsen ansatz does not produce a consistent set of equations on $\mathbb{R}^2$ even though it is possible to consider generalizations of the Ott-Antonsen ansatz that give rise to higher dimensional dynamical systems.

Eq. (2.22) defines a two-dimensional non-autonomous dynamical system on $\mathbb{R}^2$. For $\varepsilon = 0$ the Ott-Antonsen equations agree with those obtained in [134] for the system without forcing. Note that the equations make sense only on the (closed) unit disk $D = \{x^2+y^2 \leq 1\}$, bounded by the unit circle $S = \{x^2 + y^2 = 1\} = \partial D$. We check that

$$\frac{\mathrm{d}}{\mathrm{d}t}(x^2 + y^2)\Big|_S = -2\gamma < 0.$$

This implies that D remains invariant under the flow defined by Eq. (2.22) and thus the 2π-flow of Eq. (2.22) defines a Poincaré map $P : D \to D$.

We have compared the dynamics given by the low-dimensional Ott-Antonsen description, Eq. (2.22), to the corresponding full network dynamics, see Sec. 2.4.3. Fig. 2.8 and Fig. 2.9 shows the evolution of

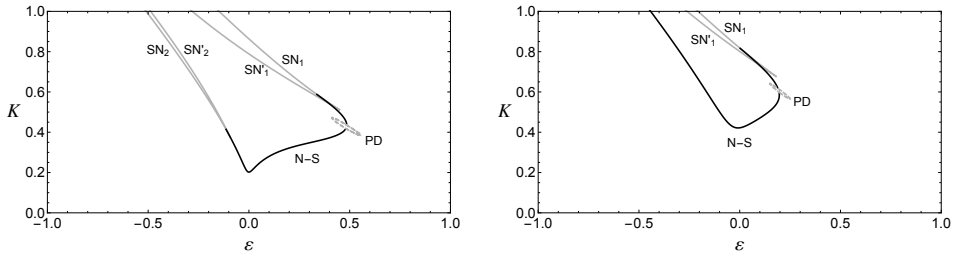

(a) $\gamma = 0.05$ (b) $\gamma = 0.1$

Figure 2.10: Bifurcation diagrams. Solid black curves represent Neimark-Sacker (N-S) bifurcations, solid gray curves represent fold (saddle-node, SN) bifurcations, and dashed gray curves represent flip (period doubling, PD) bifurcations. Saddle-node bifurcations marked by a prime (SN$'$) correspond to the collision of a saddle point with a stable node; unmarked ones (SN) correspond to the collision of a saddle point with an unstable node.

the order parameter $(x(t), y(t))$ for different values of the parameters, and the corresponding iterates of the Poincaré map g, given by points $(x(2k\pi), y(2k\pi))$ with integer k. We have found that the evolution of the order parameter in the numerical simulations (Fig. 2.9) and the one predicted by the Ott-Antonsen ansatz (Fig. 2.8 and Fig. 2.9) are qualitatively similar, thus validating the use of the Ott-Antonsen ansatz.

2.5.2 Bifurcations in the Ott-Antonsen equations

Brouwer's fixed point theorem ensures that the Poincaré map $P : D \to D$ defined by the 2π-flow of Eq. (2.22) has at least one fixed point. As the parameters (K, ε, γ) of the system change, the fixed points of P can change stability and go through bifurcations. For fixed γ, we expect to find in the (ε, K) parameter plane curves of codimension-1 bifurcations such as fold (saddle-node), flip (period-doubling), and Neimark-Sacker bifurcations [105].

We have used MatCont [50] to compute the bifurcation curves for Poincaré map P induced by the Ott-Antonsen equations in the

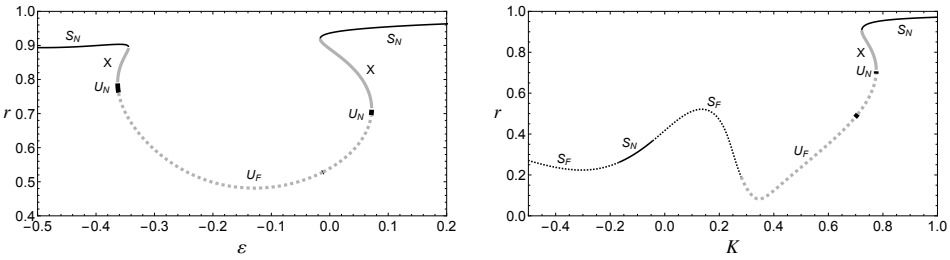

(a) Scenario 1 ($K = 0.8$) (b) Scenario 2 ($\varepsilon = 0.1$)

Figure 2.11: Bifurcation scenarios for $\gamma = 0.05$. The vertical axis depicts the distance r of the fixed point(s) from the origin. The legends are S_F (stable focus), S_N (stable node), U_F (unstable focus), U_N (unstable node), X (saddle point).

parameter range $-1 \leq \varepsilon \leq 1$, $-1 \leq K \leq 1$. The bifurcations for $\gamma = 0.05$ and $\gamma = 0.1$ are shown in Fig. 2.10—we have not found any bifurcations in this parameter range for $\gamma = 0.2$ and $\gamma = 0.3$.

For $\gamma = 0.05$ there are four 1-parameter families of saddle-node bifurcations, represented by solid gray curves and denoted SN in Fig. 2.10(a). The pairs SN_1, SN_1' and SN_2, SN_2' each meet at a cusp bifurcation. Moreover, the families SN_1 and SN_2 each meet the 1-parameter of Neimark-Sacker (N-S) bifurcations, represented by a black curve, at an 1:1 resonance. A family of flip bifurcations (PD), represented by a dashed gray loop, has been also found along the Neimark-Sacker curve. The main difference when $\gamma = 0.1$ is that two of the families of saddle-node bifurcations (SN_2 and SN_2') are no longer present.

The main common feature of these two cases is that there is a parameter region enclosed by the Neimark-Sacker and parts of the saddle-node bifurcations where the system does not have any stable fixed points. We describe this in detail by considering two bifurcation scenarios for $\gamma = 0.05$—similar bifurcation scenarios also occur for $\gamma = 0.1$.

Scenario 1. We fix $K = 0.8$ and increase ε, see Fig. 2.11a. For $\varepsilon \lessapprox -0.363$ the map has a stable node fixed point. At $\varepsilon \approxeq -0.363$,

the map P goes through a saddle-node bifurcation SN_2, where a saddle point and an unstable node are created. The unstable node almost immediately turns into an unstable focus. At slightly larger $\varepsilon \approxeq -0.345$, the map goes through a second saddle-node bifurcation SN_2' where the saddle point and the stable node collide and disappear while a stable closed invariant curve appears and the only remaining fixed point is the unstable focus. This scenario repeats in reverse between $\varepsilon \approxeq -0.016$ and $\varepsilon \approxeq 0.071$. First, a saddle-node bifurcation SN_1' on the invariant curve at $\varepsilon \approxeq -0.016$ gives rise to a saddle point and a stable node. Then, just before the final saddle-node SN_1, the unstable focus becomes an unstable node, and then it collides with the saddle point when $\varepsilon \approxeq 0.071$ for the saddle-node SN_1. This last bifurcation leaves the stable node as the only fixed point of the Poincaré map for $\varepsilon \gtrapprox 0.071$. Note, in particular, that for $-0.345 \lessapprox \varepsilon \lessapprox -0.016$ the Poincaré map has no stable fixed points and that the only stable invariant set is an invariant curve.

Scenario 2. We fix $\varepsilon = 0.1$ and increase K, see Fig. 2.11b. For $K \lessapprox 0.280$ the map has a stable fixed point which changes stability between stable node and stable focus. For $K \gtrapprox -0.045$, in particular, the fixed point is a stable focus and at $K \approxeq 0.280$ it goes through a Neimark-Sacker (N-S) bifurcation, whereas it becomes an unstable focus and simultaneously a normally stable invariant curve emanates from it. As K increases, a saddle-node bifurcation SN_1' takes place on the invariant curve at $K \approxeq 0.722$ and produces a saddle point and a stable node. The unstable focus becomes an unstable node and then at $K \approxeq 0.775$ it collides with the saddle point in the saddle-node bifurcation SN_1. For $K \gtrapprox 0.775$ the Poincaré map has only a stable fixed point. Again, note that for $0.280 \lessapprox K \lessapprox 0.722$ the system has no stable fixed points and that the only stable invariant set is the invariant curve generated at the Neimark-Sacker bifurcation.

The bifurcation diagrams give a comprehensive picture of the parameter regions where the Poincaré map has a stable fixed point. This plays an important role in Sec. 2.5.3, where we use the existence of fixed points of the Poincaré map (i.e., 2π-periodic orbits of the full system) to give an estimate of the entrainment degree.

2.5.3 Entrainment degree from the Ott-Antonsen mean field

The Ott-Antonsen equations provide low-dimensional dynamics for the evolution of the order parameter of the system. However, the order parameter gives only a macroscopic description of the dynamics and, in particular, it does not directly provide information on the entrainment degree. To recover the entrainment degree from the Ott-Antonsen order parameter we may work as follows. We first compute the evolution $z_{\mathrm{OA}}(t)$ of the order parameter using the Ott-Antonsen equations for specific values of the parameters (ε, K, γ) and starting at a random initial value. We call the obtained order parameter evolution $z_{\mathrm{OA}}(t)$ the *Ott-Antonsen mean field*. Then we consider the dynamics of an oscillator of natural frequency ω in the Ott-Antonsen mean field. The dynamics of such oscillator is given by

$$\dot{\theta} = \omega - F(t)\sin\theta, \tag{2.23a}$$

where

$$F(t) = K(1 + \mathrm{Re}(z_{\mathrm{OA}}(t))) + \varepsilon(1 + \cos t). \tag{2.23b}$$

To compute the entrainment degree for an ensemble of oscillators in the Ott-Antonsen mean field we follow two different approaches, the *direct method* and the *resonance tongue method* which we describe and compare below.

2.5.3.1 Direct method

We consider a finite ensemble of N oscillators with natural frequencies ω_i, $i = 1, \ldots, N$, following a Lorentz distribution $g(\omega)$ with mean value 1 and scale parameter γ, that is, the same Lorentz distribution that gives rise to the Ott-Antonsen mean field $z_{\mathrm{OA}}(t)$. Then the entrainment degree d_e can be computed as the percentage of oscillators that have rotation number 1.

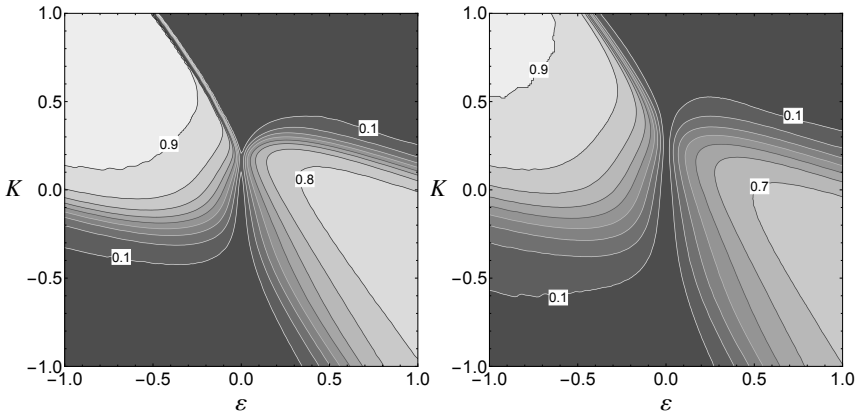

(a) $\gamma = 0.05$ (b) $\gamma = 0.1$

(c) $\gamma = 0.2$ (d) $\gamma = 0.3$

Figure 2.12: Entrainment degree as predicted by directly computing the rotation numbers of an ensemble of oscillators following the Ott-Antonsen mean field dynamics, see Sec. 2.5.3. The entrainment criterion was chosen as $|\rho - 1| < 10^{-3}$. Entrainment degree contours are equally spaced with $\Delta d_e = 0.1$ and lighter grays correspond to higher d_e. The value of d_e on some contours has been indicated in the pictures.

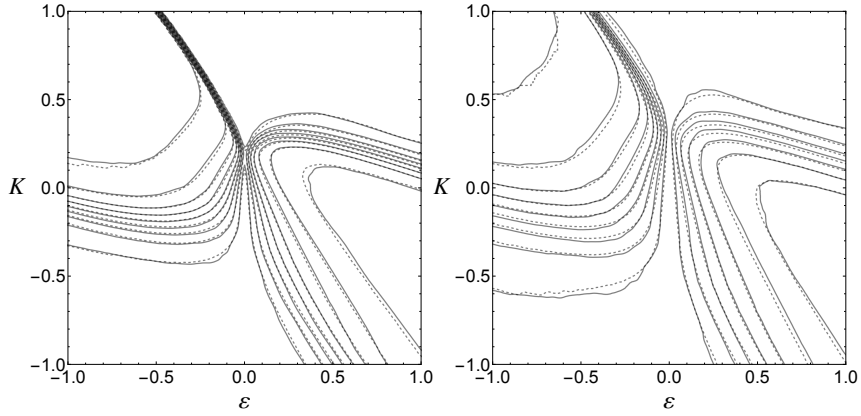

(a) $\gamma = 0.05$ (b) $\gamma = 0.1$

(c) $\gamma = 0.2$ (d) $\gamma = 0.3$

Figure 2.13: Comparison of contours in the top row (dashed lines) to those shown in Fig. 2.5 (solid lines) computed by direct integration of the full dynamics.

Practically, we compute the order parameter $z_{\mathrm{OA}}(t)$ for time $0 \leq t \leq 10^3 \cdot (2\pi)$ using a Runge-Kutta fourth order method with fixed step size $dt = 10^{-2} \cdot (2\pi)$ and we simultaneously integrate the dynamics of $N = 200$ oscillators, given by Eq. (2.23), that is interacting only with the Ott-Antonsen mean-field, using the Euler method. An oscillator with natural frequency ω_i is considered to be entrained if its rotation number ρ_i satisfies $|\rho_i - 1| < 10^{-3}$.

The results of this computation are shown in Fig. 2.12 on the (ε, K) parameter plane for different values of the scale parameter γ. The results are strikingly similar to the results in Fig. 2.5 that have been computed from the full dynamics without any theoretical approximations. This is clearly shown in Fig. 2.13 where the contours for the two methods (direct method and full dynamics) are drawn together. These results further validate the use of the Ott-Antonsen approximation to study the entrainment in this system.

2.5.3.2 Resonance tongue method

When the Ott-Antonsen Poincaré map has a stable fixed point we can estimate the entrainment degree using the theory of circle maps. In this case, the Ott-Antonsen order parameter $z_{\mathrm{OA}}(t)$, and thus also $F(t)$, are periodic with period 2π. Therefore, the dynamics, given by Eq. (2.23) for an oscillator with natural frequency ω, gives rise to a circle map whose 1:1 resonance tongue has boundaries $\omega_-(F) < \omega_+(F)$. The oscillator is entrained if $\omega \in (\omega_-(F), \omega_+(F))$ and thus the entrainment degree is given by

$$d_e = \int_{\omega_-(F)}^{\omega_+(F)} g(\omega)\, d\omega,$$

where $g(\omega)$ is a Lorentz distribution with mean value 1 and scale parameter γ, cf. the discussion in Sec. 2.2.

The results from this method are shown in Fig. 2.14 on the (ε, K) parameter plane for different values of the scale parameter γ. The black regions shown for $\gamma = 0.05$ and $\gamma = 0.1$ correspond to parameter values for which the Ott-Antonsen Poincaré map has no stable fixed points and should be compared with the corresponding bifurcation diagrams shown in Fig. 2.10. Outside these regions the obtained values for the entrainment degree are nearly identical to those obtained with the direct method. This is depicted in Fig. 2.15 where the contours for the direct and the resonance tongue method are drawn together.

2.6 Discussion and Conclusions

We have considered a system of periodically forced coupled Winfree oscillators and we have studied in detail its dynamics focusing on the question of the synchronization (entrainment) of individual oscillators to the external forcing. Through numerical simulations we have shown that the degree of entrainment decreases when the width of the natural frequency distribution increases while, in general, it increases with the strength ε of the external forcing.

First, we have considered oscillators that are influenced by the external forcing but they are not coupled to each other. We have computed the 1:1 resonance tongue and we have used it to obtain the entrainment degree for non-interacting oscillators.

We have then considered the case of identical oscillators. Here we have given a theoretical explanation of the numerically obtained results on the entrainment degree through a careful study of synchronized states and their stability.

At the next step, we have considered non-identical oscillators whose natural frequencies follow a uniform or a Lorentz distribution. For such oscillators we have numerically computed the entrainment degree, and we have presented typical state diagrams (rotation number as a function of natural frequency) and the corresponding evolution of the order parameter. Moreover, we have established a rough correspondence between the evolution of the order parameter and the entrainment degree of the system.

In the last part, we focused on systems where the oscillators follow a Lorentz distribution and we have derived the low-dimensional dynamics given by the Ott-Antonsen ansatz. The evolution of the order parameter given by the Ott-Antonsen equations compares well to the evolution computed for the full dynamics. Then we have given a description of bifurcations of fixed points in the Ott-Antonsen equations. Finally, we have used the dynamics of oscillators in the Ott-Antonsen mean field to obtain an approximation for the entrainment degree. The results match very well the results that we had earlier obtained, while they can be much more efficiently computed.

One restriction of the current study is that it has focused to the case of unimodal natural frequency distributions whose mean value Ω

equals the forcing frequency, i.e., $\Omega = 1$. A natural question to ask is what will be the effect of "detuning" the system, that is, having $\Omega \neq 1$. We expect that in this case entrainment will be weaker and increasing the detuning will lead to fewer entrained oscillators. A closely related question is to understand what will happen in the case of bimodal distributions, symmetric with respect to $\Omega = 1$. These questions will be considered in the coming chapters.

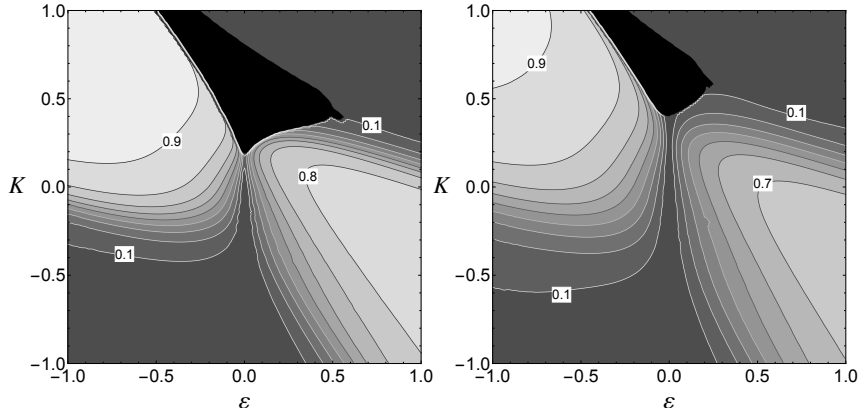

(a) $\gamma = 0.05$ (b) $\gamma = 0.1$

(c) $\gamma = 0.2$ (d) $\gamma = 0.3$

Figure 2.14: (a-d) Entrainment degree as predicted by computing the width of the resonance tongues of the Ott-Antonsen mean field dynamics for the case that the Ott-Antonsen Poincaré map has a fixed point, see Sec. 2.5.3. The black regions for $\gamma = 0.05$ and $\gamma = 0.1$ correspond to parameter values for which there is no stable fixed point. Entrainment degree contours are equally spaced with $\Delta d_e = 0.1$ and lighter grays correspond to higher d_e. The value of d_e on some contours has been indicated in the pictures.

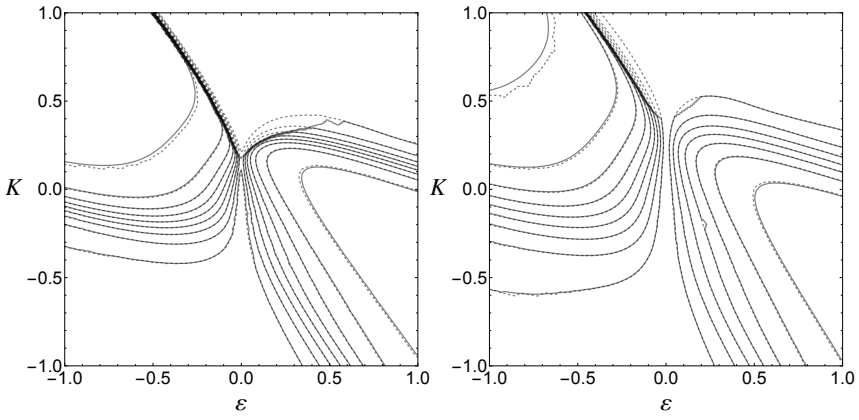

(a) $\gamma = 0.05$

(b) $\gamma = 0.1$

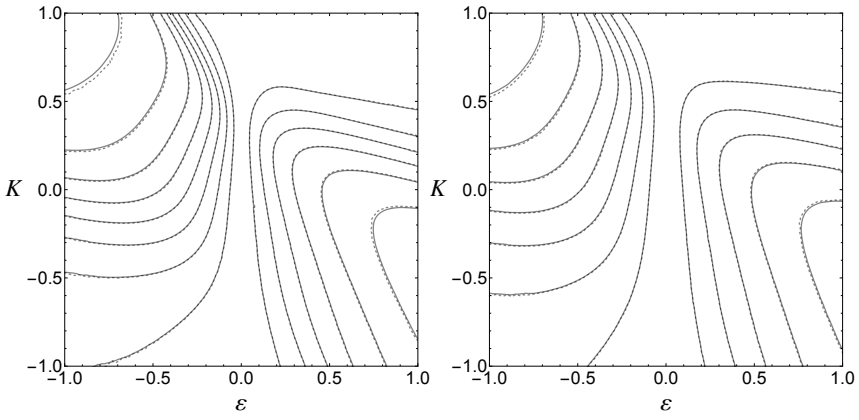

(c) $\gamma = 0.2$

(d) $\gamma = 0.3$

Figure 2.15: Comparison of contours in the top row (solid lines) to those shown in Fig. 2.12 (dashed lines) computed by finding directly how many oscillators entrain in the Ott-Antonsen mean field.

Chapter 3

Entrainment of Detuned Forced Winfree System

In Chapter 2 we have considered the case that the external forcing has the same frequency with the mean natural frequency of the oscillators. In this chapter, we investigate the entrainment when the forcing frequency differs from the mean natural frequency.

3.1 Introduction

When we talk about entrainment, we mean that the coupled oscillators are synchronized with the periodic forcing. Generally, there are several parameters, such as coupling strength, forcing strength, and the properties of the natural frequency distribution which influence the dynamics and determine how easily a group of oscillators can be entrained to the external forcing. We assumed that the oscillators' mean natural frequency equals the forcing frequency in Chapter 2. However, in this situations the oscillators' mean natural frequency differs from the forcing frequency. Detuned systems, that is, systems with nonzero frequency difference, is a topic of widespread multidisciplinary interest describing many physical, mechanical, biological and other systems [38, 42, 52, 154].

Frequency detuning is a number that quantifies how different the mean natural frequency of the oscillators is from the external forcing

frequency. A large frequency detuning can lead to a different pattern formation in oscillatory systems [81,97,203]. Some studies have shown that circadian rhythm are determined by circadian genes. Thus it makes sense to study frequency detuned system as the intrinsic periods of the genes are different from that of the dark-light cycle [98, 108, 123]. In this chapter we discuss the case where the mean frequency of the coupled oscillators is different from the frequency of the periodic external forcing.

We are considering the detuned system in Winfree system with forcing as in Eq. (2.3) which means the frequency of the periodic driving and the mean frequency of the oscillators are different. By rescaling we can either fix the frequency of the driving to 1 or fix the mean frequency to 1. In order to make the discussion easy, we choose to fix the driving frequency to 1 as we discussed for the non-detuned case. It is natural to ask how frequency detuning influences the entrainment of the Winfree system with periodic forcing. In this chapter, we investigate the effects of the detuned frequency on the entrainment degree.

3.2 Identical Oscillators

We have considered a single periodically forced oscillator and the identical oscillators where all of the oscillators have the same frequency in non-detuned case in Sec. 2.3. In this section, we have a comparable consideration for identical oscillators but in detuned systems where the forcing frequency is different from the mean natural frequency. In this section, we consider identical oscillators, thus we regard all oscillators have the same natural frequency that equals to Ω. Note that in this case, Ω is ω.

We first numerically compute entrainment degree, normal stability and resonance tongue for identical oscillators. Then we obtain the approximation of Poincaré map by a vector field from normalizing the vector field of the identically periodically forced oscillators. We find that the resonance tongues from the two methods coincide.

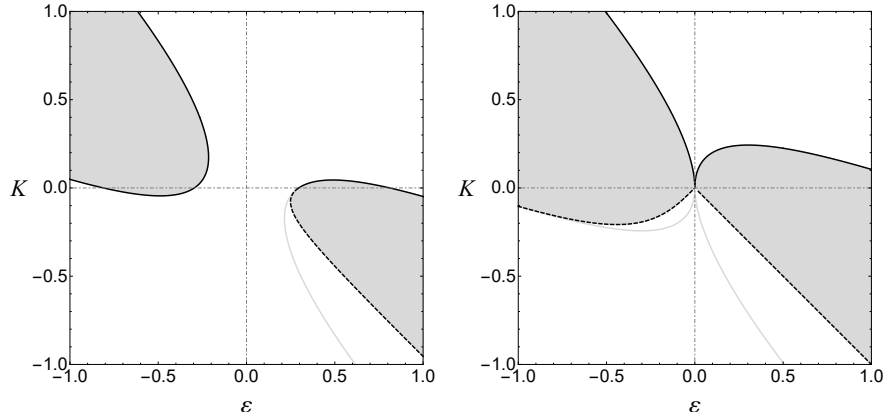

(a) $\Omega = 0.9$ (b) $\Omega = 1.0$

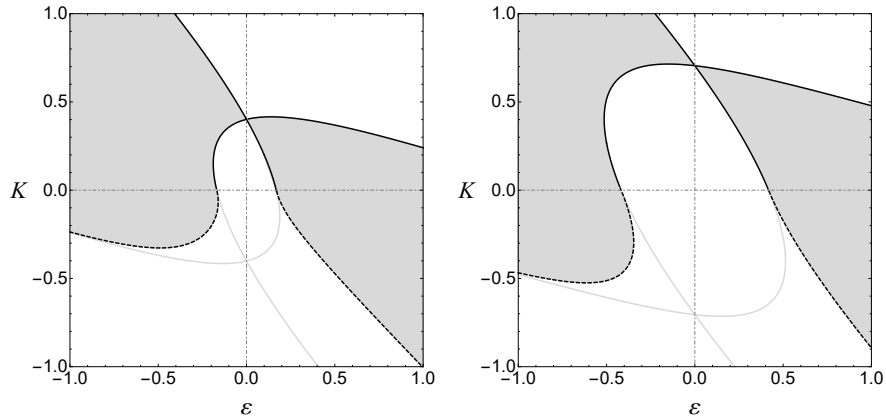

(c) $\Omega = 1.1$ (d) $\Omega = 1.3$

Figure 3.1: Computation for entrainment degree, resonance tongue and normal stability for Eq. (3.1). All oscillators are entrained to the forcing (light grey), or no oscillators are entrained (in white). Resonance Tongue (black line for $K > 0$, light grey line for $K < 0$) is computed by Matcont. Normal stability for $K < 0$ is shown in black dashed line. Boundaries of the 1:1 resonance tongue on the (ε, K)-plane for the synchronized dynamics are in black line and light grey line. The upper boundary of the tongue is exactly coincidental with the upper boundaries of the entrainment. The lower boundaries are governed by the normal stability of the periodic orbits on the synchronized manifold defined in Section 2.3.

3.2.1 Numerical results for identical oscillators

We assume that all oscillators have the same natural frequency Ω and we consider three cases with $\Omega = 0.9, \Omega = 1.1, \Omega = 1.3$. Recall that the driving frequency equals 1. We are motivated by the change of resonance tongues compared to that of the non-detuned case in Chapter 2.

Considering the dynamics on the synchronized manifold $\Sigma = \{\theta \in (\mathbb{S}^1)^n : \theta_1 = \cdots = \theta_N =: \theta_s\}$ as we defined for the non-detuned case in Section 2.3. Thus the dynamics is given by the non-autonomous first-order differential equation as following:

$$\dot{\theta}_s = \Omega - \sin\theta_s \left[K(1+\cos\theta_s) + \varepsilon(1+\cos t)\right]. \tag{3.1}$$

Here Ω varies and it is different from the frequency of the external forcing in the equation.

Fig. 3.1 shows the entrainment degree, normal stability and 1:1 resonance tongues for the system in Eq. (3.1) for different values of Ω. This is a result of the (numerically verified) fact that for all values of ε and K all oscillators attain exactly the same rotation number in grey area. It is called entrainment window, and it means oscillators and external driving has reached the same rotation number, a complete synchronization state. The entrainment degree (in light grey area) in Fig. 3.1 are computed for $N = 1000$ identical oscillators with $\Omega = 0.9, \Omega = 1.0, \Omega = 1.1$, and $\Omega = 1.3$ respectively. Their initial phases $\theta_i(0)$ are randomly chosen uniformly in $[0, 2\pi)$. Simulations were performed with the fourth-order Runge-Kutta method with time step 0.1 for time $T = 20000$. An oscillator is considered to be entrained if its rotation number ρ_i satisfies $|\rho_i - 1| < 10^{-3}$. Complete entrainment of the system means oscillators' rotation number $|\rho_i - 1| < 10^{-3}$ and its order parameter $z > 0.99$. The upper boundary of the entrainment is governed by resonance tongue which is shown by black line in Fig. 3.1. The lower boundary of the entrainment is restrained by normal stability of the system shown in black dashed line in Fig. 3.1.

3.2.2 Approximation method for identical oscillators

Here we describe an analytical approximation [86] to the resonance tongues computed numerically in Sec. 3.2.1. Recall that for numerical computations, we choose $R(\theta) = -\sin\theta, P(\theta) = 1 + \cos\theta$. It turns out that with this choice the system is in a sense degenerate which will be explained later. In this respect a better choice here is $R(\theta) = c_1\cos\theta + s_1\sin\theta, P(\theta) = 1+\cos\theta$, for $c_1 = \cos\phi$, and $s_1 = \sin\phi$ where $\phi \in [0, 2\pi]$ satisfying non-degeneracy conditions that $c_1 \neq 0$.

We consider a system of N identical oscillators. In particular we look at the dynamics on the synchronized invariant manifold with $\theta_1 = \cdots = \theta_N =: \theta_s$. In new coordinates the dynamics on $\mathbb{R}^2$ reads

$$\dot{\theta}_s = \Omega - R(\theta)(KP(\theta) + \varepsilon P(t)), \tag{3.2a}$$

$$\dot{t} = 1. \tag{3.2b}$$

A periodic solution of this equation corresponds to a periodic solution of the original equation for N oscillators. If the latter is stable we say that the system synchronizes. First we analyze the equation above, describing periodically forced single oscillators. We do this by computing a vector field approximation of the Poincaré map via a normal form transformation. The vector field approximation of the Poincaré map of a periodically forced oscillator is of the following general form

$$\dot{u} = \phi + \beta p(u)$$

where ϕ and β are parameters and p is periodic function. Now we assume that p has a Fourier series and $p(u) = \cos(u - \chi) + \cdots$ for some χ. Then, in first approximation, stationary solutions exist for $|\phi| \leq |\beta|$, a wedge shaped region in the parameter plane called a tongue. Inside the tongue the Poincaré map has stationary points, implying that the periodically forced oscillator has periodic solutions.

We are going to find a map $F_s : \mathbb{R}^2 \to \mathbb{R}^2$, such that $F_\delta(K, \varepsilon) = (\phi, \beta)$. Thus the inverse image of the general tongue in the (K, ε)-plane is a region where the periodically forced Winfree oscillator has periodic solutions. In order to find F we have to be more explicit. We

will take $\Omega = r + \delta$, where r is a rational number and δ is another small parameter. In particular we take $r = 1$.

The vector field approximation up to order two, of the Poincaré map of Eq. (3.2) reads

$$\dot{u} = \delta + \tfrac{1}{2}c_1 K - \tfrac{5}{8}K^2 - K\varepsilon - \tfrac{9}{16}\varepsilon^2 + \tfrac{1}{2}\varepsilon\cos(u-\phi) - \tfrac{3}{16}K\varepsilon\cos u.$$

Thus, the required map F_δ has the form:

$$F_\delta(K,\varepsilon) = (\delta + \tfrac{1}{2}c_1 K - \tfrac{5}{8}K^2 - K\varepsilon - \tfrac{9}{16}\varepsilon^2, \tfrac{1}{2}\varepsilon).$$

Suppose that $c_1 = \cos\phi \neq 0$, then in lowest order in the parameters we have $F_\delta(K,\varepsilon) = (\delta + \frac{1}{2}c_1 K, \frac{1}{2}\varepsilon)$. Thus at the origin the map F_δ is just linear, so the inverse image of the standard tongue is again a straight cone. Indeed, we find the resonance region from solving $F_\delta(K,\varepsilon) = (\phi, \pm\phi)$ for K and ε. Reducing the map F_δ to its essentials we find the resonance region from solving $(\delta + K, \varepsilon) = (\phi, \pm\phi)$, so $\varepsilon = \pm(\delta + K)$. If $c_1 = 0$, then we have in lowest order in the parameters $F_\delta(K,\varepsilon) = (\delta - \frac{5}{8}K^2 - K\varepsilon - \frac{9}{16}\varepsilon^2, \frac{1}{2}\varepsilon)$. The boundaries of the $1:1$-resonance region are found from solving $F_\delta(K,\varepsilon) = (\phi, \pm\phi)$. By choosing $\delta = -0.1, 0, 0.1, 0.3$, we obtain the same pictures for resonance tongues as in Fig. 3.1 from numerical computations for identical oscillators.

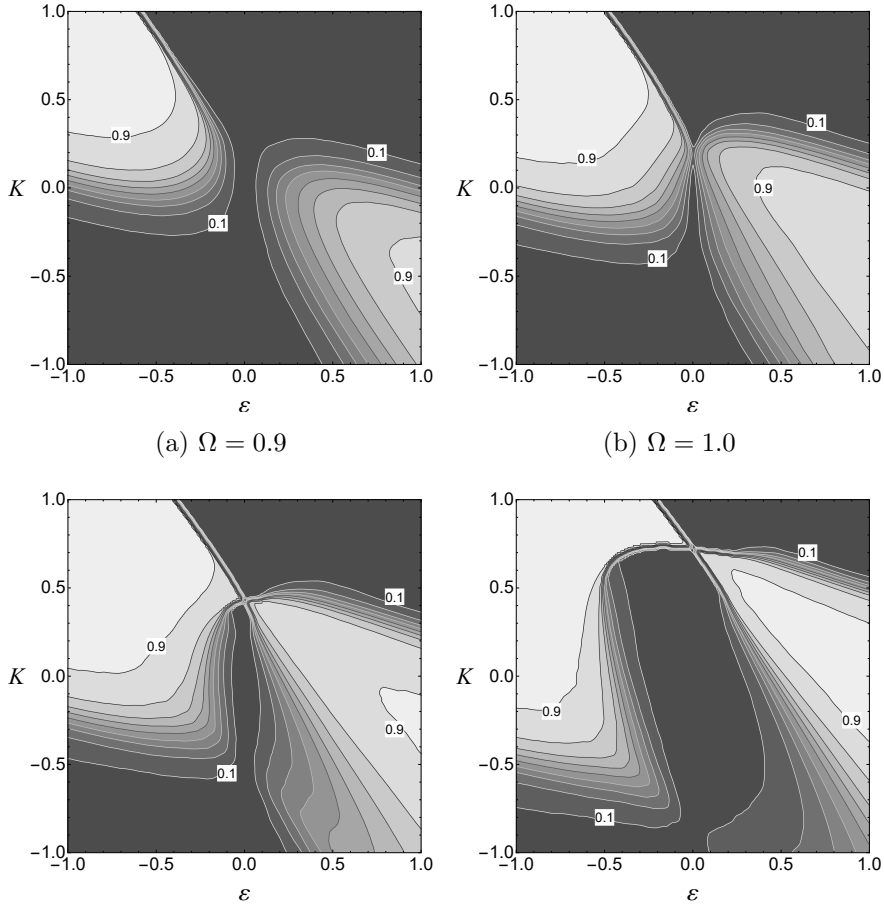

(a) $\Omega = 0.9$ (b) $\Omega = 1.0$

(c) $\Omega = 1.1$ (d) $\Omega = 1.3$

Figure 3.2: Entrainment degree is numerically computed for $N = 1000$ identical oscillators $\gamma = 0.05$. Their initial phases $\theta_i(0)$ are randomly chosen from a uniform distribution in $[0, 2\pi)$. Their natural frequencies follow a Lorentz distribution with different mean frequency $\Omega = 0.9, \Omega = 1.0, \Omega = 1.1$, and $\Omega = 1.3$. Simulations were performed with the fourth-order Runge-Kutta method with time step 0.1 for time $T = 20000$. An oscillator is considered to be entrained if its rotation number ρ_i satisfies $|\rho_i - 1| < 10^{-3}$ here. The entrainment degree is shown for the Lorentz distribution in the parameter space (ε, K) for fixed values of the scale parameters. Lighter gray levels represent larger entrainment degrees. Contours are equally spaced with step $\Delta d_e = 0.1$.

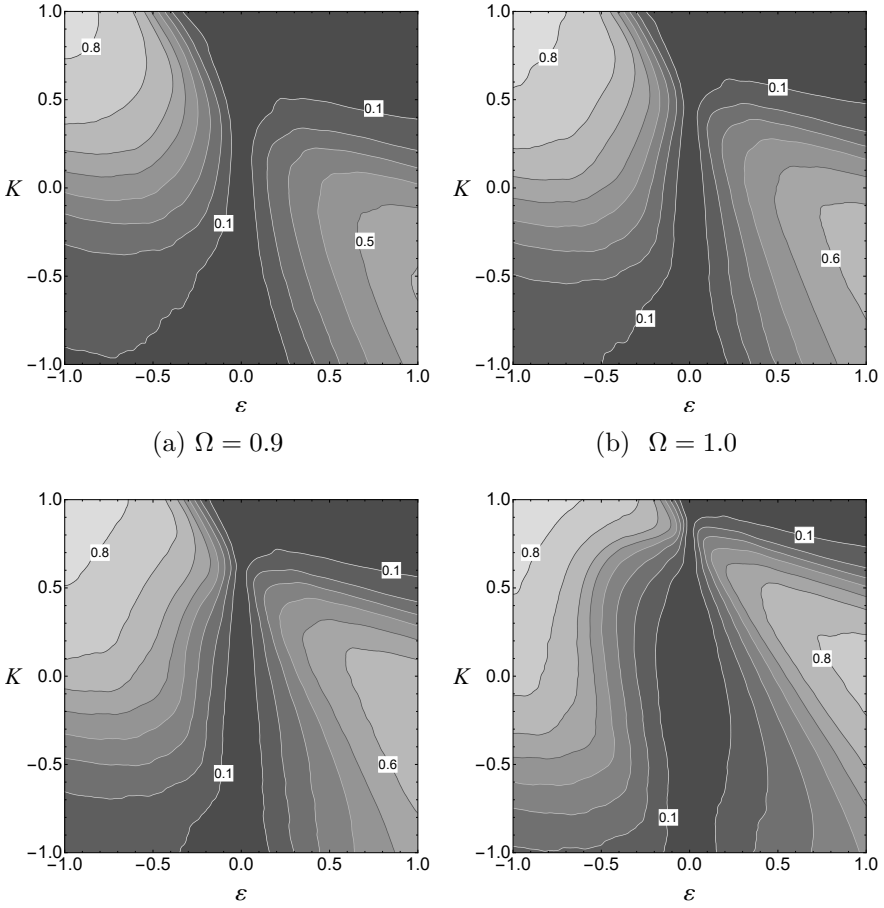

(a) $\Omega = 0.9$ (b) $\Omega = 1.0$

(c) $\Omega = 1.1$ (d) $\Omega = 1.3$

Figure 3.3: Entrainment degree is computated for $N = 1000$ identical oscillators while $\gamma = 0.2$. Their initial phases $\theta_i(0)$ are randomly chosen from a uniform distribution in $[0, 2\pi)$. Their natural frequencices follow a Lorentz distribution with different mean frequency $\Omega = 0.9, \Omega = 1.0, \Omega = 1.1$ and $\Omega = 1.3$. Simulations were performed with the fourth-order Runge-Kutta method with time step 0.1 for time $T = 20000$. An oscillator is considered to be entrained if its rotation number ρ_i satisfies $|\rho_i - 1| < 10^{-3}$ here. The entrainment degree is shown for the Lorentz distribution in the parameter space (ε, K) for fixed values of the scale parameters. Lighter gray levels represent larger entrainment degrees. Contours are equally spaced with step $\Delta d_e = 0.1$.

3.3 Non-Identical Oscillators

In this section, we focus on the oscillators whose natural frequencies follow a Lorentz distribution and the mean value Ω of the Lorentz distribution is different from the frequency of the Zeitgeber which is fixed at 1. Recall that we use the Lorentz distribution in Chapter 2 with the following form:

$$g(\omega) = \frac{\gamma}{\pi((\omega - \Omega)^2 + \gamma^2)}, \tag{3.3}$$

where ω means each oscillator's frequency, Ω is the mean natural frequency of oscillators, and γ is the scale parameter which specifies the half-width of the distribution in our thesis. We first present the numerically computed entrainment degree for different mean values of distributions by direct integration of the full dynamics.

A series of numerical simulations are shown in Fig. 3.2 and Fig. 3.3. We have computed the entrainment degree d_e for different parameter values of the system for $N = 2000$ oscillators with initial phases uniformly distributed in the interval $[0, 2\pi]$. The system evolves for time $T = 2 \cdot 10^4$, using a fourth-order Runge-Kutta method with fixed time step $\mathrm{d}t = 0.1$, and then we have computed a finite-time approximation of the rotation number for the i-th oscillator by

$$\rho_i(T) = \frac{1}{T}(\theta_i(T) - \theta_i(0)).$$

An oscillator has been marked as entrained, and thus contributed to the number of entrained oscillators, N_e, when $|\rho_i(T) - 1| < 10^{-3}$. The results of these computations are shown in Fig. 3.2 and Fig. 3.3 representing $\gamma = 0.05$ and $\gamma = 0.2$ respectively for the Lorentz distribution. From the comparison of Fig. 3.2 and Fig. 3.3, we can see the impact of parameters on detuned system. Compare Fig. 3.2a and Fig. 3.3a, we see that with Ω fixed, the smaller value on γ leads to a better entrainment on the scale of (K, ε) from $[-1, 1] \times [-1, 1]$. Compare four figures in Fig. 3.2, Ω decreases from 1 to 0.9, there is less regions are entrained in Fig. 3.2a. When Ω goes from 1 to 1.1, there are more regions in entrainment but the entrainment picture remains the similar shape. While Ω reaches 1.3, the entrainment shape has been changed.

When ε is close to zero, K has to be large to obtain entrainment, see Fig. 3.2d and Fig. 3.3d.

3.4 Low-dimensional Dynamics

The Ott-Antonsen ansatz is a major breakthrough in the study of collective dynamics in large systems of coupled phase oscillators. The macroscopic behavior of such systems can be fully described by a low-dimensional dynamics using the Ott-Antonsen ansatz. When the number of oscillators N tends to ∞, oscillators are expected to be distributed with a probability density which is continuous by considering it as a continuum limit. The detuned case can also be simplified by the Ott-Antonsen method in the same way as the non-detuned case. The details can be found in Section 2.5.1. We note the equations

$$\frac{\mathrm{d}x}{\mathrm{d}t} = -\gamma x - \Omega y + \frac{1}{2}(1 - x^2 + y^2)\big[K(1+x) + \varepsilon(1+\cos t)\big], \quad (3.4a)$$

$$\frac{\mathrm{d}y}{\mathrm{d}t} = \Omega x - \gamma y - xy\,\big[K(1+x) + \varepsilon(1+\cos t)\big]. \quad (3.4b)$$

Recall from Section 2.5.1 that x, y are the real and imaginary parts of the order parameter z respectively. In this section we present the bifurcation diagram on the (ε, K) space and compare the detuned case and the non-detuned case. Moreover, we compare the entrainment degrees of the Poincaré map with the numerical results for the full system, observing striking similarities.

3.4.1 Bifurcations in the Ott-Antonsen equations

Brouwer's fixed point theorem again ensures that the Poincaré map $P : D \to D$ defined by the 2π-flow of Eq. (3.4) has at least one fixed point in the detuned case. The system goes through bifurcations when the fixed points of P change stability as the parameters $(K, \varepsilon, \Omega, \gamma)$ change.

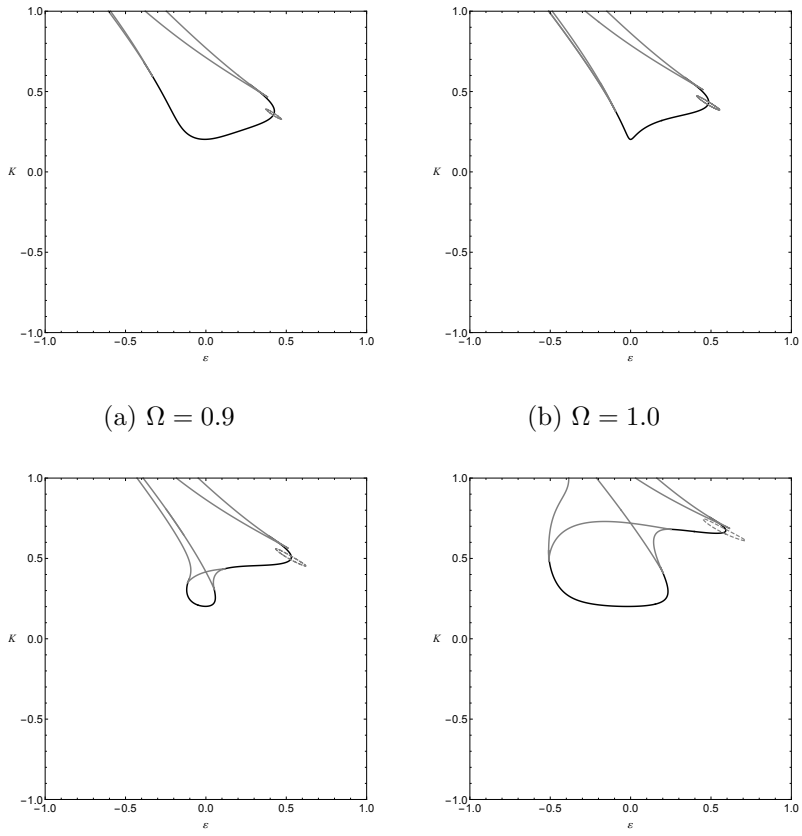

(a) $\Omega = 0.9$ (b) $\Omega = 1.0$

(c) $\Omega = 1.1$ (d) $\Omega = 1.3$

Figure 3.4: Bifurcation diagrams for the system described in Eq. (3.4). Solid black curves represent Neimark-Sacker (N-S) bifurcations, solid gray curves represent fold (saddle-node, SN) bifurcations, and dashed gray curves represent flip (period doubling, PD) bifurcations. All pictures are for $\gamma = 0.05$ and the mean natural frequency is (a) $\Omega = 0.9$, (b) $\Omega = 1.0$, (c) $\Omega = 1.1$ (d) $\Omega = 1.3$.

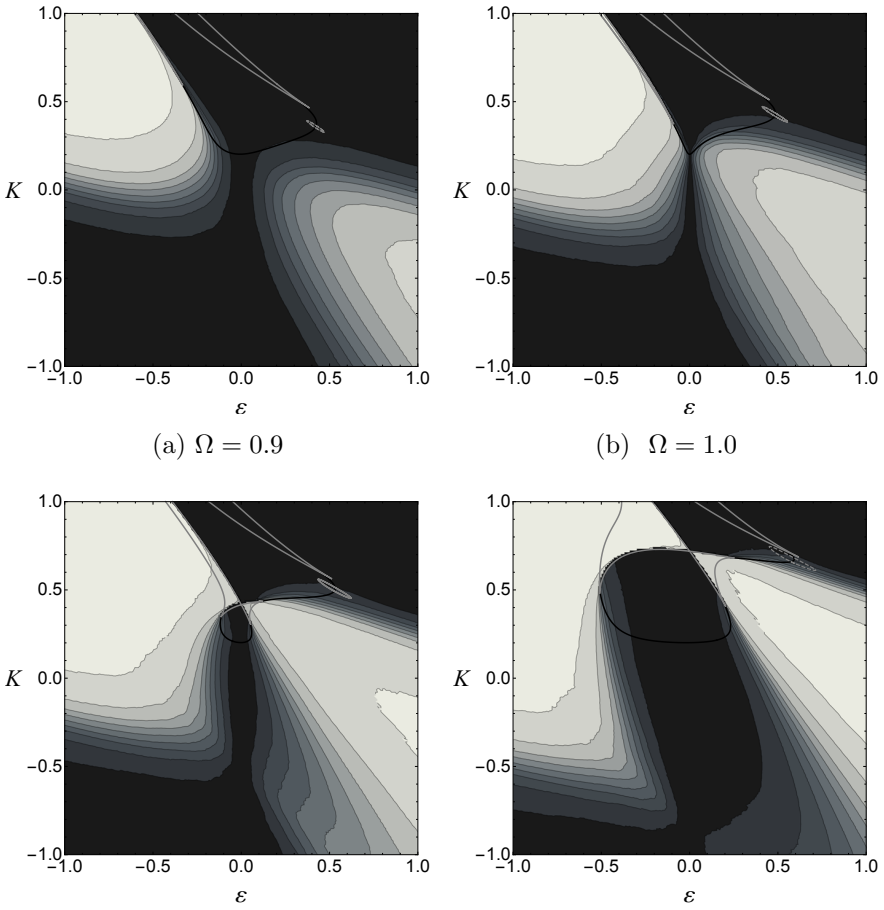

(a) $\Omega = 0.9$ (b) $\Omega = 1.0$

(c) $\Omega = 1.1$ (d) $\Omega = 1.3$

Figure 3.5: Entrainment degree for Lorentz distribution in the parameter space (ε, K) for fixed values of the scale parameters. Lighter gray levels represent larger entrainment degrees. Contours are equally spaced with step $\Delta d_e = 0.1$. In the computations $N = 1000$ oscillators were used. Bifurcation diagram for the Ott-Antonsen equations are presented for different values of Ω. All pictures are depicted for $\gamma = 0.05$.

We have used MatCont [50] to compute the bifurcation curves for Poincaré map P induced by the Ott-Antonsen equations in the parameter range $-1 \leq \varepsilon \leq 1$, $-1 \leq K \leq 1$. The bifurcations for

fixed γ with $\Omega = 0.9$, $\Omega = 1.0$, $\Omega = 1.1$ and $\Omega = 1.3$ are shown in Fig. 3.4. With increasing Ω , the bifurcation diagram becomes more complicated as we can see in Fig. 3.4c and Fig. 3.4d.

For fixed $\gamma = 0.05$, we expect to find in the (ε, K) parameter plane curves of codimension-1 bifurcations such as fold (saddle-node), flip (period-doubling), and Neimark-Sacker bifurcations [105].

With Ω increasing from 0.9 to 1.3, the area defined by the curve of flip bifurcations becomes larger. What's more, the area defined by fold bifurcations fits the entrainment better when the forcing is close to zero, especially when $\Omega \geqq 1.0$, shown in Fig. 3.5c and Fig. 3.5d.

Fig. 3.5 shows the bifurcation diagram and entrainment degree for Lorentz distribution with $\gamma = 0.05$. We find that when ε is close to 0, the entrainment boundary is governed by the saddle-node bifurcation. This is more obvious when $\Omega = 1.1$ and $\Omega = 1.3$.

3.4.2 Entrainment degree from the Ott-Antonsen mean field with different mean natural frequency

The Ott-Antonsen ansatz lowers the dimension of the system into a two-dimensional system, thus providing another way to present the evolution of the order parameter of the system. We have defined the order parameter in Sec. 2.1, which gives a macroscopic description of the dynamics. We rewrite the expression of the evolution of the order parameter $\mathrm{Re}(z_{\mathrm{OA}}(t))$ using Ott-Antonsen equations and compute it for specific values of the parameters (ε, K, ω), which is called *direct method* from the Ott-Antonsen mean field and compare it with the results in Sec. 3.2.1 by direct numerical computation from the full system. The entrainment results from the *direct method* are shown in Fig. 3.6, and its comparison with computation from full dynamics are shown in Fig. 3.7.

Afterwards, we use the *resonance tongue method*, which computes the boundaries of the entrainment degree from the Ott-Antonsen equations and we compare the results from the calculation of full system. The entrainment degree from *resonance tongue method* are shown in

Fig. 3.8, its comparsion with the results from full system is shown in Fig. 3.9.

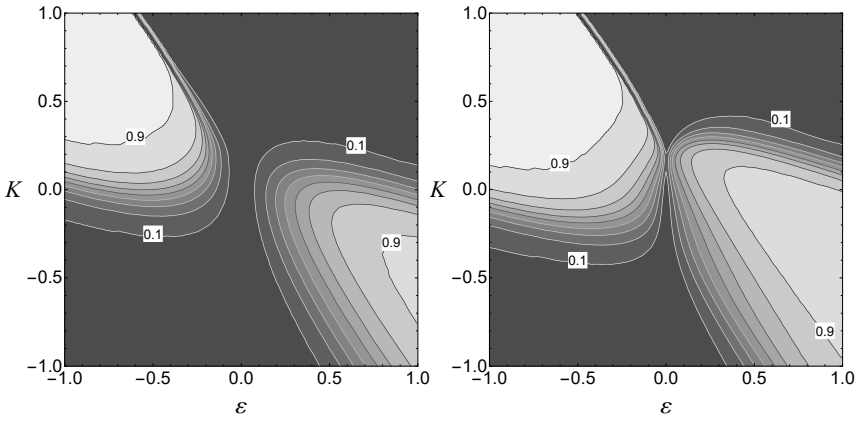

(a) $\Omega = 0.9$ (b) $\Omega = 1.0$

(c) $\Omega = 1.1$ (d) $\Omega = 1.3$

Figure 3.6: Entrainment degree as predicted by directly computing the rotation numbers of an ensemble of oscillators following the Ott-Antonsen mean field dynamics. The entrainment criterion was chosen as $|\rho - 1| < 10^{-3}$. Entrainment degree contours are equally spaced with $\Delta d_e = 0.1$ and lighter grays correspond to higher d_e. The value of d_e on some contours has been indicated in the pictures. All pictures are with $\gamma = 0.05$.

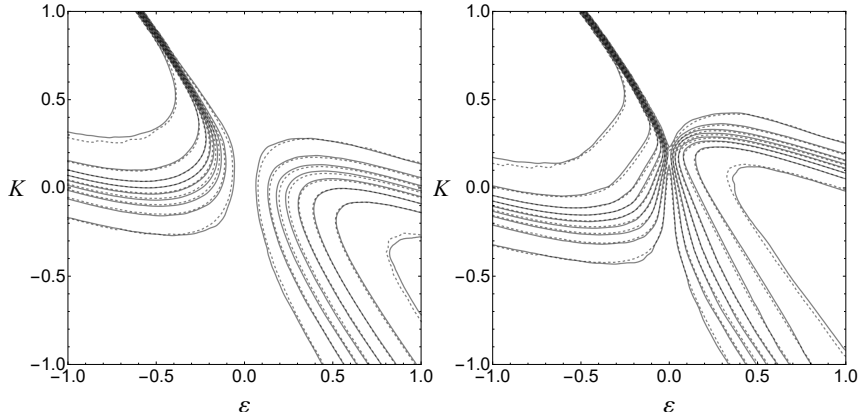

(a) $\Omega = 0.9$ (b) $\Omega = 1.0$

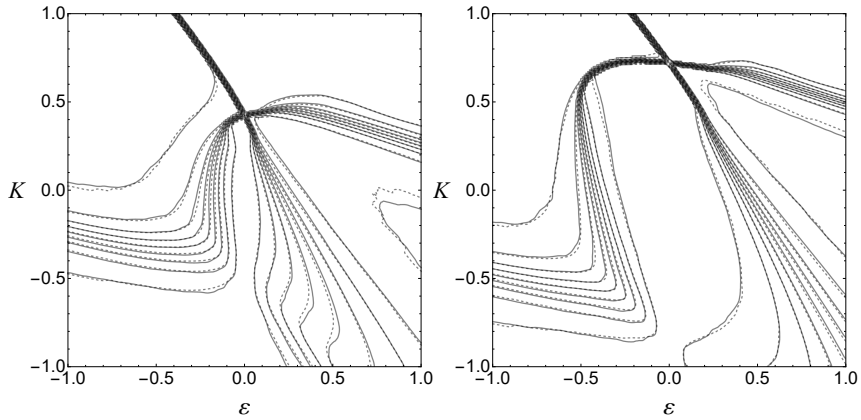

(c) $\Omega = 1.1$ (d) $\Omega = 1.3$

Figure 3.7: Comparison of contours in the top row Fig. 3.6 (dashed lines) to those shown in Fig. 3.2 (solid lines) computed by direct integration of the full dynamics.

We consider the dynamics of an oscillator of natural frequency Ω in the Ott-Antonsen mean field given by the equations:

$$\dot{\theta} = \omega - F(t)\sin\theta, \tag{3.5a}$$

where

$$F(t) = K(1 + \mathrm{Re}(z_{\mathrm{OA}}(t))) + \varepsilon(1 + \cos t). \tag{3.5b}$$

3.4.2.1 Direct method

We consider a finite ensemble of N oscillators with natural frequencies ω_i, $i = 1, \ldots, N$, following a Lorentz distribution $g(\omega)$ with four different mean values $0.9, 1.0, 1.1, 1.3$ respectively. The Lorentz distribution gives rise to the Ott-Antonsen mean field $z_{\mathrm{OA}}(t)$ and we compute the entrainment degree d_e, that is the percentage of oscillators that have rotation number 1, by using Eq. (3.5). Fig. 3.8 shows the results of entrainment degree.

We compute the order parameter $z_{\mathrm{OA}}(t)$ for time $0 \leq t \leq 10^3 \cdot (2\pi)$ using a Runge-Kutta fourth order method with fixed step size $dt = 10^{-2} \cdot (2\pi)$ and we simultaneously integrate the dynamics of $N = 200$ oscillators, given by Eq. (3.5), that is interacting only with the Ott-Antonsen mean-field, using the Euler method. Their initial phases $\theta_i(0)$ are randomly chosen uniformly in $[0, 2\pi)$. Oscillators' natural frequencies follow a Lorentz distribution with different mean value $\Omega_i = 0.9, 1.0, 1.1, 1.3$ respectively. As before, an oscillator with natural frequency ω_i is considered to be entrained if its rotation number ρ_i satisfies $|\rho_i - 1| < 10^{-3}$.

The results of this computation show the entrainment degree on the (ε, K) parameter plane for the scale parameter $\gamma = 0.05$. The results, shown in Fig. 3.6 are strikingly similar to the results in Fig. 3.2 that have been computed from the full dynamics without any theoretical approximations. This is clearly shown in Fig. 3.7 where the contours for the two methods (direct method and full dynamics) are drawn together. These results further validate the use of the Ott-Antonsen approximation to study the entrainment in this system.

3.4.2.2 Resonance tongue method

In this method we take advantage of the Poincaré map for the Ott-Antonsen equations. We estimate the entrainment degree using the theory of circle maps where there is a stable fixed point. In this case the Ott-Antonsen order parameter $z_{\mathrm{OA}}(t)$, and thus also $F(t)$,

Eq. (3.5b), are periodic with period 2π. Therefore, the dynamics gives rise to a circle map Eq. (3.5) whose 1:1 resonance tongue has boundaries $\omega_-(F) < \omega_+(F)$. The oscillator is entrained if its natural frequency $\omega \in (\omega_-(F), \omega_+(F))$ and thus the entrainment degree is given by

$$d_e = \int_{\omega_-(F)}^{\omega_+(F)} g(\omega)\, d\omega,$$

where $g(\omega)$ is a Lorentz distribution with mean value Ω and scale parameter γ.

The results from this method are shown in Fig. 3.8 on the (ε, K) parameter plane for the scale parameter $\gamma = 0.05$ and different values of the mean natural frequency Ω. The black regions shown for $\gamma = 0.05$ correspond to parameter values for which the Ott-Antonsen Poincaré map has no stable fixed points and should be compared with the corresponding bifurcation diagrams shown in Fig. 2.10. Outside these regions the obtained values for the entrainment degree are nearly identical to those obtained with the direct method. This is depicted in Fig. 3.9 where the contours for the direct and the resonance tongue method are drawn together.

3.5 Conclusions

We have considered a system of periodically forced coupled Winfree oscillators where the mean natural frequency of the oscillator is detuned from the frequency of the Zeitgeber. In this chapter, we have studied in detail its dynamics focusing on the question of the synchronization (entrainment) of individual oscillators to the external forcing. It was demonstrated that the introduction of frequency detuning significantly enriches the dynamics of Winfree system with a periodic forcing.

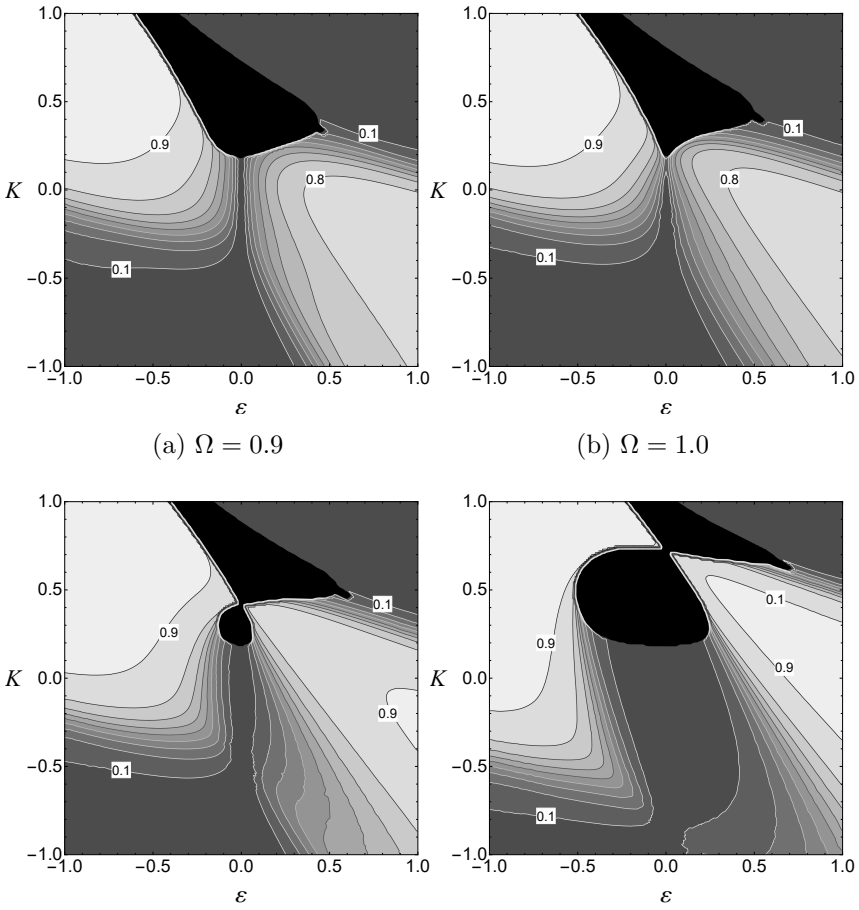

(a) $\Omega = 0.9$ (b) $\Omega = 1.0$

(c) $\Omega = 1.1$ (d) $\Omega = 1.3$

Figure 3.8: Entrainment degree as predicted by computing the width of the resonance tongues of the Ott-Antonsen mean field dynamics for the case that the Ott-Antonsen Poincaré map has a fixed point. The black regions correspond to parameter values for which there is no stable fixed point. Entrainment degree contours are equally spaced with $\Delta d_e = 0.1$ and lighter grays correspond to higher d_e. The value of d_e on some contours has been indicated in the pictures. All pictures are with $\gamma = 0.05$.

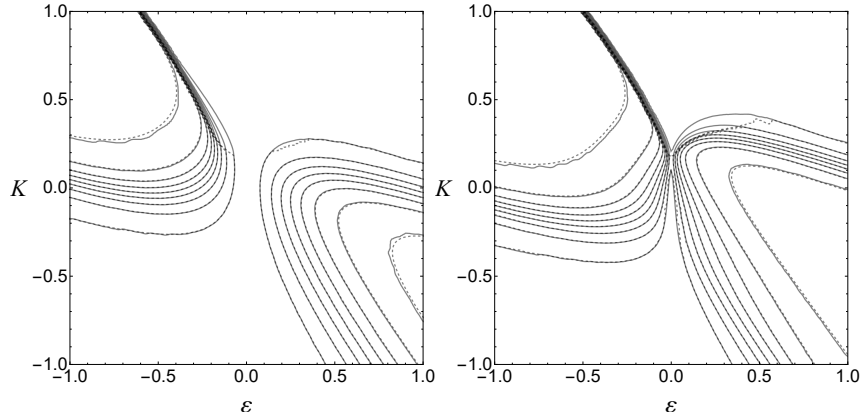

(a) $\Omega = 0.9$ (b) $\Omega = 1.0$

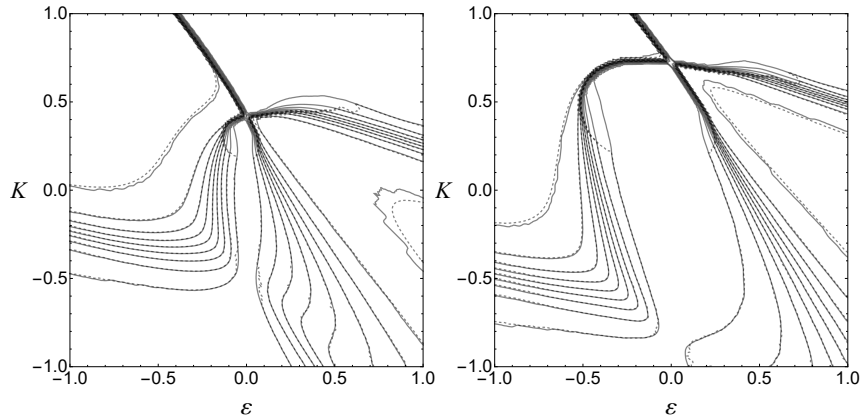

(c) $\Omega = 1.1$ (d) $\Omega = 1.3$

Figure 3.9: Comparison of contours in the top row Fig. 3.8 (solid lines) to those shown in Fig. 3.6 (dashed lines) computed by finding directly how many oscillators entrain in the Ott-Antonsen mean field.

Through numerical simulations we have shown that the entrainment properties of the set of oscillators are influenced by the amplitude of the external forcing ε, the coupling strength K and the diversity in the individual natural frequencies Ω. The degree of entrainment varies as the mean natural frequency changes.

First, we have considered the case of identical oscillators. Here we have given a theoretical explanation of the numerically obtained

results on the entrainment degree through a careful study of resonance tongues and normal stability for different values of the mean frequency of the oscillators.

Next, we have considered non-identical oscillators whose natural frequencies follow a Lorentz distribution. For such oscillators we have numerically computed the entrainment degree.

In the last part, we focused on systems where the oscillators again follow a Lorentz distribution and we have derived the low-dimensional dynamics using by the Ott-Antonsen ansatz. The evolution of the order parameter given by the Ott-Antonsen equations compares well to the evolution computed for the full dynamics for detuned cases. Then we have given a description of the bifurcation diagrams of periodic orbits in the Ott-Antonsen equations. Finally, we have connected the dynamics of oscillators in the Ott-Antonsen mean field with an approximation for the entrainment degree. The entrainment results from the Ott-Antonsen ansatz match well with the results we had earlier obtained by numerical computations, while they can be much more efficiently computed.

So far we have considered the case of unimodal natural frequency distributions. It is natural to ask what will be the effect of bimodal natural frequency distributions. We expect that the entrainment will be weaker. This question will be considered in the next chapter.

Chapter 4

Future Direction – The Bimodal Case

4.1 Introduction

Many creatures, such as dolphins, lizards and some kinds of birds have unihemispheric sleeping pattern [113]. They sleep with only one half of their brains at a time. By studying their brain waves during sleeping, it is known that the awake side is desynchronized, whereas neurons from the sleeping side of the brain are highly synchronized [93]. Synchronization has also been proved to be a central mechanism for information processing and communication between different brain regions, which constitutes a network of interacting subpopulations of neurons [69] [151]. Synchronization of interacting subpopulations of oscillatory networks play a crucial role in neuroscience and biological systems.

Some researchers mathematically model this phenomenon as collective oscillations in a system of multiple populations of limit-cycle oscillators [45]. It is known that systems with bimodal frequency distribution display rich synchronous dynamics in globally coupled phase oscillators, such as chimera states [2], twisted standing waves [197,198], transition states [184], bistability [30] and bifurcations [112]. Synchronization of two populations of phase oscillators not only in symmetric bimodal distributions but also interacting asymmetrically

are studied, such as asymmetric bimodal frequency distributions [4, 133] and asymmetric coupling functions [118]. Moreover, the effects of bimodal frequency distribution on Kuramoto model with time delay [119], the influence of entrainment under noise [127] and a trimodal natural frequency distributed population were also investigated [137]. The mechanisms of complete and partial synchronization in a system of two coupled Van der Pol oscillators under external harmonic force has been studied [9].

We have considered a forced Winfree system and its detuned case in Chapter 2 and Chapter 3. We have investigated the entrainment in different cases. The entrainment degree is influenced by several parameters, such as coupling strength, forcing strength, and the properties of the natural frequency distributions. Those factors determine how easily a group of oscillators is entrained to the external forcing.

It is natural to ask how introducing a bimodal frequency distribution influences the entrainment in Winfree system with periodic forcing. How does a periodic driving influence these two groups with different frequencies? This will be a future direction work, and in this chapter, we present some preliminary results. We explore the interacting oscillators that from two groups and each of the group has different mean frequencies. Besides their mutual coupling oscillators are also subject to a periodic forcing as we have considered in the previous chapters. Following the study for detuned case, we can study the two identical oscillators' case, non-identical oscillator case, together with Ott-Antonsen ansatz in bimodal frequency distribution case.

4.2 Investigation of the Bimodal Case

To start with, we begin our investigation with the simple case of frequency distribution with two infinitely sharp peaks. A bifurcation picture is present in Fig. 4.1. Then we compute the entrainment degree for the oscillators whose natural frequencies follow a bimodal Lorentz distribution and the mean value of the two Lorentz distribution is the same the frequency of the Zeitgeber. We give out the numerically computed entrainment degree for different cases as shown in Fig. 4.2.

We first consider the case of a bi-delta frequency distribution

$$g(\omega) = \frac{\delta(\omega - \Omega_1) + \delta(\omega - \Omega_2)}{2}. \tag{4.1}$$

In this case where the phases of all oscillators in each natural frequency group have been synchronized the dynamics of the system is described by the equations

$$\dot{\theta}_1 = \Omega_1 - \sin\theta_1 \left[\frac{K}{2}(2 + \cos\theta_1 + \cos\theta_2) + \varepsilon(1 + \cos t) \right], \tag{4.2a}$$

$$\dot{\theta}_2 = \Omega_2 - \sin\theta_2 \left[\frac{K}{2}(2 + \cos\theta_1 + \cos\theta_2) + \varepsilon(1 + \cos t) \right]. \tag{4.2b}$$

For this system, we have used MatCont [50] to compute the bifurcation diagram shown in Fig. 4.1.

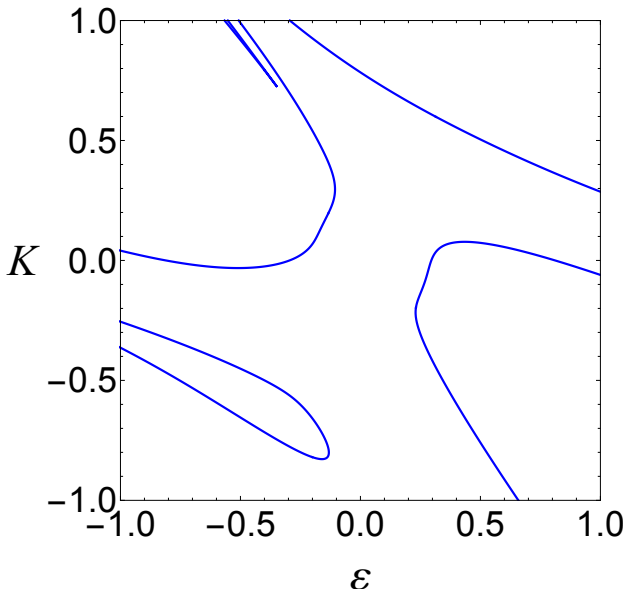

Figure 4.1: Bifurcation diagram for the system in Eq. (4.3), with $\Omega_1 = 0.9, \Omega_1 = 1.1$. The blue curves are saddle-node bifurcations.

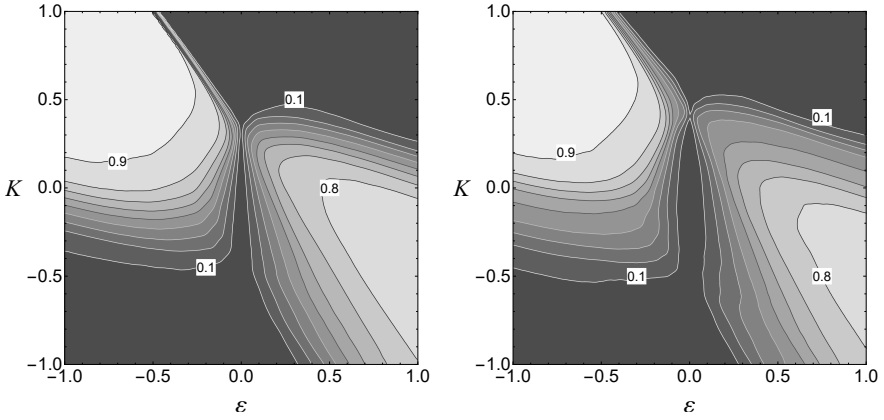

(a) $\Omega_1 = 0.95$ and $\Omega_2 = 1.05$ (b) $\Omega_1 = 0.9$ and $\Omega_2 = 1.1$

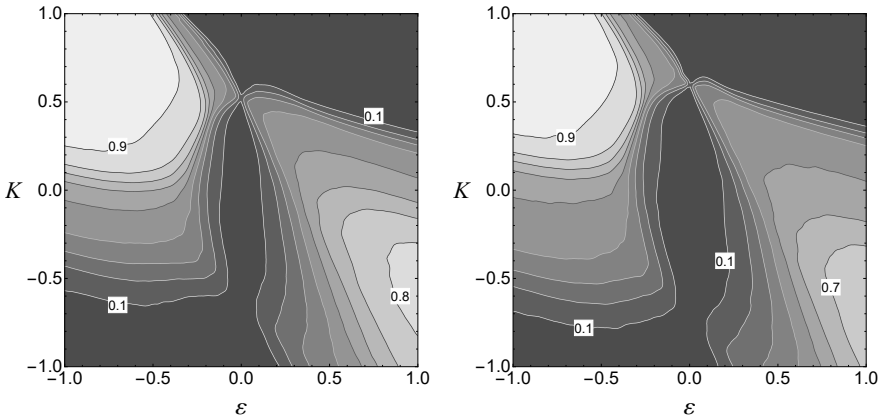

(c) $\Omega_1 = 0.85$ and $\Omega_2 = 1.15$ (d) $\Omega_1 = 0.8$ and $\Omega_2 = 1.2$

Figure 4.2: Entrainment degree for $N = 1000$ oscillators with the bimodal distribution $g(\omega)$, Eq. (4.3). Simulations were performed with the fourth-order Runge-Kutta method with time step 0.1 for time $T = 20000$. All pictures have $\gamma = 0.05$.

We also consider a bimodal distribution $g(\omega)$ that is symmetric and consists of two equally weighted Lorentzians, one centered at Ω_1 and the other is centered at Ω_2. More precisely, the natural frequency

distribution is given by

$$g(\omega) = \frac{\gamma}{2\pi}\Big(\frac{1}{(\omega-\Omega_1)^2+\gamma^2} + \frac{1}{(\omega-\Omega_2)^2+\gamma^2}\Big). \tag{4.3}$$

Note that in this case the mean natural frequency of the whole distribution $g(\omega)$ is $(\Omega_1+\Omega_2)/2$.

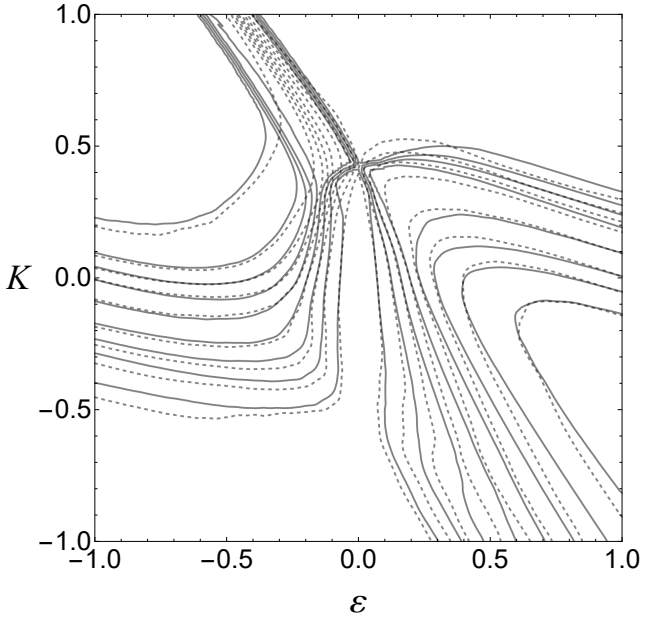

Figure 4.3: Comparison of contours in top row for entrainment degree from the average of two unimodal distribution (solid line) and a bimodal distribution (dashed line). In this computations $N = 1000$ oscillators were used. Simulations were performed with the fourth-order Runge-Kutta method with time step 0.1 for time $T = 20000$.

Fig. 4.2 depicts the entrainment degree for different values of Ω_1, Ω_2 having fixed mean value $\dfrac{\Omega_1+\Omega_2}{2}$, and fixed parameter $\gamma = 0.05$.

For the interest of knowing the impact on entrainment degree from bimodal distribution and unimodal distribution, we numerically compute the entrainment degree for two cases shown in Fig. 4.3. We

compute the average entrainment degree of two unimodal distributions when $\Omega = 0.9$ and $\Omega = 1.1$, solid line in Fig. 4.3, and compare it with the entrainment degree we obtain from a bimodal distribution where $\Omega_1 = 0.9$ and $\Omega_2 = 1.1$, dashed line in Fig. 4.3. The entrainment degree for the two cases are vary similar except in some regions for $K > 0, \varepsilon < 0$.

4.3 Derivation of the Ott-Antonsen Equations

In Chapter 2, we derived the Ott-Antonsen equations assuming that the natural frequency distribution is a Lorentz distribution. Now we investigate the more complicated situation where the natural frequency distribution is given by Eq. (4.3), i.e, the superposition of two Lorentz distributions.

The width of the two Lorentz distributions is the same, but they are centered at Ω_1 and Ω_2 respectively. We consider the continuum limit where the ensemble of discrete oscillators is replaced by a continuous distribution $\rho(\theta, t, \omega)$ expressing the probability density that an oscillator of natural frequency ω has phase θ at time t. The density ρ satisfies the normalization condition

$$\int_0^{2\pi} \rho(\theta, t, \omega)\, d\theta = 1.$$

The continuity equation takes the form

$$\frac{\partial \rho}{\partial t} + \frac{\partial}{\partial \theta}(\rho v) = 0. \tag{4.4}$$

The velocity of each oscillator is given by

$$v = \dot{\theta} = \omega - \sigma(t) \sin\theta - \varepsilon \sin\theta(1 + \cos t), \tag{4.5}$$

where $\sigma(t)$ is given in the continuum limit by

$$\sigma(t) = K \int_0^{2\pi} \int_{-\infty}^{\infty} (1 + \cos\theta)\rho(\theta, t, \omega) g(\omega)\, \mathrm{d}\theta\, \mathrm{d}\omega.$$

Note that the order parameter is given by

$$z(t) = \int_0^{2\pi} \int_{-\infty}^{\infty} e^{\mathrm{i}\theta} \rho(\theta, t, \omega) g(\omega) \, \mathrm{d}\theta \, \mathrm{d}\omega,$$

implying that

$$\sigma(t) = K\big[1 + \mathrm{Re}(z(t))\big].$$

Consider the Fourier series expansion of ρ, given by

$$\rho(\theta, t, \omega) = \frac{1}{2\pi} \sum_{n=-\infty}^{\infty} c_n(t, \omega) e^{in\theta}, \tag{4.6}$$

where $c_{-n} = \overline{c_n}$ and $c_0 = 1$. Substituting Eq. (4.6) and Eq. (4.5) into the continuity equation, Eq. (4.4), we obtain the evolution equation for the Fourier coefficients

$$\frac{\partial c_n}{\partial t} + \mathrm{i}n\omega c_n + \frac{n}{2}\big(\sigma(t) + \varepsilon(1 + \cos t)\big)(c_{n+1} - c_{n-1}) = 0. \tag{4.7}$$

Using the Fourier representation of ρ we find that

$$z(t) = \int_0^{2\pi} \int_{-\infty}^{\infty} e^{\mathrm{i}n\theta} \rho(\theta, t, \omega) g(\omega) \, \mathrm{d}\theta \, \mathrm{d}\omega = \int_{-\infty}^{\infty} c_{-1}(t, \omega) g(\omega) \, \mathrm{d}\omega. \tag{4.8}$$

Following the Ott-Antonsen ansatz we consider distributions with $c_n(t, \omega) = \alpha(t, \omega)^n$, for $n \geq 1$. Consequently, $c_n = \overline{c}_{|n|} = \overline{\alpha}^{|n|}$ for $n \leq -1$. Substituting the expression for c_n into Eq. (4.6) we find

$$\frac{\partial \alpha}{\partial t} + \mathrm{i}\,\omega\alpha + \frac{1}{2}\big(\sigma(t) + \varepsilon(1 + \cos t)\big)(\alpha^2 - 1) = 0. \tag{4.9}$$

Using Eq. (4.8) we can write the order parameter as

$$z(t) = \int_{-\infty}^{\infty} \overline{\alpha(t, \omega)} g(\omega) \, \mathrm{d}\omega. \tag{4.10}$$

Considering the case where $g(\omega)$ is the bimodal Lorentz distribution, Eq. (4.3), we obtain by calculating the residue at the poles

of $g(\omega)$ at the lower complex half-plane that the order parameter in complex form is

$$z(t) = \frac{1}{2}(z_1(t) + z_2(t)), \tag{4.11}$$

where

$$z_1(t) = \overline{\alpha(t, \Omega_1 - \mathrm{i}\gamma)}, z_2(t) = \overline{\alpha(t, \Omega_2 - \mathrm{i}\gamma)}. \tag{4.12}$$

Finally, considering the complex conjugate of Eq. (4.9) for $\omega = \Omega_1 - \mathrm{i}\gamma$, $\omega = \Omega_2 - \mathrm{i}\gamma$, we find the following two coupled complex differential equations for the order parameter:

$$\frac{\mathrm{d}z_1}{\mathrm{d}t} + (\gamma - \mathrm{i}\,\Omega_1)z_1 + \frac{1}{2}\big(K(1 + \mathrm{Re}(\frac{z_1 + z_2}{2})) + \varepsilon(1 + \cos t)\big)(z_1^2 - 1) = 0 \tag{4.13a}$$

$$\frac{\mathrm{d}z_2}{\mathrm{d}t} + (\gamma - \mathrm{i}\,\Omega_2)z_2 + \frac{1}{2}\big(K(1 + \mathrm{Re}(\frac{z_1 + z_2}{2})) + \varepsilon(1 + \cos t)\big)(z_2^2 - 1) = 0. \tag{4.13b}$$

Writing $z_1 = x_1 + \mathrm{i}y_1$, $z_2 = x_2 + \mathrm{i}y_2$ and separating the real and imaginary parts of Eq. (4.13), we obtain the equations

$$\frac{\mathrm{d}x_1}{\mathrm{d}t} = -\gamma x_1 - \Omega_1 y_1 - \frac{1}{2}(x_1^2 - y_1^2 - 1)\big[K(1 + \frac{x_1 + x_2}{2}) + \varepsilon(1 + \cos t)\big], \tag{4.14a}$$

$$\frac{\mathrm{d}y_1}{\mathrm{d}t} = \Omega_1 x_1 - \gamma y_1 - x_1 y_1 \big[K(1 + \frac{x_1 + x_2}{2}) + \varepsilon(1 + \cos t)\big], \tag{4.14b}$$

$$\frac{\mathrm{d}x_2}{\mathrm{d}t} = -\gamma x_2 - \Omega_2 y_2 - \frac{1}{2}(x_2^2 - y_2^2 - 1)\big[K(1 + \frac{x_1 + x_2}{2}) + \varepsilon(1 + \cos t)\big], \tag{4.14c}$$

$$\frac{\mathrm{d}y_2}{\mathrm{d}t} = \Omega_2 x_2 - \gamma y_2 - x_2 y_2 \big[K(1 + \frac{x_1 + x_2}{2}) + \varepsilon(1 + \cos t)\big]. \tag{4.14d}$$

Eq. (4.14) defines a four-dimensional non-autonomous dynamical system on $\mathbb{R}^4$.

So far bimodal frequency distributions have not been investigated in a large system of globally coupled phase oscillators with forcing. There are some studies on bimodal frequency distribution in the Kuramoto model. Using Ott-Antonsen ansatz, E. A. Martens et al. [112] analyze the system's stability diagram and show that in this case the infinite-dimensional problem reduces exactly to a flow in four dimensions. Note that this is similar to the system we have obtained here except that we also have a time–dependent forcing term whose strength is given by the parameter ε. Note that the case $\varepsilon = 0$ was studied for the Kuramoto model and results have been obtained on bifurcation boundaries between states [112], hysteretic phase transitions [133], full bifurcation diagrams [138] and so on. In the future work, we think it will be interesting to first understand the case $\varepsilon = 0$ on the Winfree model, and make a comparison with corresponding results for the Kuramoto model. After that, the case of small periodic forcing can be considered.

4.4 Open Problems

In this chapter, we have introduced the case of a bimodal natural frequency distribution. As the extension of the last chapter, this will be an interesting research topic to study in the future in more detail.

There are three possible future directions that we have briefly touched upon in this chapter. The first open question is the dynamical behavior of two oscillators in the system. The two oscillators can be identical or be different. We expect that in these two cases, the systems have different bifurcation diagrams or resonance tongues. We have computed the bifurcation diagram for two different oscillators, and it is quite different from the case of identical oscillators (non-detuned case and detuned case). The mechanism of this bifurcation diagram has to be found. Approximation method might help to understand the mechanism as we presented in Sec.3.2.1.

The second open question concerns the degree to which the entrainment for the obtained distribution can be obtained as a simple superposition of the entrainment for two unimodal distributions. Fig. 4.3 suggests that this may be the case, at least for some parameter values,

but a more thorough study of this question is required.

The third question worth working on is the low-dimensional dynamics. We have derived a low-dimensional system using the Ott-Antonsen ansatz in Sec. 4.3, and it is important to obtain a more clear understanding of the dynamics of the four-dimensional non-autonomous dynamical system. Moreover, it is still unclear what are the features of the bifurcation diagram of the lower dimensional system for the bimodal case. A comprehensive study of the bifurcation diagram can shed more light on the entrainment process for the bimodal case.

Chapter 5

Conclusions and Limitations

In this chapter, we will first provide a summary of this thesis. Subsequently, some limitations are discussed.

5.1 Conclusions

This thesis dealt with entrainment in forced Winfree system. Arthur Winfree has considered the general interactions among biological oscillators and regarded biological oscillators as self-sustained nearly identical coupled oscillators. This model could be used to describe the synchronization of a large system of globally coupled phase oscillators. One innovation of our thesis is considered to model the external stimuli with a periodic forcing in Winfree system, which simulates the circadian rhythms with environmental variation. We come up with the ideas from circadian rhythms, but the presented methods and results could be applied to many other oscillatory systems undergoing entrainment. The insights of this thesis highlight the entrainment phenomenon and the analysis of the built periodically forced model.

There are several scenarios we aim to understand for entrainment in this system, non-detuned case, i.e., the periodicity of the external forcing is the same with the intrinsic mean frequency of the oscillators, detuned case, i.e., the frequency of theoscillators detuned from that of the peiodic force, and the bimodal intrinsic mean frequency of oscillators in forced Winfree system. We started our research by mod-

eling a periodic forcing in Winfree system in this thesis and focus on entrainment, which means oscillators are entrained to the external periodic forcing. We study the entrainment phenomenon with the three above mentioned scenarios with a periodic forcing in Winfree system, yielding results of interest to the dynamics in the Winfree system with an external forcing as well as the entrainment patterns. We quantitatively describe entrainment by the percentage of oscillators synchronized to forcing. The entrainment behavior of the system depends on the mean frequency of the distribution of natural frequency, the coupling strength, the strength and frequency of the external force.

In the non-detuned case, we first consider a single forced oscillator and compute the 1:1 resonance tongue and use Poincaré map lift to explain the resonance tongue for the dynamics in Eq. (2.6). Then we study the normal stability on a synchronized manifold for identical oscillators. Considering the non-identical oscillators, we present dynamics states, evolution of the order parameter, and the entrainment degree of the system. The last observation in this case is the application of Ott-Antenson ansatz, and bifurcation is obtained for a better understanding of the system. Entrainment degree is coincidental for both numerical computation and Ott-Antonsen approach.

The second insight on studying entrainment on force Winfree system is the consideration for detuned case that the frequency of the oscillators differ from that of the periodic force. The entrainment properties of the detuned system and the differences with non-detuned system are studied. We study the normal stability, resonance tongue and entrainment degree for identical oscillators and compare that of in non-detuned case. Ott-Antenson ansatz works to obtain a two-dimensional dynamics and we found a very good agreement between the entrainment degree from direct numerical computations and the Ott-Antonsen approach in this case.

Additionally, we give some preliminary results and the insights on future work, entrainment in the Winfree model with a bimodal distribution constructed as the combination of two unimodal distributions.

5.2 Limitations

We have analyzed the driven Winfree model, which describes a wide class of phenomena in which systems of coupled oscillators can be entrained by an externally imposed driving force. However, there are still some limitations that can be addressed in future research.

We have studied our model using direct numerical simulations and by the low-dimensional reduction of Ott-Antonsen ansatz which has proven useful for the treatment of a wide variety of problems involving the interactions of a large number of phase oscillators. However, the validation conditions of Ott-Antonsen ansatz are not clearly acknowledged so far.

The second set of challenges relates to the fourth chapter of this thesis. We have considered the dynamics of two interacting groups of coupled oscillators. One restriction of the current study is that it has focused to the case of unimodal natural frequency distributions. It will be also interesting to study bifurcations, the entrainment degree and dynamics of the low-dimensional from the Ott-Antonsen ansatz in the bimodal cases as future research direction.

The last challenge goes well beyond the description of the mathematical model to the real world. Mathematical models are useful to describe the dynamics, but how well do the dynamics describe the real situation? How do we identify dynamics that are biologically precise, and validate and use models of these dynamics to predict the responses? On the large scale, we regard the biological oscillators as coupled oscillators, but the actual changes among the pace cells in some situations are more subtle, and therefore model-driven analyses could only be useful to have a macroscopic understanding. Insights into these fundamental questions will allow one to have more thoughts on understanding the entrainment patterns in forced Winfree model macroscopically.

Bibliography

[1] Ute Abraham, Adrián E Granada, Pål O Westermark, Markus Heine, Achim Kramer, and Hanspeter Herzel. Coupling governs entrainment range of circadian clocks. *Molecular Systems Biology*, 6(1), 2010.

[2] Daniel M Abrams, Rennie Mirollo, Steven H Strogatz, and Daniel A Wiley. Solvable model for chimera states of coupled oscillators. *Physical Review Letters*, 101(8):084103, 2008.

[3] Daniel M Abrams, Louis M Pecora, and Adilson E Motter. Introduction to focus issue: Patterns of network synchronization. *Chaos: An Interdisciplinary Journal of Nonlinear Science*, 26(9):094601, 2016.

[4] JA Acebrón, LL Bonilla, S De Leo, and R Spigler. Breaking the symmetry in bimodal frequency distributions of globally coupled oscillators. *Physical Review E*, 57(5):5287, 1998.

[5] Juan A Acebrón, Luis L Bonilla, Conrad J Pérez Vicente, Félix Ritort, and Renato Spigler. The kuramoto model: A simple paradigm for synchronization phenomena. *Reviews of Modern Physics*, 77(1):137, 2005.

[6] I Aihara. Synchronization experimentally observed in calling behaviors of japanese rain frogs (hyla-japonica). In *Proc. of 2006 Inter. Symp. on Nonlinear Theory and its Applications*, 2006.

[7] Ikkyu Aihara, Shunsuke Horai, Hiroyuki Kitahata, Kazuyuki Aihara, and Kenichi Yoshikawa. Dynamical calling behavior

experimentally observed in japanese tree frogs (hyla japonica). *IEICE Transactions on Fundamentals of Electronics, Communications and Computer Sciences*, 90(10):2154–2161, 2007.

[8] Ikkyu Aihara, Hiroyuki Kitahata, Kenichi Yoshikawa, and Kazuyuki Aihara. Mathematical modeling of frogs' calling behavior and its possible application to artificial life and robotics. *Artificial Life and Robotics*, 12(1-2):29–32, 2008.

[9] V Anishchenko, S Astakhov, and T Vadivasova. Phase dynamics of two coupled oscillators under external periodic force. *Europhysics Letters*, 86(3):30003, 2009.

[10] TM Antonsen Jr, RT Faghih, M Girvan, E Ott, and J Platig. External periodic driving of large systems of globally coupled phase oscillators. *Chaos: An Interdisciplinary Journal of Nonlinear Science*, 18(3):037112, 2008.

[11] Edward Victor Appleton. Automatic synchronization of triode oscillators. In *Proceedings of the Cambridge Philosophical Society*, volume 21, page 1923, 1922.

[12] Alex Arenas, Albert Díaz-Guilera, Jurgen Kurths, Yamir Moreno, and Changsong Zhou. Synchronization in complex networks. *Physics Reports*, 469(3):93–153, 2008.

[13] Joel T Ariaratnam and Steven H Strogatz. Phase diagram for the winfree model of coupled nonlinear oscillators. *Physical Review Letters*, 86(19):4278, 2001.

[14] Jürgen Aschoff. Freerunning and entrained circadian rhythms. In *Biological rhythms*, pages 81–93. Springer, 1981.

[15] Jürgen Aschoff and Hermann Pohl. Phase relations between a circadian rhythm and its zeitgeber within the range of entrainment. *Naturwissenschaften*, 65(2):80–84, 1978.

[16] Jürgen Aschoff and Rütger Wever. Human circadian rhythms: a multioscillatory system. In *Federation Proceedings*, volume 35, pages 236–232, 1976.

[17] Ameneh Asgari-Targhi and Elizabeth B Klerman. Mathematical modeling of circadian rhythms. *Wiley Interdisciplinary Reviews: Systems Biology and Medicine*, 11(2):e1439, 2019.

[18] Peter Ashwin, Stephen Coombes, and Rachel Nicks. Mathematical frameworks for oscillatory network dynamics in neuroscience. *The Journal of Mathematical Neuroscience*, 6(1):2, 2016.

[19] Angelo Auricchio, Christoph Stellbrink, Stefan Sack, Michael Block, J ürgen Vogt, Patricia Bakker, Christof Huth, Friedrich Schöndube, Ulrich Wolfhard, Dirk Böcker, et al. Long-term clinical effect of hemodynamically optimized cardiac resynchronization therapy in patients with heart failure and ventricular conduction delay. *Journal of the American College of Cardiology*, 39(12):2026–2033, 2002.

[20] Yernur Baibolatov, Michael Rosenblum, Zeinulla Zh Zhanabaev, Meyramgul Kyzgarina, and Arkady Pikovsky. Periodically forced ensemble of nonlinearly coupled oscillators: From partial to full synchrony. *Physical Review E*, 80(4):046211, 2009.

[21] Mauricio Barahona and Louis M Pecora. Synchronization in small-world systems. *Physical Review Letters*, 89(5):054101, 2002.

[22] Utako B Barnikol, Oleksandr V Popovych, Christian Hauptmann, Volker Sturm, Hans-Joachim Freund, and Peter A Tass. Tremor entrainment by patterned low-frequency stimulation. *Philosophical Transactions of the Royal Society A: Mathematical, Physical and Engineering Sciences*, 366(1880):3545–3573, 2008.

[23] A Barroso and B Den Brinker. Boosting circadian rhythms with lighting: A model driven approach. *Lighting Research & Technology*, 45(2):197–216, 2013.

[24] George A Bartholomew and Robert C Lasiewski. Heating and cooling rates, heart rate and simulated diving in the galapagos marine iguana. *Comparative Biochemistry and Physiology*, 16(4):573–582, 1965.

[25] Domien G. M. Beersma, Bram A. D. van Bunnik, Roelof A. Hut, and Serge Daan. Emergence of circadian and photoperiodic system level properties from interactions among pacemaker cells. *Journal of Biological Rhythms*, 23(4):362–373, 2008.

[26] Domien GM Beersma, Henk W Broer, Konstantinos Efstathiou, Kim A Gargar, and Igor Hoveijn. Pacer cell response to periodic zeitgebers. *Physica D: Nonlinear Phenomena*, 240(19):1516–1527, 2011.

[27] Domien GM Beersma, Serge Daan, and Roelof A Hut. Accuracy of circadian entrainment under fluctuating light conditions: contributions of phase and period responses. *Journal of Biological Rhythms*, 14(4):320–329, 1999.

[28] Igor V Belykh, Vladimir N Belykh, and Martin Hasler. Blinking model and synchronization in small-world networks with a time-varying coupling. *Physica D: Nonlinear Phenomena*, 195(1-2):188–206, 2004.

[29] Richard A Block. *Cognitive models of psychological time*. Psychology Press, 2014.

[30] Luis L Bonilla, John C Neu, and Renato Spigler. Nonlinear stability of incoherence and collective synchronization in a population of coupled oscillators. *Journal of Statistical Physics*, 67(1-2):313–330, 1992.

[31] Grigory Bordyugov, Ute Abraham, Adrian Granada, Pia Rose, Katharina Imkeller, Achim Kramer, and Hanspeter Herzel. Tuning the phase of circadian entrainment. *Journal of The Royal Society Interface*, 12(108):20150282, 2015.

[32] Michael R Bristow, Leslie A Saxon, John Boehmer, Steven Krueger, David A Kass, Teresa De Marco, Peter Carson, Lorenzo DiCarlo, David DeMets, Bill G White, et al. Cardiac-resynchronization therapy with or without an implantable defibrillator in advanced chronic heart failure. *New England Journal of Medicine*, 350(21):2140–2150, 2004.

[33] Emery N Brown and Harry Luithardt. Statistical model building and model criticism for human circadian data. *Journal of Biological Rhythms*, 14(6):609–616, 1999.

[34] John Buck. Synchronous rhythmic flashing of fireflies. ii. *The Quarterly Review of Biology*, 63(3):265–289, 1988.

[35] John Buck and Elisabeth Buck. Synchronous fireflies. *Scientific American*, 234(5):74–85, 1976.

[36] John Bonner Buck. Synchronous flashing of fireflies experimentally induced. *Science*, 1935.

[37] John Bonner Buck. Synchronous rhythmic flashing of fireflies. *The Quarterly Review of Biology*, 13(3):301–314, 1938.

[38] Miguel D Bustamante and Elena Kartashova. Effect of the dynamical phases on the nonlinear amplitudes' evolution. *Europhysics Letters*, 85(3):34002, 2009.

[39] Robert J Butera Jr, John Rinzel, and Jeffrey C Smith. Models of respiratory rhythm generation in the pre-botzinger complex. i. bursting pacemaker neurons. *Journal of Neurophysiology*, 82(1):382–397, 1999.

[40] Lauren M Childs and Steven H Strogatz. Stability diagram for the forced kuramoto model. *Chaos: An Interdisciplinary Journal of Nonlinear Science*, 18(4):043128, 2008.

[41] Ned J Corron, Jonathan N Blakely, and Shawn D Pethel. Beam steering by lag synchronization in wide-bandwidth, chaotic arrays. In *AIP Conference Proceedings*, volume 742, pages 45–50. AIP, 2004.

[42] Alex DD Craik. *Wave interactions and fluid flows*. Cambridge University Press, 1988.

[43] J. D. Crawford. Scaling and singularities in the entrainment of globally coupled oscillators. *Physical Review Letters*, 74:4341–4344, 1995.

[44] J. D. Crawford and K. T. R. Davies. Synchronization of globally coupled phase oscillators: singularities and scaling for general couplings. *Physica D: Nonlinear Phenomena*, 125(1–2):1–46, 1999.

[45] John David Crawford. Amplitude expansions for instabilities in populations of globally-coupled oscillators. *Journal of Statistical Physics*, 74(5-6):1047–1084, 1994.

[46] Serge Daanm and Domien GM Beersma. A single pacemaker can produce different rates of reentrainment in different overt rhythms. *Journal of Sleep Research*, 1(2):80–83, 1992.

[47] Regis A DeSilva. George ralph mines, ventricular fibrillation and the discovery of the vulnerable period. *Journal of the American College of Cardiology*, 29(6):1397–1402, 1997.

[48] R. L. Devaney. *An Introduction to Chaotic Dynamical Systems*. Number 1 in Studies in Nonlinearity. Addison-Wesley Publishing Company, Inc., 2 edition, 1989.

[49] Daniel DeWoskin, Weihua Geng, Adam R Stinchcombe, and Daniel B Forger. It is not the parts, but how they interact that determines the behaviour of circadian rhythms across scales and organisms. *Interface focus*, 4(3):20130076, 2014.

[50] A. Dhooge, W. Govaerts, Yu. A. Kuznetsov, H. G. E. Meijer, and B. Sautois. New features of the software MatCont for bifurcation analysis of dynamical systems. *Mathematical and Computer Modelling of Dynamical Systems*, 14(2):147–175, 2008.

[51] Huaiyu Duan, George M Fuller, and Yong-Zhong Qian. Collective neutrino oscillations. *Annual Review of Nuclear and Particle Science*, 60:569–594, 2010.

[52] Denys Dutykh and Elena Tobisch. Resonance enhancement by suitably chosen frequency detuning. *arXiv preprint arXiv:1411.5518*, 2014.

[53] William Henry Eccles and JH Vincent. On the variations of wave-length of the oscillations generated by three-electrode thermionic tubes due to changes in filament current, plate voltage, grid voltage, or coupling. *Proceedings of the Royal Society of London. Series A, Containing Papers of a Mathematical and Physical Character*, 96(680):455–465, 1920.

[54] Bard Ermentrout. An adaptive model for synchrony in the firefly pteroptyx malaccae. *Journal of Mathematical Biology*, 29(6):571–585, 1991.

[55] G Bard Ermentrout and David H Terman. *Mathematical foundations of neuroscience*, volume 35. Springer Science & Business Media, 2010.

[56] Juergen Fell and Nikolai Axmacher. The role of phase synchronization in memory processes. *Nature Reviews Neuroscience*, 12(2):105, 2011.

[57] Giovanni Filatrella, Arne Hejde Nielsen, and Niels Falsig Pedersen. Analysis of a power grid using a kuramoto-like model. *The European Physical Journal B*, 61(4):485–491, 2008.

[58] Kristin J Forbes and Roberto Rigobon. No contagion, only interdependence: measuring stock market comovements. *The journal of Finance*, 57(5):2223–2261, 2002.

[59] Mattia Frasca, Arturo Buscarino, Alessandro Rizzo, Luigi Fortuna, and Stefano Boccaletti. Synchronization of moving chaotic agents. *Physical Review Letters*, 100(4):044102, 2008.

[60] Pascal Fries. A mechanism for cognitive dynamics: neuronal communication through neuronal coherence. *Trends in Cognitive Sciences*, 9(10):474–480, 2005.

[61] Pascal Fries. Neuronal gamma-band synchronization as a fundamental process in cortical computation. *Annual Review of Neuroscience*, 32:209–224, 2009.

[62] Naoya Fujiwara, Jürgen Kurths, and Albert Díaz-Guilera. Synchronization in networks of mobile oscillators. *Physical Review E*, 83(2):025101, 2011.

[63] Rafael Gallego, Ernest Montbrió, and Diego Pazó. Synchronization scenarios in the winfree model of coupled oscillators. *Physical Review E*, 96(4):042208, 2017.

[64] Rafael Gallego, Ernest Montbrió, and Diego Pazó. Synchronization scenarios in the Winfree model of coupled oscillators. *Physical Review E*, 96:042208, Oct 2017.

[65] AK Ghosh, B Chance, and EK Pye. Metabolic coupling and synchronization of nadh oscillations in yeast cell populations. *Archives of Biochemistry and Biophysics*, 145(1):319–331, 1971.

[66] Brian C Goodwin. Oscillatory behavior in enzymatic control processes. *Advances in Enzyme Regulation*, 3:425–437, 1965.

[67] Cynthia A Graham and William C McGrew. Menstrual synchrony in female undergraduates living on a coeducational campus. *Psychoneuroendocrinology*, 5(3):245–252, 1980.

[68] Adrián E Granada and Hanspeter Herzel. How to achieve fast entrainment? the timescale to synchronization. *PLOS One*, 4(9):e7057, 2009.

[69] Charles M Gray, Peter König, Andreas K Engel, and Wolf Singer. Oscillatory responses in cat visual cortex exhibit intercolumnar synchronization which reflects global stimulus properties. *Nature*, 338(6213):334, 1989.

[70] Claude Gronfier, Kenneth P Wright, Richard E Kronauer, and Charles A Czeisler. Entrainment of the human circadian pacemaker to longer-than-24-h days. *Proceedings of the National Academy of Sciences*, 104(21):9081–9086, 2007.

[71] Andreas Groth and Michael Ghil. Synchronization of world economic activity. *Chaos: An Interdisciplinary Journal of Nonlinear Science*, 27(12):127002, 2017.

[72] Seung-Yeal Ha, Eunhee Jeong, and Moon-Jin Kang. Emergent behaviour of a generalized viscek-type flocking model. *Nonlinearity*, 23(12):3139, 2010.

[73] Seung-Yeal Ha, Dongnam Ko, Jinyeong Park, and Sang Woo Ryoo. Emergent dynamics of Winfree oscillators on locally coupled networks. *Journal of Differential Equations*, 260(5):4203–4236, 2016.

[74] Seung-Yeal Ha, Jinyeong Park, and Sang Woo Ryoo. Emergence of phase-locked states for the Winfree model in a large coupling regime. *Discrete and Continuous Dynamical Systems, Series A*, 35(8):3417–3436, 2015.

[75] Ruth Halaban. Effects of light quality on the circadian rhythm of leaf movement of a short-day-plant. *Plant Physiology*, 44(7):973–977, 1969.

[76] Constance Hammond, Hagai Bergman, and Peter Brown. Pathological synchronization in parkinson's disease: networks, models and treatments. *Trends in neurosciences*, 30(7):357–364, 2007.

[77] E Newton Harvey et al. Living light. 1940.

[78] J Woodland Hastings and Beatrice M Sweeney. A persistent diurnal rhythm of luminescence in gonyaulax polyedra. *The Biological Bulletin*, 115(3):440–458, 1958.

[79] Michael H Hastings and Erik D Herzog. Clock genes, oscillators, and cellular networks in the suprachiasmatic nuclei. *Journal of Biological Rhythms*, 19(5):400–413, 2004.

[80] Ted Heath, Kurt Wiesenfeld, and Robert A York. Manipulated synchronization: Beam steering in phased arrays. *International Journal of Bifurcation and Chaos*, 10(11):2619–2627, 2000.

[81] Christopher Hemming and Raymond Kapral. Turbulent fronts in resonantly forced oscillatory systems. *Faraday discussions*, 120:371–382, 2002.

[82] Hyunsuk Hong, Moo-Young Choi, and Beom Jun Kim. Synchronization on small-world networks. *Physical Review E*, 65(2):026139, 2002.

[83] KI Honma and TSUTOMU Hiroshige. Internal synchronization among several circadian rhythms in rats under constant light. *American Journal of Physiology-Regulatory, Integrative and Comparative Physiology*, 235(5):R243–R249, 1978.

[84] Sato Honma, Wataru Nakamura, Tetsuo Shirakawa, and Kenichi Honma. Diversity in the circadian periods of single neurons of the rat suprachiasmatic nucleus depends on nuclear structure and intrinsic period. *Neuroscience Letters*, 358(3):173–176, 2004.

[85] Frank C Hoppensteadt and Joseph B Keller. Synchronization of periodical cicada emergences. *Science*, 194(4262):335–337, 1976.

[86] Igor Hoveijn. Stability pockets of a periodically forced oscillator in a model for seasonality. *Indagationes Mathematicae*, 27(5):1204–1218, 2016.

[87] Christiaan Huygens. Oeuvres completes de christiaan huygens, vol. 5. *The Hague: Martinus Nijhoff.(Includes works from 1665.)*, pages 241–262, 1893.

[88] Christiaan Huygens. *Horologium oscillatorium: 1673*. Dawson, 1966.

[89] Oleg A Igoshin, Alex Mogilner, Roy D Welch, Dale Kaiser, and George Oster. Pattern formation and traveling waves in myxobacteria: theory and modeling. *Proceedings of the National Academy of Sciences*, 98(26):14913–14918, 2001.

[90] Yuichi Ikeda, Hideaki Aoyama, Yoshi Fujiwara, Hiroshi Iyetomi, Kazuhiko Ogimoto, Wataru Souma, and Hiroshi Yoshikawa. Coupled oscillator model of the business cycle with fluctuating goods markets. *Progress of Theoretical Physics Supplement*, 194:111–121, 2012.

[91] John Jalife. Mutual entrainment and electrical coupling as mechanisms for synchronous firing of rabbit sino-atrial pace-maker cells. *The Journal of Physiology*, 356(1):221–243, 1984.

[92] Valerii P Kandidov and Andrey V Kondrat'ev. Generation dynamics of laser arrays with diffraction coupling. In *Laser Optics' 98: Fundamental Problems of Laser Optics*, volume 3685, pages 34–41. International Society for Optics and Photonics, 1999.

[93] Herbert Kattler, DERK-JAN DIJK, and Alexander A Borbely. Effect of unilateral somatosensory stimulation prior to sleep on the sleep eeg in humans. *Journal of Sleep Research*, 3(3):159–164, 1994.

[94] Dongnam Ko. Practical synchronization of winfree oscillators in a random environment. *Journal of Statistical Physics*, 174(6):1263–1287, 2019.

[95] Hiroshi Kori and Alexander S Mikhailov. Entrainment of randomly coupled oscillator networks by a pacemaker. *Physical Review Letters*, 93(25):254101, 2004.

[96] Hiroshi Kori and Alexander S Mikhailov. Strong effects of network architecture in the entrainment of coupled oscillator systems. *Physical Review E*, 74(6):066115, 2006.

[97] Aneta Koseska, Evgenij Volkov, and Juergen Kurths. Detuning-dependent dominance of oscillation death in globally coupled synthetic genetic oscillators. *Europhysics Letters*, 85(2):28002, 2009.

[98] Richard E Kronauer, Charles A Czeisler, Samuel F Pilato, Martin C Moore-Ede, and Elliot D Weitzman. Mathematical model of the human circadian system with two interacting oscillators. *American Journal of Physiology-Regulatory, Integrative and Comparative Physiology*, 242(1):R3–R17, 1982.

[99] Sandra J Kuhlman, Rae Silver, Joseph Le Sauter, Abel Bult-Ito, and Douglas G McMahon. Phase resetting light pulses induce

per1 and persistent spike activity in a subpopulation of biological clock neurons. *Journal of Neuroscience*, 23(4):1441–1450, 2003.

[100] Y. Kuramoto. Self-entrainment of a population of coupled nonlinear oscillators. In H. Araki, editor, *International Symposium on Mathematical Problems in Theoretical Physics*, volume 39 of *Lecture Notes in Physics*, pages 420–422. Springer, 1975.

[101] Yoshiki Kuramoto. Self-entrainment of a population of coupled non-linear oscillators. In *International Symposium on Mathematical Problems in Theoretical Physics*, pages 420–422. Springer, 1975.

[102] Yoshiki Kuramoto. *Chemical oscillations, waves, and turbulence*. Courier Corporation, 2003.

[103] Yoshiki Kuramoto and Ikuko Nishikawa. Statistical macrodynamics of large dynamical systems. case of a phase transition in oscillator communities. *Journal of Statistical Physics*, 49(3-4):569–605, 1987.

[104] Gen Kurosawa and Albert Goldbeter. Amplitude of circadian oscillations entrained by 24-h light–dark cycles. *Journal of Theoretical Biology*, 242(2):478–488, 2006.

[105] Y. A. Kuznetsov. *Elements of Applied Bifurcation Theory*, volume 112 of *Applied Mathematical Sciences*. Springer, 2 edition, 1998.

[106] Carlo R. Laing. *Phase oscillator network models of brain dynamics*, chapter 37, pages 505–517. Wiley-Blackwell, 2017.

[107] Jean-Christophe Leloup and Albert Goldbeter. Toward a detailed computational model for the mammalian circadian clock. *Proceedings of the National Academy of Sciences*, 100(12):7051–7056, 2003.

[108] Chen Liu, David R Weaver, Steven H Strogatz, and Steven M Reppert. Cellular construction of a circadian clock: period determination in the suprachiasmatic nuclei. *Cell*, 91(6):855–860, 1997.

[109] Zhixin Lu, Kevin Klein-Cardeña, Steven Lee, Thomas M Antonsen, Michelle Girvan, and Edward Ott. Resynchronization of circadian oscillators and the east-west asymmetry of jet-lag. *Chaos: An Interdisciplinary Journal of Nonlinear Science*, 26(9):094811, 2016.

[110] Rosario N Mantegna. Hierarchical structure in financial markets. *The European Physical Journal B-Condensed Matter and Complex Systems*, 11(1):193–197, 1999.

[111] Eve Marder and Dirk Bucher. Central pattern generators and the control of rhythmic movements. *Current Biology*, 11(23):R986–R996, 2001.

[112] Erik Andreas Martens, Ernest Barreto, Steven H Strogatz, Edward Ott, Paul So, and Thomas M Antonsen. Exact results for the kuramoto model with a bimodal frequency distribution. *Physical Review E*, 79(2):026204, 2009.

[113] Christian G Mathews, John A Lesku, Steven L Lima, and Charles J Amlaner. Asynchronous eye closure as an anti-predator behavior in the western fence lizard (sceloporus occidentalis). *Ethology*, 112(3):286–292, 2006.

[114] Martha K McClintock. Menstrual synchrony and suppression. *Nature*, 1971.

[115] Brian K Meadows, Ted H Heath, Joseph D Neff, Edgar A Brown, David W Fogliatti, MICHAEL Gabbay, Visarath In, Paul Hasler, Stephen P Deweerth, and William L Ditto. Nonlinear antenna technology. *Proceedings of the IEEE*, 90(5):882–897, 2002.

[116] Donald C Michaels, Edward P Matyas, and Jose Jalife. Mechanisms of sinoatrial pacemaker synchronization: a new hypothesis. *Circulation Research*, 61(5):704–714, 1987.

[117] J Mills. *Biological aspects of circadian rhythms*. Springer Science & Business Media, 2012.

[118] Ernest Montbrió, Jürgen Kurths, and Bernd Blasius. Synchronization of two interacting populations of oscillators. *Physical Review E*, 70(5):056125, 2004.

[119] Ernest Montbrió, Diego Pazó, and Jürgen Schmidt. Time delay in the kuramoto model with bimodal frequency distribution. *Physical Review E*, 74(5):056201, 2006.

[120] Carolina A Moreira and Marcus AM de Aguiar. Global synchronization of partially forced kuramoto oscillators on networks. *Physica A: Statistical Mechanics and its Applications*, 514:487–496, 2019.

[121] Masayo Morofushi, Kazuyuki Shinohara, Toshiya Funabashi, and Fukuko Kimura. Positive relationship between menstrual synchrony and ability to smell 5α-androst-16-en-3α-ol. *Chemical Senses*, 25(4):407–411, 2000.

[122] Arthur J Moss, W Jackson Hall, David S Cannom, Helmut Klein, Mary W Brown, James P Daubert, NA Mark Estes III, Elyse Foster, Henry Greenberg, Steven L Higgins, et al. Cardiac-resynchronization therapy for the prevention of heart-failure events. *New England Journal of Medicine*, 361(14):1329–1338, 2009.

[123] Emi Nagoshi, Camille Saini, Christoph Bauer, Thierry Laroche, Felix Naef, and Ueli Schibler. Circadian gene expression in individual fibroblasts: cell-autonomous and self-sustained oscillators pass time to daughter cells. *Cell*, 119(5):693–705, 2004.

[124] Z Néda, A Nikitin, and T Vicsek. Synchronization of two-mode stochastic oscillators: a new model for rhythmic applause and

much more. *Physica A: Statistical Mechanics and its Applications*, 321(1-2):238–247, 2003.

[125] Zoltán Néda, Erzsébet Ravasz, Yves Brechet, Tamás Vicsek, and A-L Barabási. Self-organizing processes: The sound of many hands clapping. *Nature*, 403(6772):849, 2000.

[126] Zoltán Néda, Erzsébet Ravasz, Tamás Vicsek, Yves Brechet, and Albert-Lázló Barabási. Physics of the rhythmic applause. *Physical Review E*, 61(6):6987, 2000.

[127] Koji Okuda and Yoshiki Kuramoto. Mutual entrainment between populations of coupled oscillators. *Progress of Theoretical Physics*, 86(6):1159–1176, 1991.

[128] Edward Ott and Thomas M Antonsen. Low dimensional behavior of large systems of globally coupled oscillators. *Chaos: An Interdisciplinary Journal of Nonlinear Science*, 18(3):037113, 2008.

[129] W. Oukil, A. Kessi, and Ph. Thieullen. Synchronization hypothesis in the winfree model. *Dynamical Systems*, 32(3):326–339, 2017.

[130] Kevin P O'Keeffe, Hyunsuk Hong, and Steven H Strogatz. Oscillators that sync and swarm. *Nature communications*, 8(1):1504, 2017.

[131] Derek A Paley, Naomi Ehrich Leonard, Rodolphe Sepulchre, Daniel Grunbaum, and Julia K Parrish. Oscillator models and collective motion. *IEEE Control Systems Magazine*, 27(4):89–105, 2007.

[132] Theodosios Pavlidis. A model for circadian clocks. *The Bulletin of Mathematical Biophysics*, 29(4):781–791, 1967.

[133] Diego Pazó and Ernest Montbrió. Existence of hysteresis in the kuramoto model with bimodal frequency distributions. *Physical Review E*, 80(4):046215, 2009.

[134] Diego Pazó and Ernest Montbrió. Low-dimensional dynamics of populations of pulse-coupled oscillators. *Physical Review X*, 4(1):011009, 2014.

[135] Louis M Pecora and Thomas L Carroll. Master stability functions for synchronized coupled systems. *Physical Review Letters*, 80(10):2109, 1998.

[136] Charles S Peskin. Mathematical aspects of heart physiology. *Courant Institute of Mathematical Sciences*, 1975.

[137] Bastian Pietras, Nicolás Deschle, and Andreas Daffertshofer. Equivalence of coupled networks and networks with multimodal frequency distributions: Conditions for the bimodal and trimodal case. *Physical Review E*, 94(5):052211, 2016.

[138] Bastian Pietras, Nicolás Deschle, and Andreas Daffertshofer. First-order phase transitions in the kuramoto model with compact bimodal frequency distributions. *Physical Review E*, 98(6):062219, 2018.

[139] Arkady Pikovsky, Michael Rosenblum, Jurgen Kurths, and Jürgen Kurths. *Synchronization: a universal concept in nonlinear sciences*, volume 12. Cambridge University Press, 2003.

[140] Arkady S Pikovsky, Michael G Rosenblum, Grigory V Osipov, and Jürgen Kurths. Phase synchronization of chaotic oscillators by external driving. *Physica D: Nonlinear Phenomena*, 104(3-4):219–238, 1997.

[141] Colin S Pittendrigh and Serge Daan. A functional analysis of circadian pacemakers in nocturnal rodents. *Journal of Comparative Physiology*, 106(3):223–252, 1976.

[142] Collin S Pittendrigh. An oscillator model for biological clocks. *Rhythmic and Synthetic Processes in Growth*, pages 75–109, 1957.

[143] Oleksandr V Popovych and Peter A Tass. Macroscopic entrainment of periodically forced oscillatory ensembles. *Progress in biophysics and molecular biology*, 105(1-2):98–108, 2011.

[144] C Ladd Prosser. Comparative physiology and biochemistry: status and prospects. *Comparative Biochemistry and Physiology*, 11(1):1–7, 1964.

[145] D. Dane Quinn, Richard H. Rand, and Steven Strogatz. Synchronization in the winfree model of coupled nonlinear oscillators. In *5th EUROMECH Nonlinear Oscillations Conference*, 2005.

[146] D. Dane Quinn, Richard H. Rand, and Steven H. Strogatz. Singular unlocking transition in the Winfree model of coupled oscillators. *Physical Review E*, 75(3):036218, 2007.

[147] Filippo Radicchi and Hildegard Meyer-Ortmanns. Entrainment of coupled oscillators on regular networks by pacemakers. *Physical Review E*, 73(3):036218, 2006.

[148] Rohit Rajeev, M Govind, and Bipin Balaram. Effect of external force on the dynamics of nonlinearly coupled self excited oscillators. *Procedia Engineering*, 144:1007–1014, 2016.

[149] A Reinberg. Methodologic considerations for human chronobiology. *Biological Rhythm Research*, 2(1):1–15, 1971.

[150] Francisco A. Rodrigues, Thomas K. DM. Peron, Peng Ji, and Jürgen Kurths. The kuramoto model in complex networks. *Physics Reports*, 610:1–98, 2016.

[151] Pieter R Roelfsema, Andreas K Engel, Peter König, and Wolf Singer. Visuomotor integration is associated with zero time-lag synchronization among cortical areas. *Nature*, 385(6612):157, 1997.

[152] Till Roenneberg, Zdravko Dragovic, and Martha Merrow. Demasking biological oscillators: properties and principles of entrainment exemplified by the neurospora circadian clock. *Proceedings of the National Academy of Sciences*, 102(21):7742–7747, 2005.

[153] Till Roenneberg and Martha Merrow. The network of time: understanding the molecular circadian system. *Current Biology*, 13(5):R198–R207, 2003.

[154] Fabien Rogister and Rajarshi Roy. Localized excitations in arrays of synchronized laser oscillators. *Physical Review Letters*, 98(10):104101, 2007.

[155] Michael Rosenblum and Arkady Pikovsky. Synchronization: from pendulum clocks to chaotic lasers and chemical oscillators. *Contemporary Physics*, 44(5):401–416, 2003.

[156] Tarun Kanti Roy and Avijit Lahiri. Synchronized oscillations on a kuramoto ring and their entrainment under periodic driving. *Chaos, Solitons and Fractals*, 45(6):888–898, 2012.

[157] Christian Rummel, Marc Goodfellow, Heidemarie Gast, Martinus Hauf, Frédérique Amor, Alexander Stibal, Luigi Mariani, Roland Wiest, and Kaspar Schindler. A systems-level approach to human epileptic seizures. *Neuroinformatics*, 11(2):159–173, 2013.

[158] Hidetsugu Sakaguchi. Cooperative phenomena in coupled oscillator systems under external fields. *Progress of Theoretical Physics*, 79(1):39–46, 1988.

[159] Hidetsugu Sakaguchi and Yoshiki Kuramoto. A soluble active rotater model showing phase transitions via mutual entertainment. *Progress of Theoretical Physics*, 76(3):576–581, 1986.

[160] Hidetsugu Sakaguchi, Shigeru Shinomoto, and Yoshiki Kuramoto. Mutual entrainment in oscillator lattices with nonvariational type interaction. *Progress of Theoretical Physics*, 79(5):1069–1079, 1988.

[161] Eur Schöll. Synchronization patterns and chimera states in complex networks: interplay of topology and dynamics. *The European Physical Journal Special Topics*, 225(6-7):891–919, 2016.

[162] Arthur Sherman and John Rinzel. Collective properties of insulin-secreting cells. In *Cell to Cell Signalling*, pages 61–75. Elsevier, 1989.

[163] Arthur Sherman and John Rinzel. Model for synchronization of pancreatic beta-cells by gap junction coupling. *Biophysical Journal*, 59(3):547–559, 1991.

[164] Arthur Sherman, JOHN RiNZEL, and Joel Keizer. Emergence of organized bursting in clusters of pancreatic beta-cells by channel sharing. *Biophysical Journal*, 54(3):411–425, 1988.

[165] Wolf Singer and Charles M Gray. Visual feature integration and the temporal correlation hypothesis. *Annual Review of Neuroscience*, 18(1):555–586, 1995.

[166] Nikos S Skantzos, Isaac Pérez Castillo, and Jonathan PL Hatchett. Cavity approach for real variables on diluted graphs and application to synchronization in small-world lattices. *Physical Review E*, 72(6):066127, 2005.

[167] H. M. SMITH. Synchronous flashing of fireflies. *Science*, 82:151, 1935.

[168] S. H. Strogatz. From kuramoto to Crawford: exploring the onset of synchronization in populations of coupled oscillators. *Physica D: Nonlinear Phenomena*, 143(1–4):1–20, 2000.

[169] SH Strogatz, CM Marcus, RM Westervelt, and RE Mirollo. Simple model of collective transport with phase slippage. *Physical Review Letters*, 61(20):2380, 1988.

[170] Steven H Strogatz. *Sync: How order emerges from chaos in the universe, nature, and daily life*. Hachette UK, 2012.

[171] Steven H Strogatz and Renato E Mirollo. Stability of incoherence in a population of coupled oscillators. *Journal of Statistical Physics*, 63(3-4):613–635, 1991.

[172] John William Strutt and Baron Rayleigh. *The theory of sound*. Dover, 1945.

[173] Jeppe Sturis, Eve Van Cauter, John D Blackman, and Kenneth S Polonsky. Entrainment of pulsatile insulin secretion by oscillatory glucose infusion. *The Journal of Clinical Investigation*, 87(2):439–445, 1991.

[174] Joseph S Takahashi, Fred W Turek, and Robert Y Moore. *Handbook of behavioral neurobiology: circadian clocks*. Kluwer Academic/PlenumPublishers, 2001.

[175] Vincent Torre. A theory of synchronization of heart pace-maker cells. *Journal of Theoretical Biology*, 61(1):55–71, 1976.

[176] Peter Uhlhaas, Gordon Pipa, Bruss Lima, Lucia Melloni, Sergio Neuenschwander, Danko Nikolić, and Wolf Singer. Neural synchrony in cortical networks: history, concept and current status. *Frontiers in Integrative Neuroscience*, 3:17, 2009.

[177] Peter J Uhlhaas and Wolf Singer. Neural synchrony in brain disorders: relevance for cognitive dysfunctions and pathophysiology. *Neuron*, 52(1):155–168, 2006.

[178] Shimon Ullman. Sequence seeking and counter streams: a computational model for bidirectional information flow in the visual cortex. *Cerebral Cortex*, 5(1):1–11, 1995.

[179] Koichiro Uriu, Saúl Ares, Andrew C Oates, and Luis G Morelli. Dynamics of mobile coupled phase oscillators. *Physical Review E*, 87(3):032911, 2013.

[180] Anthony N van den Pol. The hypothalamic suprachiasmatic nucleus of rat: intrinsic anatomy. *Journal of Comparative Neurology*, 191(4):661–702, 1980.

[181] Balth Van der Pol. On relaxation-oscillations. *The London, Edinburgh, and Dublin Philosophical Magazine and Journal of Science*, 2(11):978–992, 1926.

[182] Eddy A Van der Zee, Koen Jansen, and Menno P Gerkema. The suprachiasmatic nucleus in organotypic slice cultures of the common vole (microtus arvalis): comparison of development with

rat and hamster and the effect of age. *Journal of Biological Rhythms*, 15(1):37–47, 2000.

[183] Thomas J Walker. Acoustic synchrony: two mechanisms in the snowy tree cricket. *Science*, 166(3907):891–894, 1969.

[184] Huobin Wang, Wenchen Han, and Junzhong Yang. Synchronous dynamics in the kuramoto model with biharmonic interaction and bimodal frequency distribution. *Physical Review E*, 96(2):022202, 2017.

[185] Xiao-Jing Wang. Neurophysiological and computational principles of cortical rhythms in cognition. *Physiological Reviews*, 90(3):1195–1268, 2010.

[186] Yongqiang Wang and Francis J Doyle. Exponential synchronization rate of kuramoto oscillators in the presence of a pacemaker. *IEEE Rransactions on Automatic Control*, 58(4):989–994, 2012.

[187] Shinya Watanabe and Steven H Strogatz. Integrability of a globally coupled oscillator array. *Physical Review Letters*, 70(16):2391, 1993.

[188] Shinya Watanabe and Steven H Strogatz. Constants of motion for superconducting josephson arrays. *Physica D: Nonlinear Phenomena*, 74(3-4):197–253, 1994.

[189] David K Welsh, Diomedes E Logothetis, Markus Meister, and Steven M Reppert. Individual neurons dissociated from rat suprachiasmatic nucleus express independently phased circadian firing rhythms. *Neuron*, 14(4):697–706, 1995.

[190] R Wever. Pendulum versus relaxation oscillation. *Circadian Clocks*, pages 74–83, 1965.

[191] Norbert Wiener. *Cybernetics or Control and Communication in the Animal and the Machine*, volume 25. MIT press, 1965.

[192] Norbert Wiener. Nonlinear problems in random theory. *Nonlinear Problems in Random Theory, by Norbert Wiener, pp.*

142. ISBN 0-262-73012-X. Cambridge, Massachusetts, USA: The MIT Press, August 1966.(Paper), page 142, 1966.

[193] Kurt Wiesenfeld, Pere Colet, and Steven H Strogatz. Frequency locking in josephson arrays: Connection with the kuramoto model. *Physical Review E*, 57(2):1563, 1998.

[194] Arthur T Winfree. Biological rhythms and the behavior of populations of coupled oscillators. *Journal of Theoretical Biology*, 16(1):15–42, 1967.

[195] Kong-Fatt Wong and Xiao-Jing Wang. A recurrent network mechanism of time integration in perceptual decisions. *Journal of Neuroscience*, 26(4):1314–1328, 2006.

[196] Kenneth P Wright, Rod J Hughes, Richard E Kronauer, Derk-Jan Dijk, and Charles A Czeisler. Intrinsic near-24-h pacemaker period determines limits of circadian entrainment to a weak synchronizer in humans. *Proceedings of the National Academy of Sciences*, 98(24):14027–14032, 2001.

[197] Yuan Xie, Shuangjian Guo, Lan Zhang, Qionglin Dai, and Junzhong Yang. Twisted states in nonlocally coupled phase oscillators with bimodal frequency distribution. *Communications in Nonlinear Science and Numerical Simulation*, 68:139–146, 2019.

[198] Yuan Xie, Lan Zhang, Shuangjian Guo, Qionglin Dai, and Junzhong Yang. Twisted states in nonlocally coupled phase oscillators with frequency distribution consisting of two lorentzian distributions with the same mean frequency and different widths. *PlOS one*, 14(3):e0213471, 2019.

[199] Shun Yamaguchi, Hiromi Isejima, Takuya Matsuo, Ryusuke Okura, Kazuhiro Yagita, Masaki Kobayashi, and Hitoshi Okamura. Synchronization of cellular clocks in the suprachiasmatic nucleus. *Science*, 302(5649):1408–1412, 2003.

[200] Robert A York and Richard C Compton. Quasi-optical power combining using mutually synchronized oscillator arrays. *IEEE*

Transactions on Microwave Theory and Techniques, 39(6):1000–1009, 1991.

[201] Minoru Yoshimoto, Kenichi Yoshikawa, and Yoshihito Mori. Coupling among three chemical oscillators: synchronization, phase death, and frustration. *Physical Review E*, 47(2):864, 1993.

[202] Di Yuan, Jun-Long Tian, Fang Lin, Dong-Wei Ma, Jing Zhang, Hai-Tao Cui, and Yi Xiao. Periodic synchronization in a system of coupled phase oscillators with attractive and repulsive interactions. *Frontiers of Physics*, 13(3):130504, 2018.

[203] M Zalalutdinov, Keith L Aubin, Manoj Pandey, Alan Taylor Zehnder, Richard H Rand, Harold G Craighead, Jeevak M Parpia, and Brian H Houston. Frequency entrainment for micromechanical oscillator. *Applied Physics Letters*, 83(16):3281–3283, 2003.

Summary

Rhythmic behavior is widely present in living organisms. The rhythms can be innate and usually they are externally stimulated by the environment. One such stimulus is the 24 h natural light–dark cycle which governs the activity–inactivity cycle of many plants, animals and humans. The cells in the suprachiasmatic nucleus that govern our circadian rhythms are ideally regarded as a group of biological oscillators. In the Winfree model, the biological oscillators are regarded as coupled oscillators. The Winfree model was used to describe the synchronization of a large system of globally coupled phase oscillators. Considering that external stimuli and environmental factors, such as the change of light and darkness, have great influence on the rhythmic behavior, a periodic forcing is added to Winfree system.

We first introduce the background of the synchronization history and its applications on biology, physics, science and finance in Chapter 1. Then we talk about the synchronization in circadian rhythm, the motivation of the project and the setting of the thesis in the same chapter.

The second chapter of the thesis focuses on a case where the mean natural frequency of the oscillators is the same with the frequency of the external forcing. A simple case is analyzed with the Poincaré map for only one forced oscillator. Then through a careful study of synchronized states and stability on identical oscillators, we obtain the entrainment degree. For a more general case, we study the state diagrams of non-identical oscillators whose natural frequencies follow a uniform or a Lorentz distribution. The Ott-Antonsen is used to give a low-dimensional dynamical description of the system.

The third chapter of the thesis contains comparable considerations

as the second chapter but in the case of detuned systems. We investigate the difference between the detuned and non-detuned cases for identical oscillators and understand the entrainment patterns using stability theory. In the last part of the third chapter, we again use the Ott-Antonsen ansatz to lower the dimension of the forced Winfree system. The entrainment degree obtained through the Ott-Antonsen ansatz is then compared to the results we get from the numerical computations.

In the fourth chapter of the thesis we point out the possibilities for future work. We investigate the routes to synchronization in the Winfree model with a bimodal distribution constructed as combination of two unimodal distributions and present questions for future work.

Finally, in the fifth chapter we summarize the most important insights and contributions of this thesis. In addition, we discuss some limitations of this work.

Samenvatting

Ritmisch gedrag is wijd en zijd aanwezig in levende organismen. De ritmes kunnen aangeboren zijn en meestal worden ze van buitenaf gestimuleerd door de omgeving. Een van deze stimulansen is de 24-uurs natuurlijke licht-donker cyclus die de activiteit-inactiviteit cyclus van veel planten, dieren en mensen regelt. De cellen in de suprachiasmatische kern die onze circadische ritmes regelen, worden idealiter beschouwd als een groep biologische oscillatoren. In het Winfree model worden de biologische oscillatoren beschouwd als gekoppelde oscillatoren. Het Winfree model werd gebruikt om de synchronisatie van een groot systeem van globaal gekoppelde fase-oscillatoren te beschrijven. Gezien het feit dat externe prikkels en omgevingsfactoren, zoals de verandering van licht en duisternis, grote invloed hebben op het ritmische gedrag, wordt een periodiekeaandrijving toegevoegd aan het Winfreesysteem.

In hoofdstuk 1 introduceren we eerst de achtergrond van de synchronisatiegeschiedenis en de toepassingen hiervan op het gebied van biologie, natuurwetenschappen en financiën. Vervolgens spreken we in hetzelfde hoofdstuk over de synchronisatie in het circadiane ritme, de motivatie van project en de setting van het proefschrift.

Het tweede hoofdstuk van de proefschrift richt zich op een geval waarin de gemiddelde natuurlijke frequentie van de oscillatoren gelijk is aan de frequentie van de externe aandrijving. Een eenvoudig geval wordt geanalyseerd met de Poincare-kaart voor slechts één geforceerde oscillator. Vervolgens wordt door een zorgvuldige studie van gesynchroniseerde toestanden en stabiliteit op identieke oscillatoren de entrainment graad verkregen. Voor een meer algemeen geval bestuderen we de toestandsdiagrammen van niet-identieke oscillatoren waarvan de

natuurlijke frequenties een uniforme of een Lorentz-verdeling volgen. De Ott-Antonsen wordt gebruikt om een laagdimensionale dynamische beschrijving van het systeem te geven.

Het derde hoofdstuk van de proefschrift bevat vergelijkbare overwegingen als het tweede hoofdstuk, maar dan in het geval van detuned (ontstemde) systemen. We onderzoeken het verschil tussen de detuned en de non-detuned gevallen voor identieke oscillatoren en komen tot het begrip van de entrainment patronen met behulp van de stabiliteitstheorie. In het laatste deel van het derde hoofdstuk gebruiken we opnieuw de Ott-Antonsen ansatz om de dimensie van het geforceerde Winfree systeem te verlagen. De entrainment graad verkregen via de Ott-Antonsen ansatz wordt dan vergeleken met de resultaten die we krijgen uit de numerieke berekeningen.

In het vierde hoofdstuk van het proefschrift wijzen we op de mogelijkheden voor toekomstig werk. We onderzoeken de routes naar synchronisatie in het Winfree model met een bimodale verdeling die is opgebouwd als een combinatie van twee unimodale verdelingen en de huidige vragen voor toekomstig werk.

Tot slot vatten we in het vijfde hoofdstuk de belangrijkste inzichten en bijdragen van deze thesis samen. Daarnaast bespreken we enkele beperkingen van dit werk.

Acknowledgements

How time flies! I has been living in Groningen four years. It is time to draw the conclusion, similar to drawing conclusions for scientific articles. I still remembered the day I arrived at the train station in the early morning on the 1st October in 2016. Everything was so fresh to me, and so the life was. I have experienced many ups and downs in the past four years, but full of gratitude. This doctoral thesis could never be written without many people's help, trust and support in many ways, directly or indirectly. I would like to express my gratitude to them here.

First of all, I am very grateful to my supervisor, Dr.Konstantinos Efstathiou. Thank you for giving me the opportunity to do my PhD under your supervisor. Your meticulous attitudes on scientific research made me a deep impression. In the past four years, we had many weekly meetings which got me continuous progress on my research. You were so nice waiting for me at the Groningen station with your family on my first arrival day four years ago. In Kunshan, you also helped me a lot to start my study and continue my research. I am very grateful that you are helping me on my research and supporting me during my difficulties. I cannot list all of them, but they are all my precious and well-appreciated memory. Your guidance, support, and encouragement means a lot to me through my PhD life.

I am thankful to my superior Prof. H. W Broer. I felt myself luck to have you as my supervisor and promoter, this gave me the opportunity to benefit from your knowledge and experience to become a better researcher.

I am thankful to my collaborator Dr. Igor Hoveijn. You are a knowledgeable scholar and a delightful collaborator. I appreciate your

thoughts, your guidance and your contribution on the third part of my research. I am grateful to you for many things I have learned from you, from our weekly meetings, and from your patient explanations of some knowledge.

I wish to thank the members of the assessment committee, Prof. Gert Vegter, Prof. Angel Jorba, Prof. Lidong Wang for accepting to evaluate and comment on my thesis. I am grateful to Lidong for all your support for my PhD study.

Many thanks to all the staff at the Bernoulli Institute for Mathematics, Computer Science and Artificial Intelligence for creating such a good research environment. Special thanks to Holger Waalkens for taking me into your courses, dynamical system. The same thanks to Daniel and Bart for allowing me to take your course, mathematical modelling. I am also grateful to Alef Sterk and Fred Wubs for the talks we had. I would like to thank the secretaries Elina, Renske and Ineke for many help for making my study successful.

I wish to thank my friends and colleagues from the University of Groningen. In particular, I would like to thank Dirk, Mahdi, Nikolay, Pan Li, Pariya, Reza and Vladimire who have left the university already. I wish to thank Benjamin, Chengtao, Eric, Jiajia, Junjie, Lorenzo, Markus and Georg, Gariel, Rui, Tune, Xiaokun, Xueyi, Zizhao for creating the pleasant, friendly and stimulating atmosphere. We also had many happy time for activities, lunch, traveling, dinner and coffee time together. Special thanks should be given to Jian and Bohuan for supporting me, discussing my topic and sharing ideas.

There are more people to mention who gave me a wonderful experience in Groningen. Bingquan Zhang, Bing jiang, Fei Wu, Huala Wu, Haiyan Ni, Haoqi Chen, Heng Li, Jin Li,Jinrui Zhang, Jiacong Wei, Jingyao Li, Lu Han, Luo Ge, Minghui Li, Mingming Shi, Rufang Zhang, Rongjing Zhang, Qian Chen, Qingqing Cai, Qifeng Guo, Qifeng Guo, Shuxian Hu, Shun Fang, Si Chen, Shaomin Hou, Shandong Han, Tian Xie, Taojun Wang, Ting Huang, Wenze Guo, Xinyu Zhou, Xiaoyan Wang, Xinhui Wu, Xingchen Yan, Xiaohong Peng, Xiaoxiang, Xiaodong Wang, Xing WanChengtao Ji, Xukai Zhang, Xuelai Wang, Yongyu Zhang, Yu Li, Yuchen Du, Yehan Tao, Zhen Cheng, Zhiwen Wang.

I can not forget the joy I had together with Marina, Rodrigo,

Vivian, Renske and Julian for our memory on Phd Day 2019. This gave me a lot of pleasure during my PhD time.

Finally, I would like to give my thanks to my family.

谢谢爸爸妈妈给我无条件的爱和支持. 爸爸正直宽厚乐观积极的人生态度是我一生学习的榜样, 妈妈善良坚强给了我生活的底色. 是你们一如既往的爱护, 理解, 鼓励和支持是我人生温暖的避风港, 是我前行的动力, 更是我克服一切困难的勇气.

Yongjiao Zhang
July, 2020